

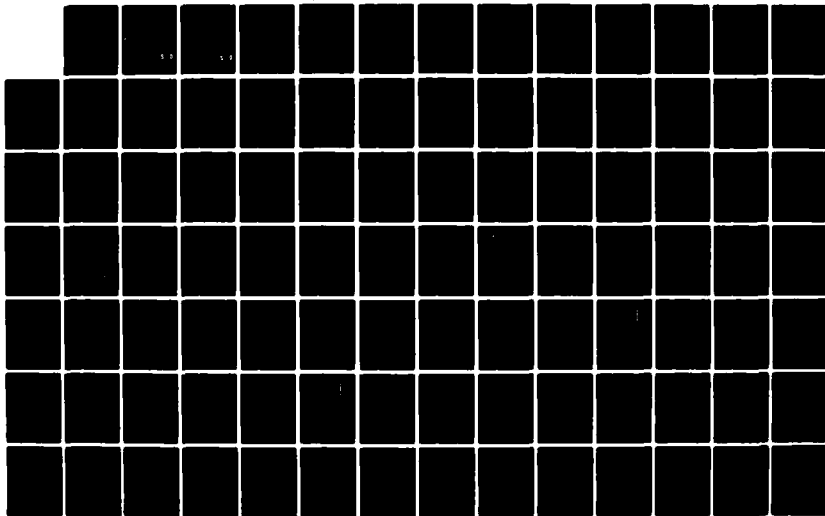
AD-A127 303

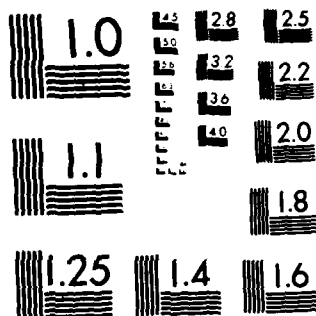
THE CALCULATION OF LATE-TIME SURFACE BURST EMP
(ELECTROMAGNETIC PULSE) FI... (U) AIR FORCE INST OF TECH
WRIGHT-PATTERSON AFB OH SCHOOL OF ENGI... J R DOWNEY
MAR 83 AFIT/GNE/PH/83M-5 F/G 18/3

1/2

UNCLASSIFIED

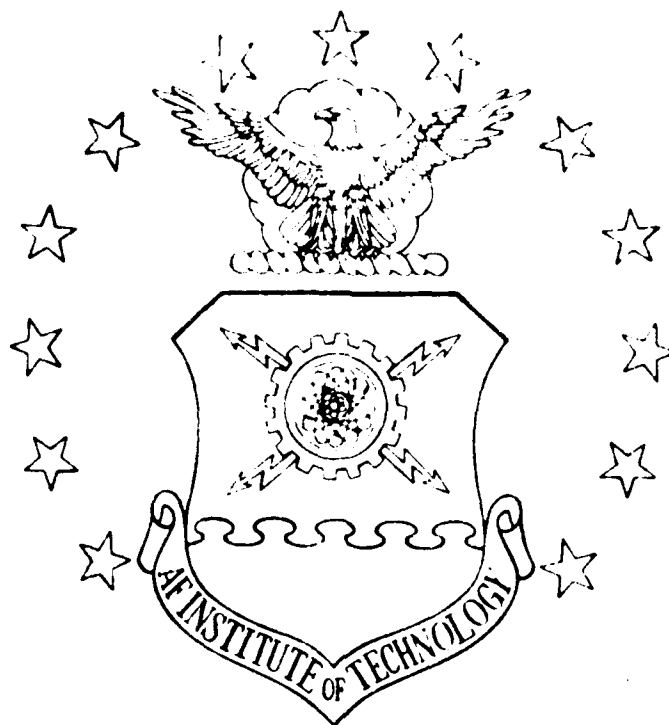
NL





MICROCOPY RESOLUTION TEST CHART
NATIONAL BUREAU OF STANDARDS-1963-A

AD A127303



THE CALCULATION OF LATE-TIME
SURFACE BURST EMP FIELDS USING
A TIME-INDEPENDENT NUMERICAL METHOD
THESIS

AFIT/GNE/PH/83M-5

James R. Downe
Lt USA

DTIC FILE COPY

DEPARTMENT OF THE AIR FORCE
AIR UNIVERSITY (ATC)
AIR FORCE INSTITUTE OF TECHNOLOGY

DTIC
ELECTE
S D
APR 28 1983
E

Wright-Patterson Air Force Base, Ohio

This document has been approved
for public release and sales in
unlimited quantities

83 04 28 091

AFIT/GNE/PH/83M-5

THE CALCULATION OF LATE-TIME
SURFACE BURST EMP FIELDS USING
A TIME-INDEPENDENT NUMERICAL METHOD
THESIS

AFIT/GNE/PH/83M-5

James R. Downey
2Lt USAF

DTIC
ELECTE
APR 28 1983
S D
E

Approved for Public Release; Distribution Unlimited

AFIT/GNE/PH/83M-5

THE CALCULATION OF LATE-TIME
SURFACE BURST EMP FIELDS USING
A TIME-INDEPENDENT NUMERICAL METHOD

THESIS

Presented to the Faculty of the School of Engineering
of the Air Force Institute of Technology

Air University
in Partial Fulfillment of the
Requirements for the Degree of
Master of Science

by

James R. Downey, B.S.

2Lt

USAF

Graduate Nuclear Engineering

March 1983

Accession For	
NTIS GRA&I	<input checked="checked" type="checkbox"/>
DTIC TAB	<input type="checkbox"/>
Unannounced	<input type="checkbox"/>
Justification	
By	
Distribution/	
Availability Codes	
Dist	Avail and/or Special
A	



Approved for Public Release; Distribution Unlimited

Preface

The purpose of this study was to calculate the electric fields in the air resulting from a surface nuclear burst. To achieve this, a computer program was developed which used curve fits for the source terms and the electron air chemistry parameters to find a solution to Maxwell's equations in the quasi-static EMP phase. The results of these calculations were compared to approximate analytic solutions.

Since the solution in the late-time phase is time-independent, the computer program in Appendix F should be useful because of the relatively fast execution time. This allows many variations in parameters to be studied easily.

I would first like to thank Maj. Gary Knutson of the Air Force Weapons Laboratory for suggesting this project.

A great deal of appreciation must, also, be extended to my faculty advisor Lt. Col. John Erkkila. He guided me when things went poorly and gave me the freedom to do my own work. This combination greatly enhanced the knowledge I gained.

Finally, I would like to thank my wife, Monica, for her patience and support at all times. This thesis truly belongs to both of us.

James R. Downey

Contents

	<u>Page</u>
Preface	ii
List of Figures	v
List of Tables	viii
Abstract	ix
I. Introduction	1
Background	1
Problem	3
Scope and Assumptions	3
General Approach	4
Overview	4
II. Background Quasi-Static EMP Theory	6
Maxwell's Equations	6
Approximate Solution	8
Air Chemistry	10
Limit of Approximate Solution	11
III. An Improved Analytic and Equivalent Finite Difference Solution	13
Legendre Polynomial Expansion	13
Numerical Solution Development	15
Solution Algorithm	17
Boundary Conditions	19
Computer Solution	20
IV. Initial Numerical Results	21
Field Calculations	21
Comparison with Expected Conductivity	23
Comparison with Approximate Expressions	31
Limits of Grover's Model	33
V. Late-Time EMP Sources and Air Chemistry Parameters	34
Late-Time Sources	34
Air Chemistry Parameters	41

	<u>Page</u>
VI. An Improved Numerical Method	44
Solution Development	44
Solution Technique	51
VII. Results	52
Test Problem	52
Theta Dependence	57
Boundary Condition at $r = 0$	58
Field Dependence	58
Effect of J_0	59
Variation in Electron Mobility	59
Summary	64
VIII. Parametric Studies	67
Code Accuracy	67
Time Dependence	68
Yield Dependence	70
Water Vapor Dependence	74
IX. Conclusions and Recommendations	78
Conclusions	78
Recommendations	79
Bibliography	80
Appendix A: Finite Differences in Initial Solution . .	82
Appendix B: Initial Numerical Results	85
Appendix C: Analytic Fits for Sources and Air Chemistry Parameters	94
Appendix D: Romberg Integration	98
Appendix E: Parametric Studies	101
Appendix F: Program Description and Listing	114
Vita	137

List of Figures

<u>Figure</u>		<u>Page</u>
1	Surface Burst Geometry	2
2	Expected Conductivity Compared to Grover's Model (3), $\sigma_o = 178.0$	25
3	Expected Conductivity Compared to Grover's Model (3), $\sigma_o = 143.2$	26
4	E_r vs Radius, Initial Solution	27
5	E_r vs Angle, Initial Solution	28
6	- E_θ vs Radius, Initial Solution	29
7	- E_θ vs Angle, Initial Solution	30
8	Electronic and Ionic Conductivity vs Radius for Initial Problem	32
9	Ionization Rate vs Radius at Four Angles . . .	36
10	Radial Compton Current ($-J_r$) vs Radius at Four Angles	37
11	Theta Compton Current (J_θ) vs Radius at Three Angles	38
12	- J_r and J_θ vs Time	40
13	Electron Attachment Rate vs Total Field . . .	42
14	Electron Mobility vs Total Field	43
15	E_r vs Radius, Full Solution	53
16	E_r vs Angle, Full Solution	54
17	- E_θ vs Radius, Full Solution	55
18	- E_θ vs Angle, Full Solution	56
19	E_r vs Radius, Field Independent	60
20	- E_θ vs Radius, Field Independent	61
21	E_r vs Radius, $J_\theta = 0$	62

List of Figures
(continued)

<u>Figure</u>		<u>Page</u>
22	- E_{θ} vs Radius, $J_{\theta} = 0$	63
23	E_r vs Radius, Electron Mobility Not Limited	65
24	- E_{θ} vs Radius, Electron Mobility Not Limited	66
25	Total Field vs Time, $\theta = 90^{\circ}$	69
26	Total Field vs Time, $\theta = 0^{\circ}$	71
27	Total Field vs Yield, $\theta = 90^{\circ}$	72
28	Total Field vs Yield, $\theta = 0^{\circ}$	73
29	Total Field vs Water Vapor Content, $\theta = 90^{\circ}$.	75
30	Total Field vs Water Vapor Content, $\theta = 0^{\circ}$. .	76
31	E_r vs Radius, Simplified Sources $\sigma_O = 178.0$	86
32	E_r vs Angle, Simplified Sources $\sigma_O = 178.0$	87
33	- E_{θ} vs Radius, Simplified Sources $\sigma_O = 178.0$	88
34	- E_{θ} vs Angle, Simplified Sources $\sigma_O = 178.0$	89
35	E_r vs Radius, Simplified Sources $\sigma_O = 143.2$	90
36	E_r vs Angle, Simplified Sources $\sigma_O = 143.2$	91
37	- E_{θ} vs Radius, Simplified Sources $\sigma_O = 143.2$	92
38	- E_{θ} vs Angle, Simplified Sources $\sigma_O = 143.2$	93
39	Generalized Romberg Terms	99
40	Romberg Algorithm	100

List of Figures
(continued)

<u>Figure</u>		<u>Page</u>
41	Total Field vs Radius, Full Solution $t = 10^{-2}$ sec	102
42	Total Field vs Angle, Full Solution $t = 10^{-2}$ sec	103
43	Total Field vs Radius, Full Solution $t = 10^{-1}$ sec	104
44	Total Field vs Angle, Full Solution $t = 10^{-1}$ sec	105
45	Total Field vs Radius, Full Solution Yld = 1000 KT	106
46	Total Field vs Angle, Full Solution Yld = 1000 KT	107
47	Total Field vs Radius, Full Solution Yld = 100 KT	108
48	Total Field vs Angle, Full Solution Yld = 100 KT	109
49	Total Field vs Radius, Full Solution Wvc = 0.00	110
50	Total Field vs Angle, Full Solution Wvc = 0.00	111
51	Total Field vs Radius, Full Solution Wvc = 0.04	112
52	Total Field vs Angle, Full Solution Wvc = 0.04	113
53	Program Flow Diagram	115

List of Tables

<u>Table</u>		<u>Page</u>
I	Computer Code Parameters Used in Calculations	68
II	Analytic Source Functions	95
III	Mobility and Attachment Rate Equations	97

Abstract

A numerical solution was developed to find the quasi-static EMP fields resulting from a surface nuclear burst. By ignoring the time derivatives in Maxwell's equations and expanding the electrostatic potential in Legendre polynomials, a set of differential equations was obtained that was dependent on r only (r = radius from burst). By employing finite differences, a tri-diagonal matrix equation was obtained that was non-linear in the electric field. This equation was solved using an iterative scheme.

Analytic curve fits based on Monte Carlo data were used to determine the air ionization rate and Compton current. This permitted the angular variation of these sources to be included in the calculations. In addition, the electron air chemistry parameters were allowed to vary with the local electric field and water vapor content of the air. This was accomplished by the use of previously developed equations for these terms.

Field calculations were made and compared to previous analytic results. The differences were found to be as great as 50 percent for peak field values. A limited parametric study was performed to consider the effects of varying the time, the yield, and the water vapor content. The computer program documented in this report should be useful for late-

time EMP calculations because of the short execution time.
Furthermore, the code was written such that improvements in
the various fits could easily be incorporated.

THE CALCULATION OF LATE-TIME
SURFACE BURST EMP FIELDS USING
A TIME-INDEPENDENT NUMERICAL METHOD

I. Introduction

Background

In recent years interest has increased in determining the electromagnetic pulse (EMP) produced by surface nuclear bursts. Of special concern is the EMP that occurs in the late-time regime ($\approx 10^{-4}$ to 1 seconds, retarded time). This has largely been motivated by changing system requirements and a desire to explain such things as the lightning strokes observed during the MIKE test shot (Ref 16).

When a surface nuclear burst occurs, electric currents are set up in the air as a result of Compton scattered electrons. The gamma rays penetrating the ground are highly attenuated; thus, the EMP source region is basically a hemisphere above the surface. The generated Compton currents are primarily in the radial direction producing a radial electric field; however, the presence of the ground creates transverse field components which can exist well beyond the source region (Ref 6:31-32). The geometry for the source region is shown in Figure 1.

The problem of late-time EMP has been investigated by several authors (Ref 4; 8; 9; and 17). The basis of the

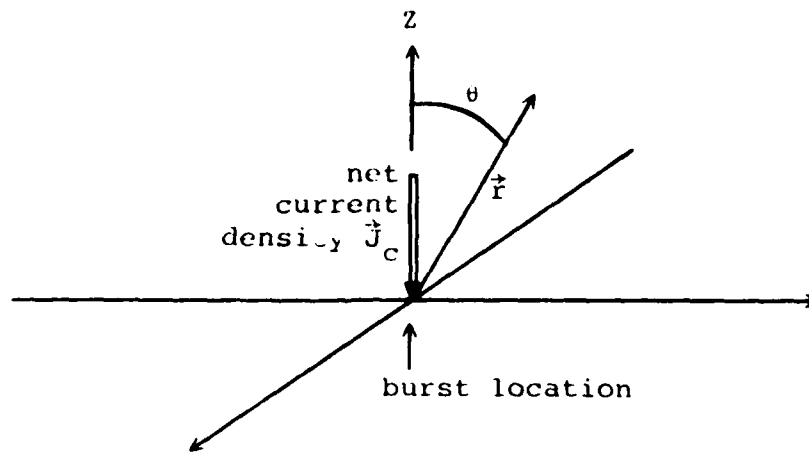


Figure 1. Surface Burst Geometry

theory assumes that the time derivatives in Maxwell's equations will be small at times greater than approximately 100 μ s and can be ignored. This assumption is known as the quasi-static approximation. The electric field is then derivable from a scalar potential $E = -\text{grad } \phi$.

Longmire (Ref 8), Hill (Ref 4), and Wyatt (Ref 17) assumed that the radial component of the electric field would be much smaller than the polar component; therefore they ignored it in their calculations. More recently, Grover (Ref 2) considered the problem of quasi-static EMP without making any assumptions about the field components. Using simplified air conductivity models and expanding the electric potential in Legendre polynomials, Grover obtained analytic solutions for the electric fields.

Though Grover's analytic results are useful, the solutions are limited by several factors: (1) the simplified conductivity models Grover used are only valid for certain

space-time regimes (Ref 2:23-25), (2) the source terms (air ionization rate and radial Compton current) are restricted because no polar variation is allowed, and (3) the electron mobility and attachment rate are assumed to be independent of the electric field and water vapor content of the air. These assumptions are necessary to obtain analytic results.

Problem

The problem investigated in this study is to determine the magnitude of the electric field in the air during the quasi-static phase resulting from a surface nuclear burst.

The angular dependence of the source terms and variations in the air chemistry parameters are included in the calculations.

Scope and Assumptions

The time range of interest in this report is from 10^{-4} to 10^{-1} seconds. This range includes the time frame of the reported nuclear lightning (≈ 1 ms) and allows for the dominance of ground or air capture sources.

The conductivity of the ground is usually much larger than that of the air, especially for later times and smaller yields; therefore it will be considered infinite. This will permit the use of simplified boundary conditions for the solution of Maxwell's equations.

Self-consistent effects between the generated fields and the source currents are ignored in all calculations. This is done to simplify the solution technique.

General Approach

The first phase in this study was the development of a numerical solution which did not include the polar variation of the sources or any variations in the air chemistry parameters. This allowed a comparison and confirmation of the results presented by Grover and provided a basis for comparison with later calculations. The next step was to derive an angular and field dependent solution (ignoring self-consistency) using curve fits for the source terms (Ref 10) and air chemistry parameters (Ref 7). The results obtained here were then compared to the earlier calculations. Finally, limited parametric studies were performed to consider the effects of varying the time, the weapon yield, and the water vapor content.

Overview

In Chapter II the background theory of quasi-static EMP is discussed. The development of the initial solution using the simplified models is presented in Chapter III. The results of calculations using the first solution technique and a comparison with one of Grover's models are given in Chapter IV. In Chapter V the angular dependence of the source terms and the field and water vapor dependence of the air chemistry parameters are discussed. The field and polar dependent derivation and solution algorithm are given in Chapter VI. Chapter VII presents a comparison of the results obtained using the new model with the previous

calculations. A series of parametric studies are given in Chapter VIII and conclusions and recommendations are presented in Chapter IX.

II. Background Quasi-Static EMP Theory

By making a number of simplifying approximations, the quasi-static EMP fields can be found by analytic solutions to Maxwell's equations. In this chapter the basic theory behind these approximate results is presented. The limitations of this theory, also, are discussed.

Maxwell's Equations

As mentioned in the introduction, it is commonly assumed that at times greater than approximately 100 μ s after a surface nuclear burst the electric fields become quasi-static. Consequently, the time derivatives in Maxwell's equations are small, compared to the other terms, and can be set equal to zero (Ref 9:44). Hence,

$$\vec{\nabla} \times \vec{E} = 0 \quad (2.1)$$

$$\frac{1}{\mu_0} \vec{\nabla} \times \vec{B} = \sigma \vec{E} + \vec{J}_c \quad (2.2)$$

where \vec{E} is the electric field (volts/m), \vec{B} is the magnetic field (webers/m²), σ is the conductivity of the air (mho/m), \vec{J}_c is the source current density (Amps/m²), and μ_0 is the magnetic permeability (henries/m).

From vector analysis it is known that $\vec{\nabla} \times (\vec{\nabla} \phi) = 0$, where ϕ is some scalar; therefore, \vec{E} can be defined as

$$\vec{E} = -\vec{\nabla} \phi \quad (2.3)$$

where ϕ is the scalar electric potential (volts). The individual field components are found by

$$E_r = -\frac{\partial \phi}{\partial r} \quad (2.4)$$

$$E_\theta = -\frac{1}{r} \frac{\partial \phi}{\partial \theta} \quad (2.5)$$

where r is the radius from the burst (meters). E_ϕ is zero from symmetry.

The permeability in Eq (2.2) is assumed to be constant. Thus, the equation can be rewritten such that

$$\vec{\nabla} \cdot \left(\frac{1}{\mu_0} \vec{\nabla} \times \vec{B} \right) = 0 \quad (2.6)$$

or

$$\vec{\nabla} \cdot (\sigma \vec{E} + \vec{J}_c) = 0 \quad (2.7)$$

Substituting Eq (2.3) into Eq (2.7) gives

$$\vec{\nabla} \cdot (\sigma \vec{\nabla} \phi) = \vec{\nabla} \cdot \vec{J}_c \quad (2.8)$$

Expanding Eq (2.8) in spherical coordinates and assuming azimuthal symmetry leads to

$$\begin{aligned} & \frac{1}{r^2} \frac{\partial}{\partial r} \left(r^2 \frac{\partial \phi}{\partial r} \right) + \frac{1}{r^2 \sin \theta} \frac{\partial}{\partial \theta} \left(\sin \theta \frac{\partial \phi}{\partial \theta} \right) + \frac{1}{\sigma} \frac{\partial \sigma}{\partial r} \frac{\partial \phi}{\partial r} \\ & + \frac{1}{\sigma r^2} \frac{\partial \sigma}{\partial \theta} \frac{\partial \phi}{\partial \theta} = \frac{1}{\sigma r^2} \frac{\partial}{\partial r} (r^2 J_r) + \frac{1}{\sigma r \sin \theta} \frac{\partial}{\partial \theta} (\sin \theta J_\theta) \end{aligned} \quad (2.9)$$

This is the equation that must be solved to find the electric field in the air.

Approximate Solution

Longmire (Ref 9), Hill (Ref 4), and Wyatt (Ref 17) have shown that an analytic solution to Eq (2.9) can be found if some simplifying assumptions are made.

Since $E_r \ll E_0$ at late times it is set equal to zero. In addition the air conductivity and radial Compton current are assumed to be independent of the polar angle theta. Finally, Monte Carlo studies have shown (Refs 5 and 10) that the theta component of the Compton current source is much smaller than the radial component, except for small r; thus J_θ is ignored.

Using all of the above assumptions Eq (2.9) reduces to

$$-\frac{1}{r \sin \theta} \frac{\partial}{\partial \theta} (\sin \theta E_0) = \frac{1}{\sigma r^2} \frac{\partial}{\partial r} (r^2 J_r) \quad (2.10)$$

Longmire has shown (Ref 8) that the radial Compton current can be fairly well approximated by

$$J_r = J_0 \frac{e^{-r/\lambda}}{r^2} \text{ (Amps/m}^2\text{)} \quad (2.11)$$

where J_0 is a constant for a given time and yield, and λ is the effective gamma ray mean free path (meters).

Substituting this equation into Eq (2.10) leads to

$$-\frac{r}{\sin \theta} \frac{\partial}{\partial \theta} (\sin \theta E_0) = \frac{-1}{\sigma \lambda} J_0 e^{-r/\lambda} \quad (2.12)$$

or

$$\frac{r}{\sin \theta} \frac{\partial}{\partial \theta} (\sin \theta E_0) = \frac{r^2}{\sigma \lambda} J_r \quad (2.13)$$

Integrating with respect to θ gives

$$\sin\theta E_\theta = \frac{r}{\lambda} \frac{J_r}{\sigma} (1 - \cos\theta) \quad (2.14)$$

or

$$E_\theta = \frac{r}{\lambda} \frac{J_r}{\sigma} \tan \frac{\theta}{2} \quad (2.15)$$

This is Longmire's result. By including J_θ , Wyatt obtained the following (Ref 17:8)

$$E_\theta = \frac{1}{\sigma} \left(\frac{r}{\lambda} \frac{J_r}{\sigma} \tan \frac{\theta}{2} - J_\theta \right) \quad (2.16)$$

which reduces to Eq (2.15) if $J_\theta = 0$.

From Eq (2.1) and the assumption that $E_r = 0$, one sees that E_θ must satisfy the following

$$\frac{1}{r} \frac{\partial}{\partial r} (r E_\theta) = 0 \quad (2.17)$$

or

$$E_\theta \propto \frac{1}{r} \quad (2.18)$$

For the above condition to be true the ratio of J_r over σ must be

$$\frac{J_r}{\sigma} \propto \frac{1}{r^2} \quad (2.19)$$

As will be shown below, this requirement places a restriction on the range over which Eq (2.15) applies.

Air Chemistry

To solve for the electric field, the conductivity must be known. The total conductivity consists of contributions from free electrons and positive and negative ions.

The electron conductivity can be written (Ref 6:21-22)

$$\sigma_e = e \mu_e \frac{S}{\alpha_e} \text{ (mho/m)} \quad (2.20)$$

where e is the charge on an electron (coulombs), μ_e is the electron mobility ($\text{m}^2/\text{V}\cdot\text{sec}$), S is the local ionization rate (ion pairs/ $\text{m}^3\cdot\text{sec}$), and α_e is the electron attachment rate (sec^{-1}). Both μ_e and α_e are dependent on the total field, but for now are considered field independent.

At late times most of the electrons are attached; thus, the number of positive ions (N_+) is approximately the same as the number of negative ions (N_-) and the ionic conductivity can be written as

$$\sigma_I = 2 \cdot e \mu_I \sqrt{\frac{S}{\gamma_I}} \text{ (mho/m)} \quad (2.21)$$

where μ_I is the ion mobility ($\text{m}^2/\text{V}\cdot\text{sec}$) and γ_I is the ion-ion recombination rate (m^3/sec). The two represents the fact that $N_+ = N_-$.

The ionization rate in Eqs (2.20) and (2.21) is assumed (Ref 8) to be of the form

$$S = S_0 \frac{e^{-r/\lambda}}{r^2} \left(\frac{\text{ion pairs}}{\text{m}^3 \cdot \text{sec}} \right) \quad (2.22)$$

where S_0 is a constant for a given time and yield.

The total conductivity can then be written (using Eq (2.22) for S)

$$\sigma_T = e \mu_e \frac{S_0 e^{-r/\lambda}}{a_e r^2} + 2e\mu_I \frac{e^{-r/2\lambda}}{r} \sqrt{\frac{S_0}{\gamma_I}} \quad (2.23)$$

As seen in the radial dependence, electrons should dominate the conductivity close to the burst and ions farther out.

Limit of Approximate Solution

If electrons dominate the conductivity, J_r / σ is nearly independent of r . Thus it would be expected that the Longmire model would be inaccurate at shorter ranges from the burst. If ions dominate, the ratio becomes

$$\frac{J_r}{\sigma} \propto \frac{e^{-r/2\lambda}}{r} \propto \frac{1}{r^2} \quad (2.24)$$

or

$$r e^{-r/2\lambda} = \text{constant} \quad (2.25)$$

Longmire (Ref 9:57) states that this requirement is not accurately valid and he limits the range of applicability to 0.2 to 2.0 kilometers with a maximum variation of ± 30 percent.

EMP theory predicts, and others have shown (Ref 13), that the electron conductivity will be important even out to

approximately 1000 meters. This obviously presents a problem for the model discussed above. In the next chapter an analytic solution will be derived which is not limited by the above requirements.

III. An Improved Analytic and Equivalent Finite Difference Solution

In the last chapter an analytic solution to Maxwell's equations was found by making several simplifying assumptions. Recently, Grover (Ref 2) obtained an improved solution by expanding the electric potential in Legendre polynomials and by using simplified models for the air conductivity.

In this chapter the basis of Grover's analytic solution is presented along with an equivalent finite difference method. The numerical solution was developed to provide a basis for comparison with the analytic results (Ref 2) and the more general results presented later in this report.

Legendre Polynomial Expansion

Longmire and Wyatt assumed that the radial component of the field would be smaller than the theta component and they ignored it in their calculations. Grover (Ref 2), however, found an analytic solution without making such an approximation.

By expanding the potential in a series of Legendre polynomials, a set of ordinary differential equations was obtained which only depended on r (Ref 2:7). The potential is written as

$$\phi(r, \theta) = \sum_{\ell=\text{odd}}^{\infty} A_{\ell}(r) P_{\ell}(\cos \theta) \quad (3.1)$$

where $A_l(r)$ are unknown coefficients to be determined, and $P_l(x)$ are the Legendre polynomials ($x = \cos\theta$). The angle θ is measured from the vertical such that $\theta = 0^\circ$ points straight up and $\theta = 90^\circ$ lies along the ground.

Choosing the summation over odd l 's satisfies the boundary conditions on the field: namely, that the radial component of the electric field must be zero at $\theta = 90^\circ$ for an infinite conductivity ground plane, and the polar component must be zero at $\theta = 0^\circ$ due to symmetry.

To solve the problem analytically, Grover assumed that the radial Compton current and the ionization rate were independent of θ . The expressions presented earlier, Eqs (2.11) and (2.22), were used for these parameters.

Instead of using the actual air chemistry, Grover approximated the conductivity by three simplified models. Model (1) was designed to represent the early-time regime when the conductivity is dominated by electrons. Model (2) approximated the late-time regime when ions dominate. Model (3) was used for intermediate times when electrons dominate in close and ions farther out (Ref 2:7). These models were necessary to obtain analytic solutions.

The purpose of this work was not to get Grover's analytic solution; consequently their derivation is left to the reader (Ref 2). Rather, an equivalent numerical method is presented below. This solution was derived to provide a basis for comparison to Grover's results and act as a stepping stone to the more general results presented later.

Numerical Solution Development

Recalling the differential equation presented in Eq (2.9) and substituting Eq (3.1) for the potential leads to

$$\sum_{\ell=\text{odd}}^{\infty} P_{\ell}(x) \frac{\partial^2 A_{\ell}(r)}{\partial r^2} + \left(\frac{2}{r} + \frac{1}{\sigma} \frac{\partial \sigma}{\partial r} \right) \sum_{\ell=\text{odd}}^{\infty} P_{\ell}(x) \frac{\partial A_{\ell}(r)}{\partial r} + \frac{1}{r^2 \sin \theta} \frac{\partial}{\partial \theta} \left(\sin \theta \sum_{\ell=\text{odd}}^{\infty} A_{\ell}(r) P_{\ell}(x) \right) = \frac{1}{\sigma} \frac{\partial J_r}{\partial r} + \frac{2}{\sigma r} J_r \quad (3.2)$$

where J_{θ} is assumed to be zero.

From Legendre's differential equation it can be shown (Ref 14:134) that

$$\frac{1}{\sin \theta} \frac{\partial}{\partial \theta} \left(\sin \theta \frac{\partial P_{\ell}(x)}{\partial \theta} \right) = -\ell(\ell+1) P_{\ell}(x) \quad (3.3)$$

Substituting this relationship into Eq (3.2) and rearranging the terms gives

$$\sum_{\ell=\text{odd}}^{\infty} P_{\ell}(x) \left[\frac{\partial^2 A_{\ell}(r)}{\partial r^2} + \left(\frac{2}{r} + \frac{1}{\sigma} \frac{\partial \sigma}{\partial r} \right) \frac{\partial A_{\ell}(r)}{\partial r} - \frac{\ell(\ell+1) A_{\ell}(r)}{r^2} \right] = \frac{1}{\sigma} \frac{\partial J_r}{\partial r} + \frac{2}{\sigma r} J_r \quad (3.4)$$

From the orthogonality of Legendre polynomials, the following is obtained (Ref 14:131)

$$\int_{-1}^{+1} P_m(x) P_n(x) dx = \begin{matrix} 0 & m \neq n \\ \frac{2}{2n+1} & m = n \end{matrix} \quad (3.5)$$

For odd or even polynomials

$$\int_0^1 P_m(x) P_n(x) dx = \frac{1}{2} \int_{-1}^{+1} P_m(x) P_n(x) dx = \begin{cases} 0 & m \neq n \\ \frac{1}{2n+1} & m = n \end{cases} \quad (3.6)$$

Therefore, the summation in Eq (3.4) can be eliminated by multiplying both sides of the differential equation by $P_m(x)$ and integrating from 0 to 1. Thus

$$\begin{aligned} \frac{\partial^2 A_\ell(r)}{\partial r^2} + \left(\frac{2}{r} + \frac{1}{\sigma} \frac{\partial \sigma}{\partial r} \right) \frac{\partial A_\ell(r)}{\partial r} - \frac{\ell(\ell+1)}{r^2} A_\ell(r) \\ = (2\ell+1) \int_0^1 P_\ell(x) \left[\frac{1}{\sigma} \frac{\partial J_r}{\partial r} + \frac{2}{\sigma r} J_r \right] dx \end{aligned} \quad (3.7)$$

The term in brackets on the right-hand side of the equation can be removed from the integral because J_r and σ do not depend on theta. Consequently, Eq (3.7) becomes

$$\begin{aligned} \frac{\partial^2 A_\ell(r)}{\partial r^2} + \left(\frac{2}{r} + \frac{1}{\sigma} \frac{\partial \sigma}{\partial r} \right) \frac{\partial A_\ell(r)}{\partial r} - \frac{\ell(\ell+1)}{r^2} A_\ell(r) \\ = (2\ell+1) \left[\frac{1}{\sigma} \frac{\partial J_r}{\partial r} + \frac{2J_r}{\sigma r} \right] \int_0^1 P_\ell(x) dx \end{aligned} \quad (3.8)$$

Note that the angular dependence which originally existed in the differential equation, Eq (2.9), has been integrated out and a series of one-dimensional equations remain. Though different from Grover's radial equations, the solution should yield the same results. Since Eq (3.8) is solved numerically, it has the added advantage of not

requiring a simplified model for the conductivity. The assumed air chemistry equations can be used.

Solution Algorithm

To solve Eq (3.8), finite differences were used. Letting $r_n = n \cdot \Delta r$ where n is the n 'th radial position where fields are to be found, all the derivatives in the equation are replaced by their equivalent central difference approximations. It can be shown (see Appendix A), after substitution of the difference operators and a rearrangement of terms, Eq (3.8) becomes

$$a_n A_{\ell, n+1} + b_{\ell, n} A_{\ell, n} + c_n A_{\ell, n-1} = R_{\ell, n} \quad (3.9)$$

where a_n , $b_{\ell, n}$, c_n , and $R_{\ell, n}$ are terms that can be determined at any range point n . Hence, for each given ℓ the equation is solved to find $A_{\ell, n}$ at all range points.

Eq (3.9) is a tri-diagonal matrix equation. The method that was used to solve it was a two-sweep algorithm sometimes known as the Thomas method. The algorithm is outlined below.

Assume that the coefficients $A_{\ell, n}$ can be written such that $A_{\ell, n+1}$ is a function of the previous coefficient $A_{\ell, n}$, i.e.

$$A_{\ell, n+1} = A_{\ell, n} \cdot e_n + f_n \quad (3.10)$$

Likewise

$$A_{\ell, n} = A_{\ell, n-1} \cdot e_{n-1} + f_{n-1} \quad (3.11)$$

Substituting Eq (3.10) into Eq (3.9) gives

$$a_n \left[A_{\ell,n} e_n + f_n \right] + b_{\ell,n} A_{\ell,n} + c_n A_{\ell,n-1} = R_{\ell,n} \quad (3.12)$$

Collecting all the terms with $A_{\ell,n}$ on the left-hand side of the equation

$$A_{\ell,n} \left[a_n e_n + b_{\ell,n} \right] = R_{\ell,n} - a_n f_n - c_n A_{\ell,n-1} \quad (3.13)$$

and dividing through by $(a_n e_n + b_{\ell,n})$ gives

$$A_{\ell,n} = \left[\frac{-c_n}{a_n e_n + b_{\ell,n}} \right] A_{\ell,n-1} + \left[\frac{R_{\ell,n} - a_n f_n}{a_n e_n + b_{\ell,n}} \right] \quad (3.14)$$

Comparing this equation with Eq (3.11) shows that

$$f_{n-1} = \frac{R_{\ell,n} - a_n f_n}{a_n e_n + b_{\ell,n}} \quad (3.15)$$

and

$$e_{n-1} = \frac{-c_n}{a_n e_n + b_{\ell,n}} \quad (3.16)$$

In the two-sweep algorithm the first sweep determines all the f_n 's and e_n 's and once these are known the second sweep gives the $A_{\ell,n}$'s for all the range points.

Once the coefficients $A_{\ell,n}$ are determined the electric field components are found by recalling that $E = -\text{grad } \phi$.

Thus

$$E_r = - \frac{\partial \phi}{\partial r} = - \sum_{\ell=\text{odd}}^{\infty} \frac{\partial A_{\ell}(r)}{\partial r} P_{\ell}(x) \quad (3.17)$$

Approximating $\frac{\partial A_\ell(r)}{\partial r}$ by its finite difference equivalent gives

$$E_{r_n} = - \sum_{\ell=\text{odd}}^{\infty} \left[\frac{A_{\ell,n+1} - A_{\ell,n-1}}{2\Delta r} \right] P_\ell(x) \quad (3.18)$$

Similarly, E_θ is found by

$$E_\theta = - \frac{\partial \phi}{\partial \theta} \frac{1}{r} = \frac{1}{r} \sum_{\ell=\text{odd}}^{\infty} A_\ell(r) P_\ell^1(x) \quad (3.19)$$

or

$$E_{\theta_n} = \frac{1}{r_n} \sum_{\ell=\text{odd}}^{\infty} A_{\ell,n} P_\ell^1(x) \quad (3.20)$$

where $P_\ell^1(x)$ is the 1'st Associated Legendre polynomial.

Once again $x = \cos(\theta)$. By symmetry the azimuthal component (E_ϕ) is zero.

Boundary Conditions

To find all the f_n 's and e_n 's in Eqs (3.15) and (3.16), boundary conditions must be applied on the fields at $r = 0$ and $r = r_N$ (N = maximum number of range points).

At $r = 0$ the electric field must be finite. Inspection of Eq (3.19) shows that this boundary condition is satisfied if

$$\phi = 0 \text{ at } r = 0 \quad (3.21)$$

Thus, from Eq (3.10)

$$A_{\ell,1} = A_{\ell,0} \cdot e_o + f_o \quad (3.22)$$

or

$$A_{\ell,1} = f_0 \quad (3.23)$$

As r increases to its maximum value it is assumed that the radial field approaches zero (actually $E_r = 0$ at $r = \infty$). From Eq (3.17) one sees that this condition is met if

$$\phi_{N+1} = \phi_N \quad (3.24)$$

Hence

$$A_{\ell,N+1} = A_{\ell,N} = A_{\ell,N} \cdot e_N + f_N \quad (3.25)$$

which requires $f_N = 0$ and $e_N = 1$.

With the boundary conditions satisfied, a complete solution is obtained.

Computer Solution

Applying the derivation and the algorithm presented above, a program was written and used to find the electric field assuming simplified sources. The results of these initial numerical calculations are presented in the next chapter.

IV. Initial Numerical Results

Using the algorithm developed in the last chapter and simplified sources, the electric fields were calculated for a specific yield/time combination. The results are discussed in this chapter and compared to Grover's analytic solution for the same problem. In addition, a comparison is made between the solution using Grover's Model (3) conductivity (Ref 2:13) and the approximate air chemistry equations presented earlier.

Field Calculations

To solve for the electric field, the source terms and air chemistry parameters must be known. The particular case investigated was a 10 megaton surface burst. The field was calculated at 10^{-3} sec (retarded time) after the burst. This example was chosen to allow a direct comparison to Grover's calculations (Ref 2:25).

The ionization rate is found from Eq (2.22), i.e.

$$S = S_0 \frac{e^{-r/\lambda}}{r^2} \left(\frac{\text{ion pairs}}{\text{m}^3 \cdot \text{sec}} \right) \quad (4.1)$$

A value of $S_0 = 1.1 \times 10^{30}$ ion-pairs/m³·sec was chosen for this problem (Ref 2:25). 320 meters was used for λ (Ref 2:20).

The radial Compton current is approximately proportional to the local ionization rate (Ref 8). Thus, J_r can be

written as

$$J_r = C \cdot S \quad (4.2)$$

where C is the constant of proportionality. The value of C used was $C = -8.2 \times 10^{-24}$. This number was based on an average of various reported values (Ref 2:20). Recalling Eq (2.11) for J_r , it can be seen that

$$J_o = C \cdot S_o \quad (4.3)$$

Hence, for the example considered here

$$J_r = -9.02 \times 10^6 \frac{e^{-r/\lambda}}{r^2} \text{ (Amps/m}^2\text{)} \quad (4.4)$$

As discussed earlier, Grover used simplified models for the conductivity instead of the approximate air chemistry equations. In the calculations presented in this work, Grover's Model (3) was used (Ref 2:13). This model was designed to provide the best fit for the conductivity. Using this model, σ is found as

$$\sigma = \sigma_o \frac{e^{-r/2\lambda}}{r^2} \text{ (mho/m)} \quad (4.5)$$

where σ is determined by a fit to the expected true form

$$\sigma = \sigma_e + \sigma_I.$$

In his calculations, Grover assumed (Ref 2:25):

$$\frac{J_o}{\sigma_o} = -63 \text{ kV/m}$$

Thus, from Eq (4.4) $\sigma_0 = 143.2$. It was found, however, that this number was inconsistent with a plot of the function shown in Grover's report (Ref 2:14). From the curve an average value of $\sigma_0 \approx 178.0$ was estimated. The discrepancy could not be explained; therefore calculations were made using both values for σ_0 .

Plots of the radial and polar electric fields that were found using the above sources and $\sigma_0 = 178.0$ are given in Appendix B. The answers agreed quite well with those found by Grover; varying only a percent or two for shorter ranges. The difference is most likely due to the uncertainty in the value of σ_0 . Calculations, also, were made using $\sigma_0 = 143.2$. These results are given in Appendix B. The fields found using this value of σ_0 were slightly larger than the ones obtained by Grover.

Comparison with Expected Conductivity

The problem encountered in the above calculations points out one of the limiting factors of the simplified conductivity models; the value of σ_0 must be determined from the expected true form of the conductivity. From Eqs (2.21) and (2.22) it was shown that

$$\sigma = e \mu_e \frac{S}{a_e} + 2e \mu_I \sqrt{\frac{S}{\gamma_I}} \quad (4.6)$$

As will be seen in the next section, the electron mobility and attachment rate are dependent on the total

electric field and water vapor content of the air. However, the ratio μ_e/α_e is not as dependent for lower water vapor contents and these parameters are often approximated by average values.

Shown in Figures 2 and 3 are plots of Grover's Model (3) conductivity (using $\sigma_0 = 178.0$ and $\sigma_0 = 143.2$) and the expected true form given by Eq (4.6). The following average values were assumed for the air chemistry parameters (Ref 2; 8; 9)

$$\begin{aligned}\mu_e &= 0.25 & (\text{m}^2/\text{V}\cdot\text{sec}) \\ \alpha_e &= 1.5 \times 10^8 & (\text{sec}^{-1}) \\ \mu_I &= 2.5 \times 10^{-4} & (\text{m}^2/\text{V}\cdot\text{sec}) \\ \gamma_I &= 2.0 \times 10^{-12} & (\text{m}^3/\text{sec})\end{aligned}$$

These values have a reported uncertainty of ± 30 to 50 percent (Ref 2).

As can be seen in both figures, the model provides a good estimate of the expected conductivity over much of the range.

Since the calculations made in this report were done numerically, Eq (4.6) could be used to find the conductivity instead of Grover's model. The results of these calculations are shown in Figures 4-7. The fields found here were slightly larger than those obtained by Grover. This might be expected since the conductivity is lower in the middle part of the range (Figures 2-3). The model appears, however,

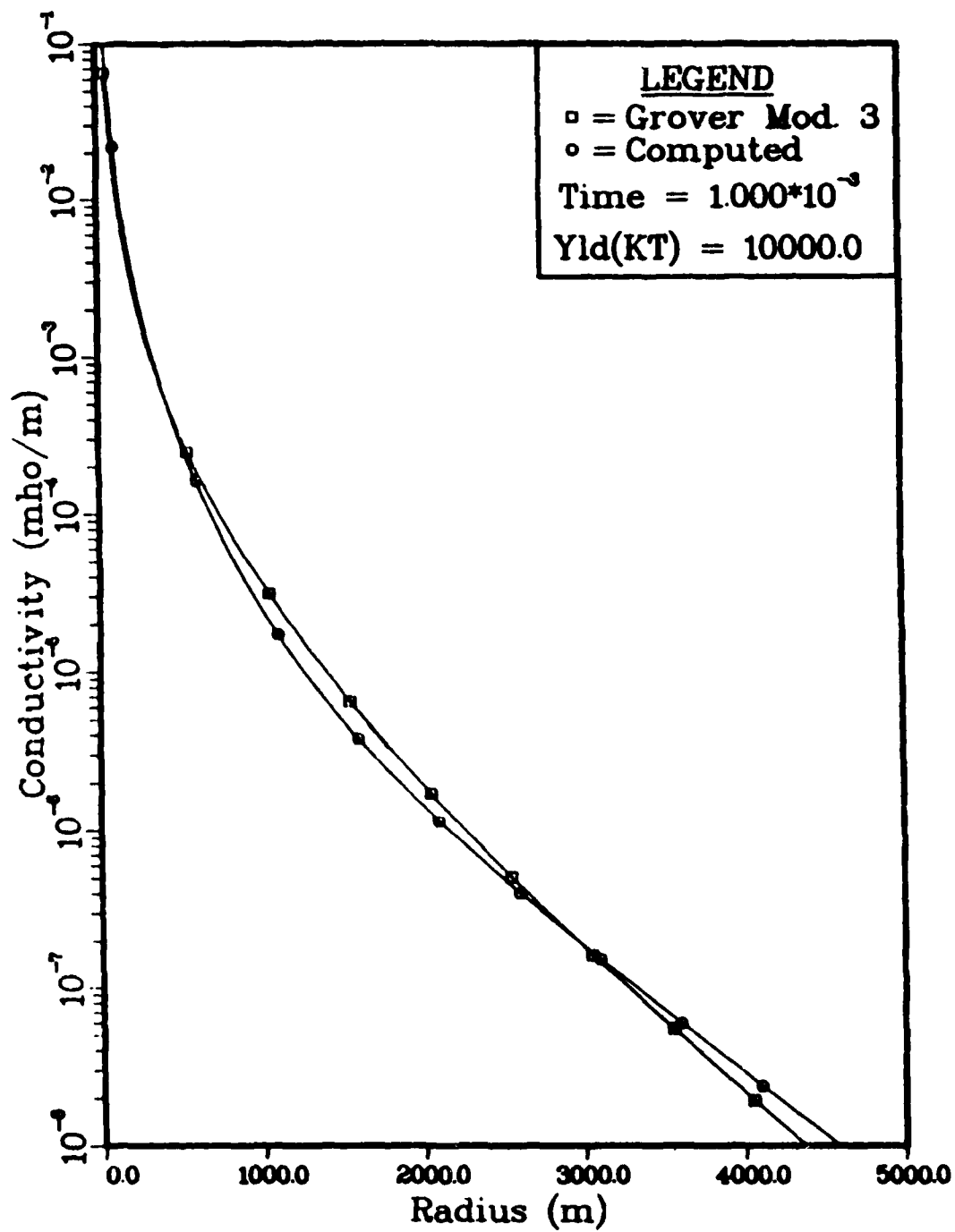


Figure 2. Expected Conductivity Compared to Grover's Model (3), $\sigma_o = 178.0$

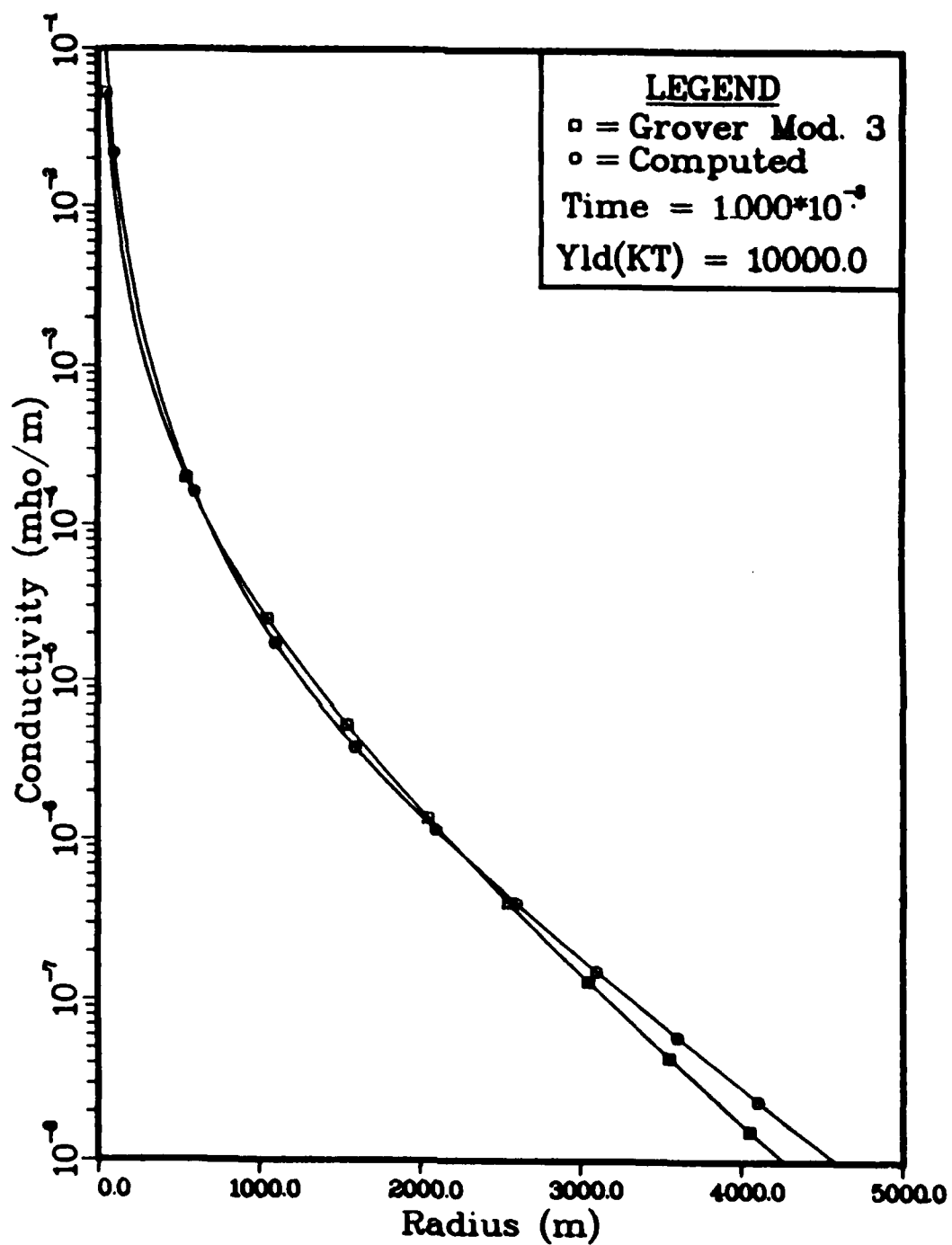


Figure 3. Expected Conductivity Compared to Grover's Model (3), $\sigma_o = 143.2$

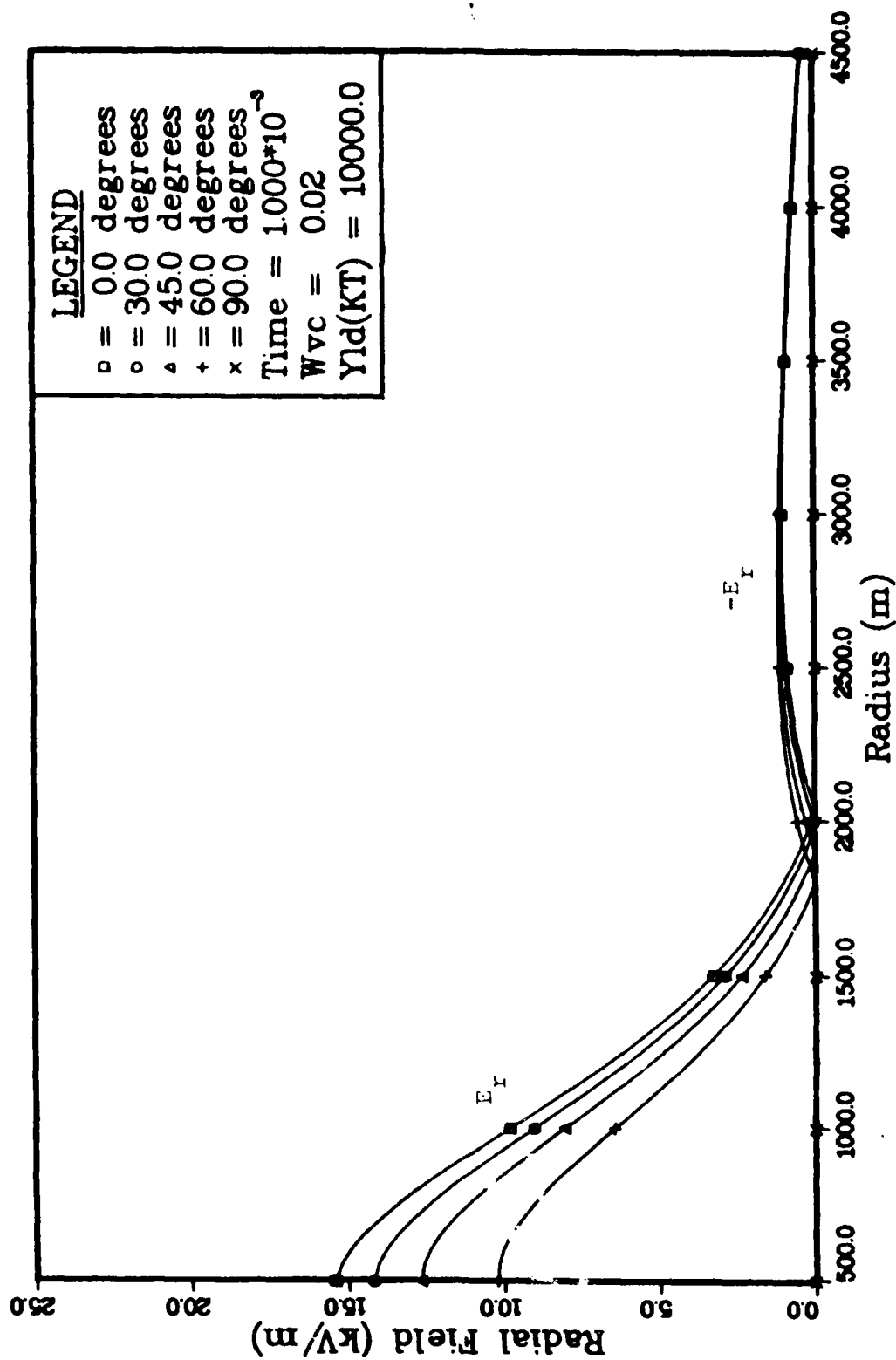


Figure 4. E_r vs Radius, Initial Solution

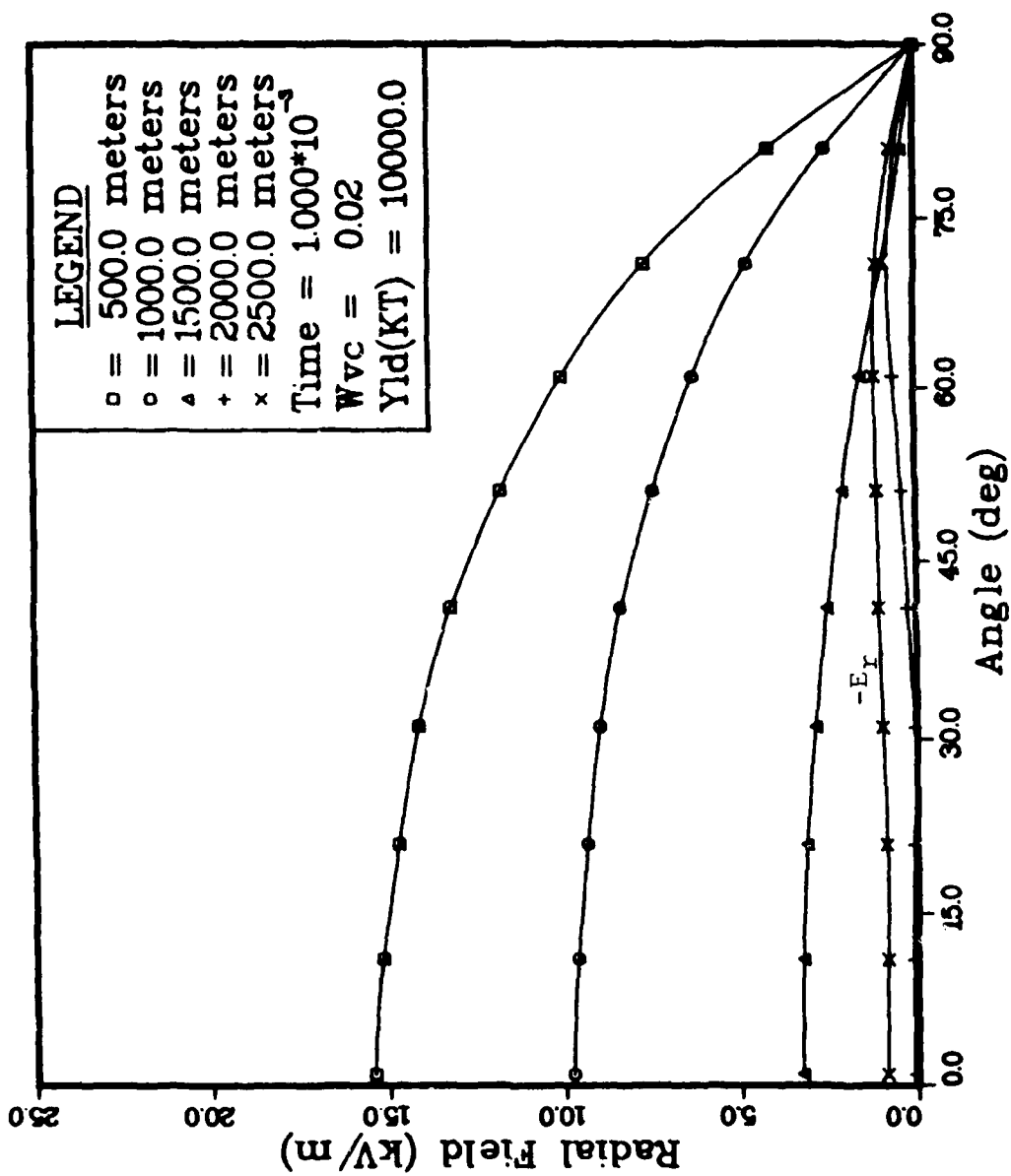


Figure 5. E_r vs Angle, Initial Solution

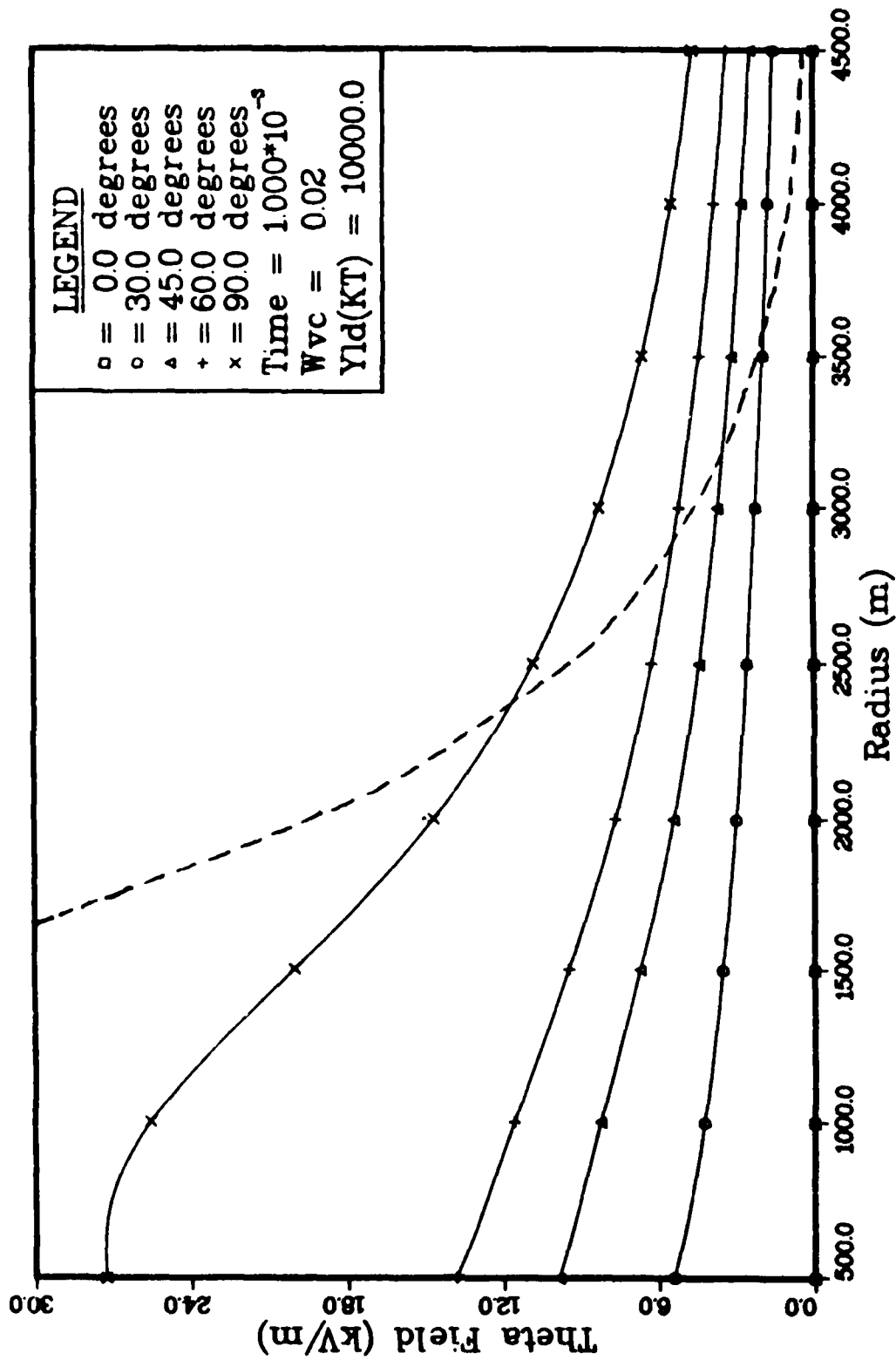


Figure 6. - E_θ vs Radius, Initial Solution
 Eq. 2.15 Shown as a Dashed Line ($\theta = 90^\circ$)

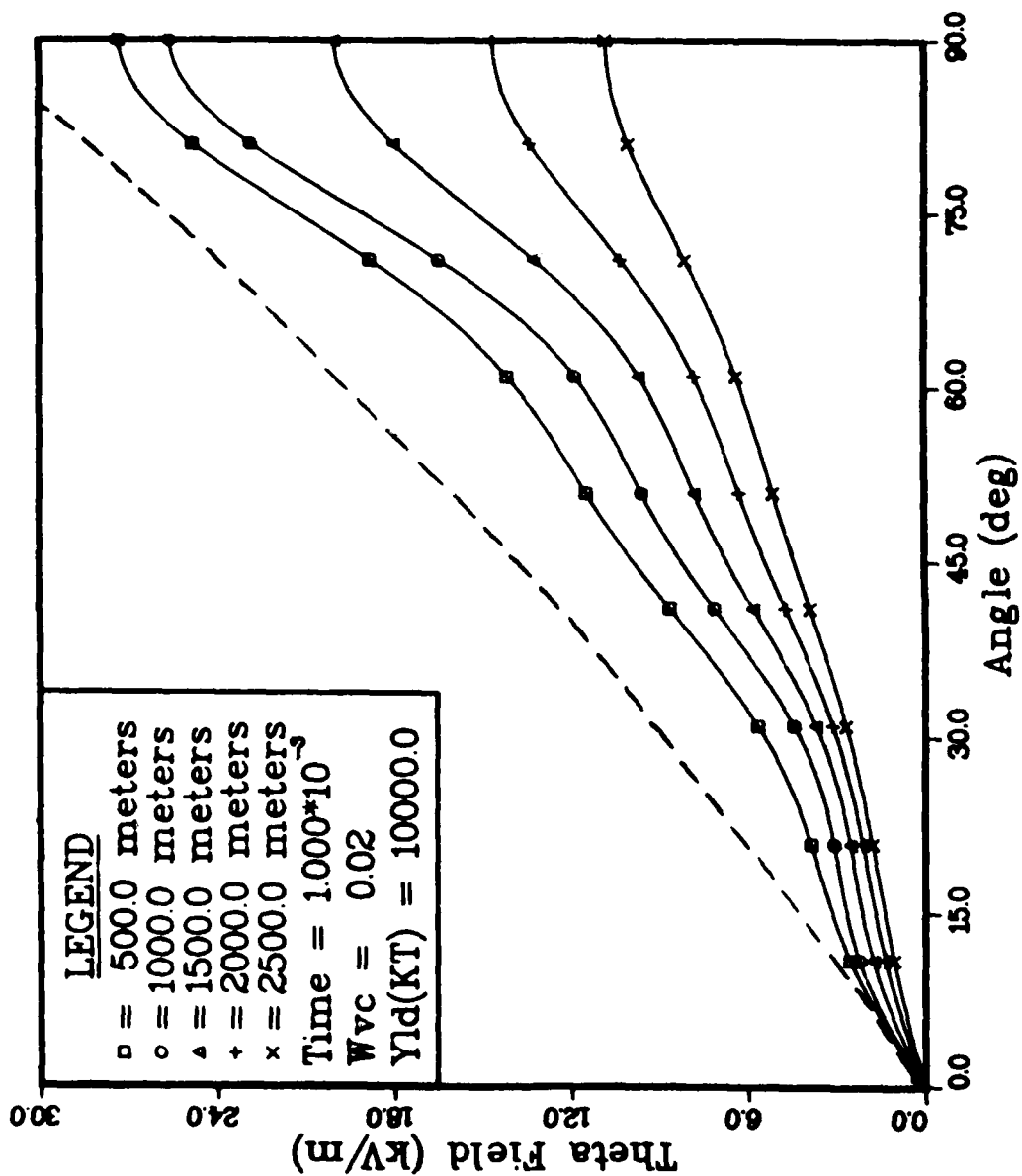


Figure 7. - E_{θ} vs Angle, Initial Solution
 Eq. 2.15 Shown as a Dashed Line ($r = 1500m$)

to predict quite well the electric fields that would be expected if the air chemistry equations were used.

Comparison with Approximate Expressions

From the work of Longmire and Wyatt, it was found that if E_r was ignored, an analytic expression, Eq (2.15), for E_θ could be derived. This approximate result is compared to the Grover-type solution in Figures 6 and 7. The major difference between the two derivations was the inclusion of E_r by Grover. He concluded (Ref 2):

"... it is found that the neglect of the radial component of the electric field is not justified when electrons contribute significantly to the air conductivity ... even in the special case where ions dominate the air conductivity, the previous approximate solutions ... are only qualitatively correct." (Ref 2:7-8)

In Figure 8 the electronic and ionic components of the conductivity from Eq (4.6) are plotted as a function of radius from the burst. It is seen that electrons do indeed dominate sigma out to approximately 1000 m; hence their effect can not be ignored.

As shown in Chapter II, E_θ was required to be \propto to $1/r$. This came from the equation for the curl of \vec{E} , i.e.

$$\frac{1}{r} \left[\frac{\partial}{\partial r} r E_\theta - \frac{\partial E_r}{\partial \theta} \right] = 0 \quad (4.7)$$

where in the previous work $\partial E_r / \partial \theta$ was assumed small, and consequently, ignored. This proved to be incorrect if electron conductivity was important and partially limited

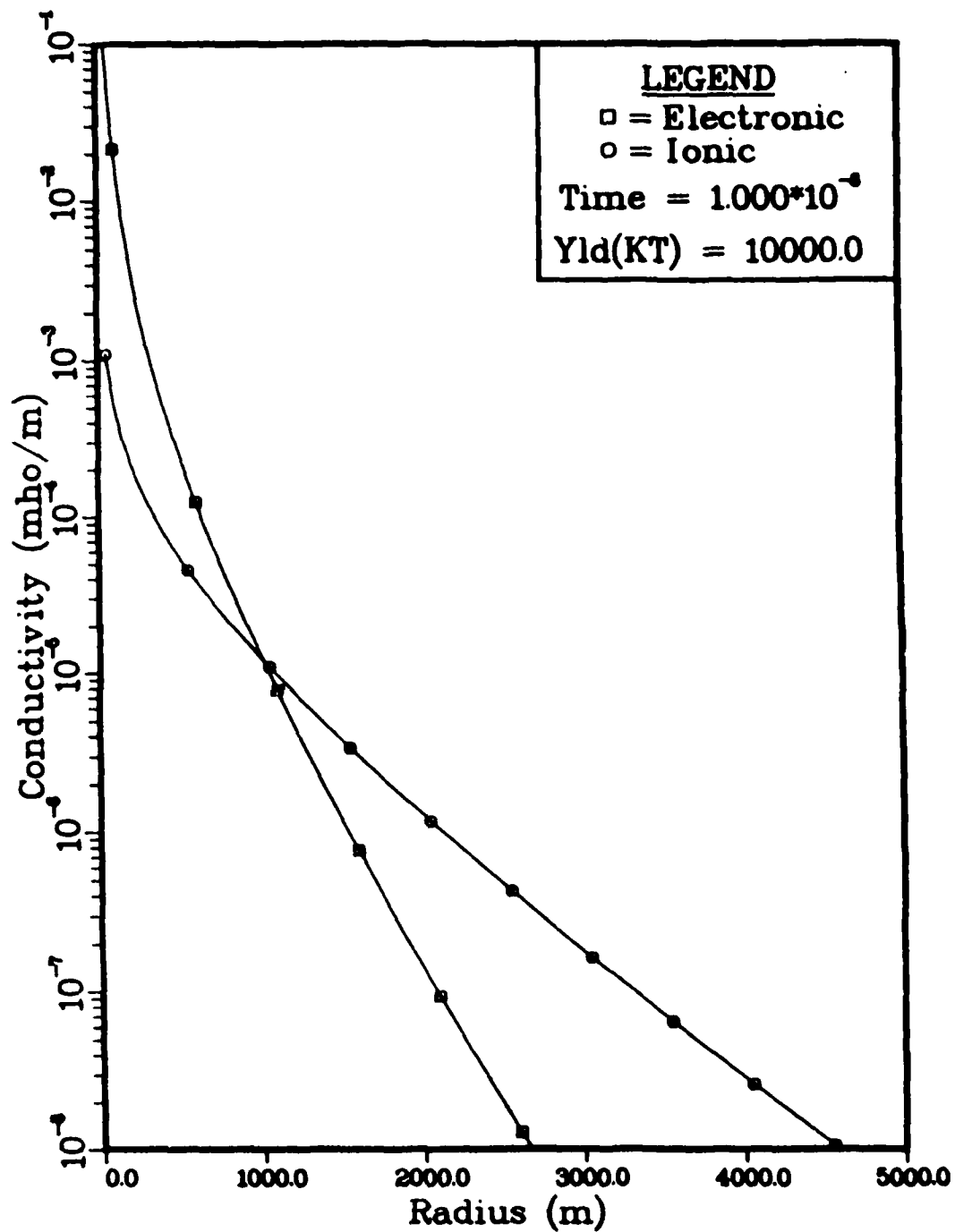


Figure 8. Electronic and Ionic Conductivity vs Radius for Initial Problem

for ion dominated conductivity. By contrast, Eq (4.7) is satisfied exactly by Grover's model. Recalling the defining equations for E_r and E_θ , Eqs (3.17) and (3.19), one sees

$$\frac{1}{r} \left[\frac{\partial}{\partial t} \left(r \frac{-1}{r} \frac{\partial \phi}{\partial \theta} \right) + \frac{\partial}{\partial \theta} \frac{\partial \phi}{\partial r} \right] = 0 \quad (4.8)$$

or

$$\frac{\partial}{\partial r} \frac{\partial}{\partial \theta} (\phi) = \frac{\partial}{\partial \theta} \frac{\partial}{\partial r} (\phi) \quad (4.9)$$

In other words the term involving E_r is the same as the one with E_θ .

Limits of Grover's Model

It appears from the above discussion that Grover's analytic model provides an improved picture of the quasi-static EMP. However, the fact that the results are analytic places some restriction on the answers. Grover points out (Ref 2:21-24) that each of the simplified conductivity models is limited by time and range values. In addition, the polar variation of the source terms and variations in the air chemistry parameters are not considered.

V. Late-Time EMP Sources and Air Chemistry Parameters

In the calculations performed by Grover and the equivalent numerical results presented in the last chapter, it was assumed that the source terms (ionization rate and Compton current) were independent of the polar angle theta and the air chemistry parameters were constant. This was an obvious requirement to obtain analytic results. Monte Carlo studies have shown, however, that the theta dependence of the source terms can be significant, especially, for ground capture sources (Refs 5 and 10). Furthermore, the electron air chemistry parameters are known to be dependent on the total electric field and, also, the water vapor content of the air.

In this chapter the late-time EMP sources are discussed. The field and water vapor dependence of the air chemistry parameters, also, are presented.

Late-Time Sources

In the late-time regime, the dominant EMP sources result from ground and air capture neutron interactions (Ref 6:13). The gamma rays released in these processes interact with the atmosphere producing ionization and the Compton current which drives the EMP.

From approximately 10^{-4} to 5×10^{-3} seconds, the major

gamma source comes from neutrons which are captured in the ground near the burst. The gammas emitted in this process are angularly dependent due to the presence of the ground. Gammas emitted normal to the surface will suffer less attenuation than those escaping horizontally. Consequently, the ionization rate and current sources resulting from this gamma flux will vary with theta. In developing curve fits for the source terms from Monte Carlo calculations, O'Dell, et al. (Ref 10) determined that the ionization rate varied by at least 2.3 between the horizontal and vertical directions. The difference was found to be even greater for larger ranges. More significant was the theta dependence of J_r . Currents pointing straight up ($\theta = 0^\circ$) were as much as 17 times larger than the currents along the ground. The variation in J_θ was not as significant. As would be expected from symmetry, J_θ approached zero for $\theta = 0^\circ$ and had its maximum value at $\theta = 90^\circ$. To model this a theta dependence of $(1 - \cos\theta)$ was used (Ref 10:38).

From about 5×10^{-3} to 10^{-1} seconds, the dominant gamma ray source will come from neutron interactions with the atmosphere. As a result, the ionization rate and Compton current are nearly independent of theta (Ref 10:22). O'Dell, et al. found a variation of 1.3 in the ionization rate and 2.3 for the radial current. J_θ was found to be much smaller than J_r and was ignored.

Shown in Figures 9, 10, and 11 are plots of the ionization rate, the radial component of the Compton current, and

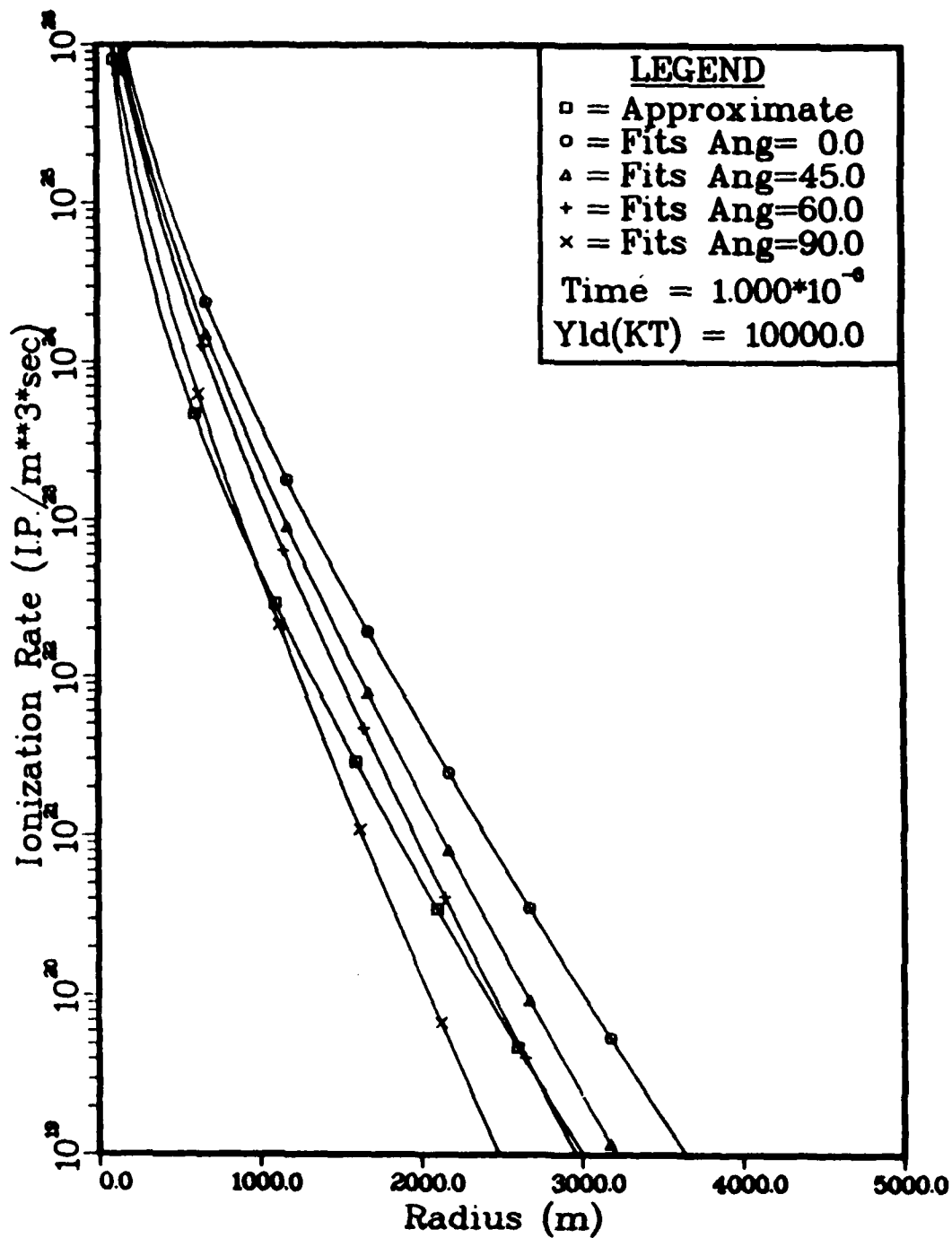


Figure 9. Ionization Rate vs Radius at Four Angles, Theta Independent Approximation (Eq 2.22) Shown for Comparison

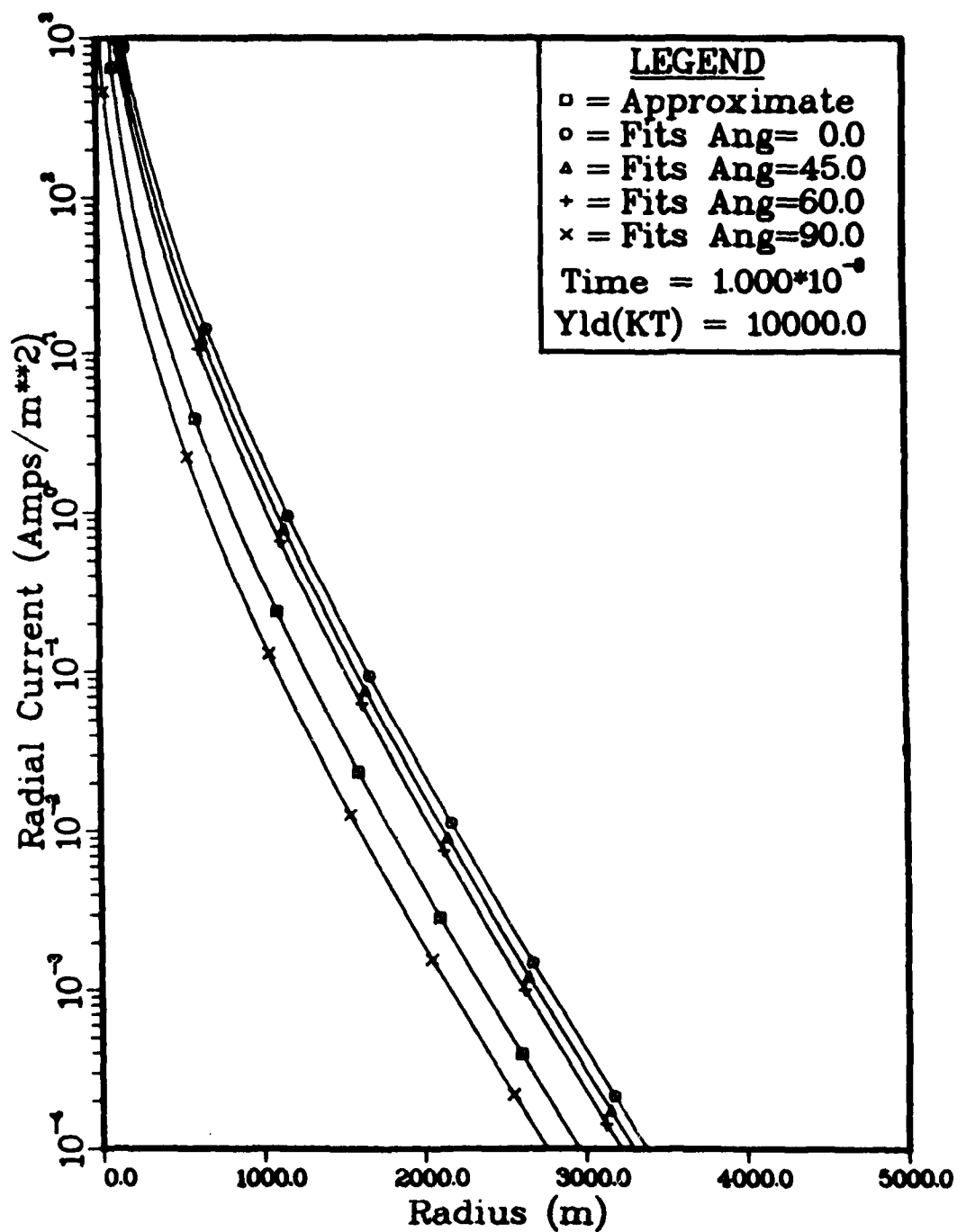


Figure 10. Radial Compton Current ($-J_r$) vs Radius at Four Angles, Theta Independent Approximation (Eq 2.11) Shown for Comparison

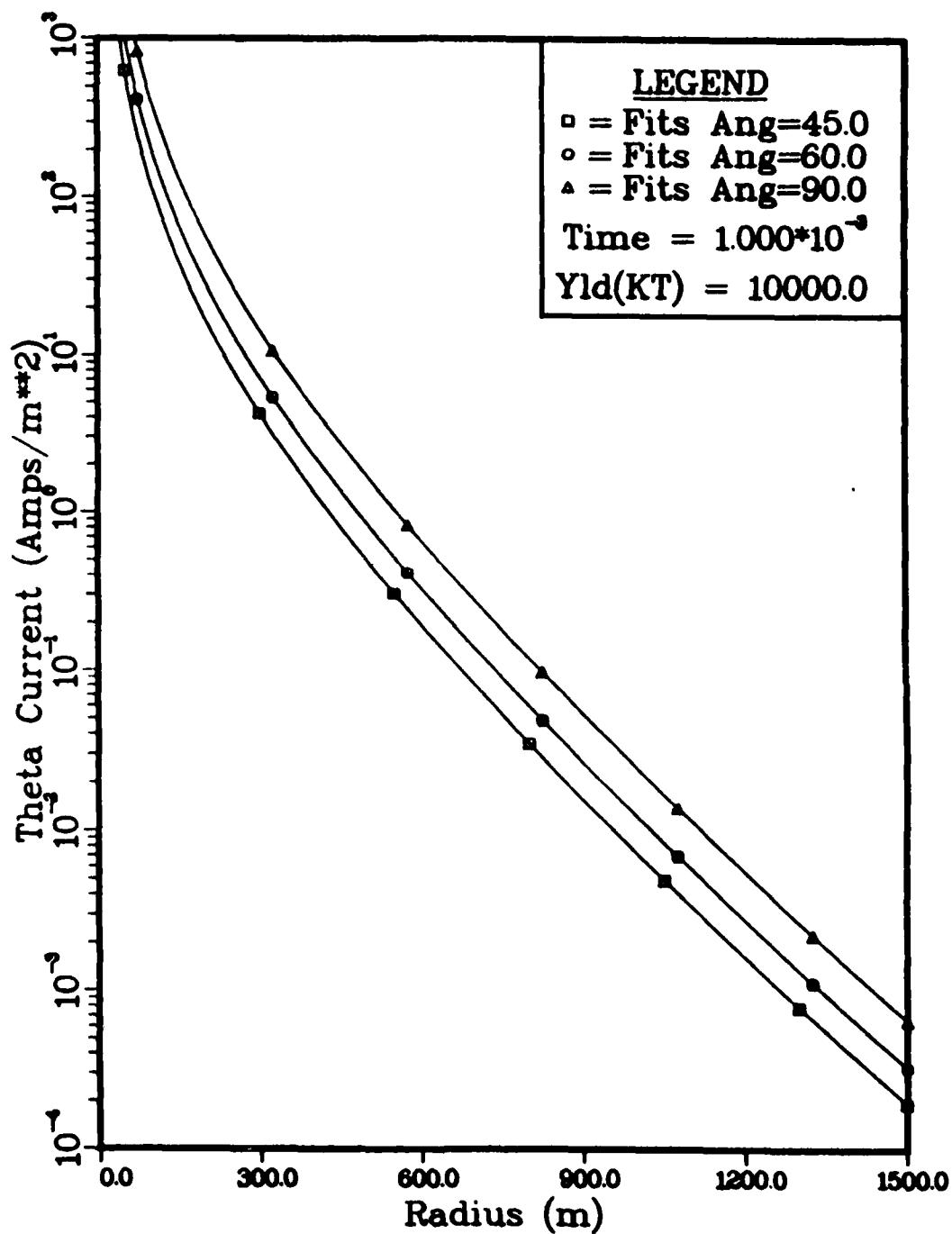


Figure 11. Theta Compton Current (J_{θ}) vs Radius at Three Angles

the polar component (J_θ) at several different angles. The plots were generated from the fits described above. The curves correspond to a time of one millisecond after a 10 megaton surface burst. For comparison, the equations used in the earlier calculations [see Eqs (2.11) and (2.22)] are plotted in Figures 9 and 10. It can be seen that for angles off the ground, the theta independent approximations underestimate the values found using the fits. In addition, the theta dependence of the ionization rate is a function of range and, as shown in Figure 9, varies substantially from the approximate result for distances of 2000 meters or more. Note that J_θ falls off very rapidly with distance and is the largest at $\theta = 90^\circ$ as expected.

Figure 12 shows the time dependence of J_r and J_θ at a particular range (1000 m). The radial component is given at $\theta = 90^\circ$ and $\theta = 0^\circ$. As discussed earlier, the polar variation of J_r reduces with time as the dominate source switches from ground to air capture gammas. J_θ is seen to fall off quite rapidly once the ground capture sources are gone. The time dependence of the ionization rate is the same as that of the radial current.

The curve fits outlined above were developed to represent a "typical" thermonuclear weapon. They were biased toward ranges of 2 kilometers or less partly because of statistical uncertainties in the Monte Carlo data at greater ranges. Also, this is the range of interest in most EMP calculations. In addition, self-consistent effects between

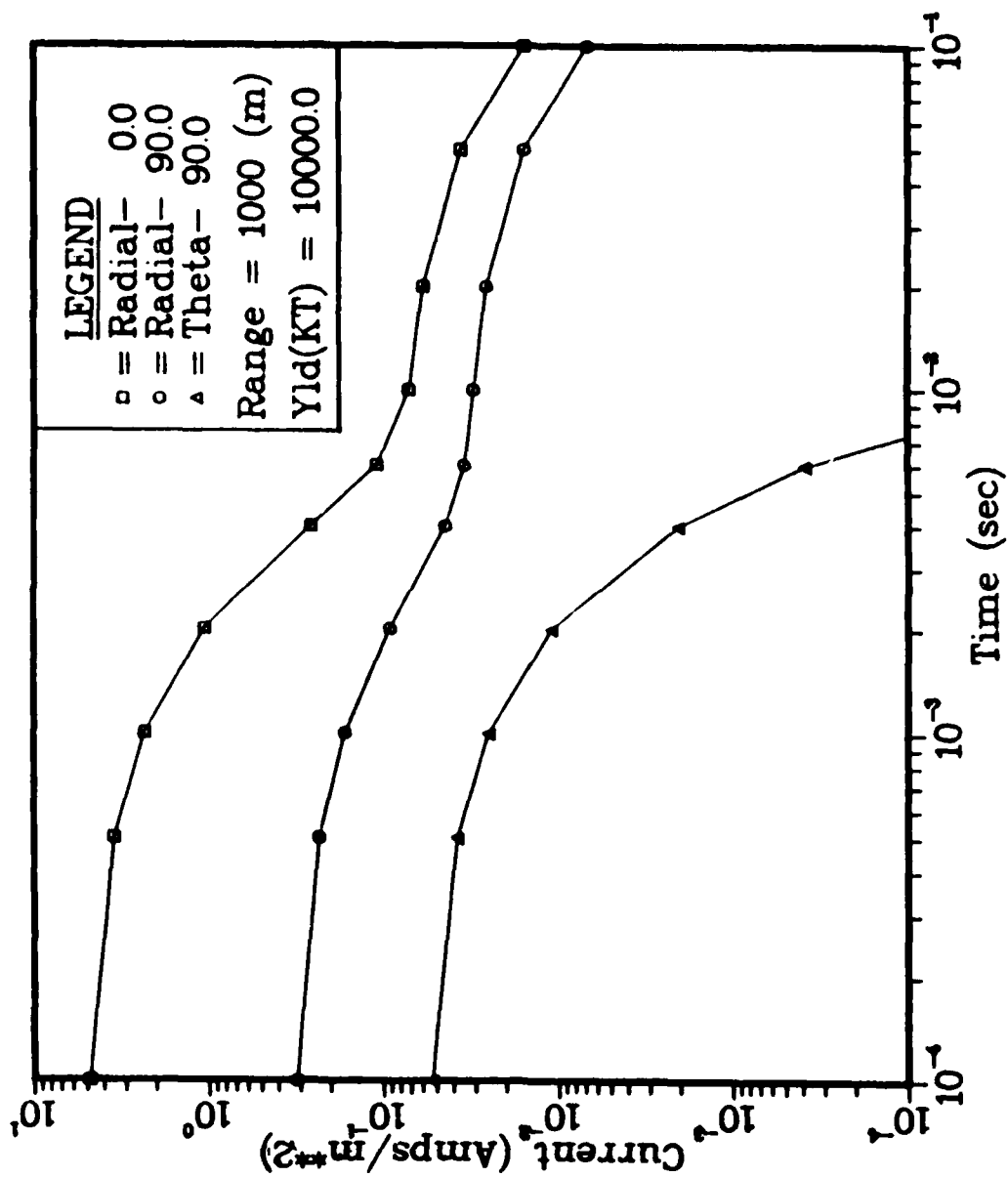


Figure 12. $-J_r$ and J_θ vs Time

the fields and currents were not included. Although this can be important, the approximation is probably not bad at late times (Ref 10:36). The exact form of the fits and the numbers used to generate Figures 9-12 is given in Appendix C.

Air Chemistry Parameters

To obtain analytic solutions, the air chemistry parameters used to determine the conductivity were assumed to be constant. If ions dominate the conductivity, this is a good approximation. As was demonstrated earlier, however, electrons outnumber the ions at shorter ranges. As will be seen below, the electron mobility and attachment rate are dependent on the electric field and water vapor content of the air. Thus for points close to the burst, the calculation of sigma is complicated by these variations.

This problem has been investigated by several authors. In general, the variations in μ_e and α_e have been modeled by curve fits to the available experimental data. Many EMP codes employ the analytic expressions developed by Longley and Longmire (Ref 7). Shown in Figure 13 is the fit for the electron attachment rate as a function of the total field for various water vapor contents. The electron mobility is plotted in Figure 14. The curves are given for sea level air pressure and normal density.

Recently, a question has been raised as to the accuracy of the data from which Longley's fits were derived. Based

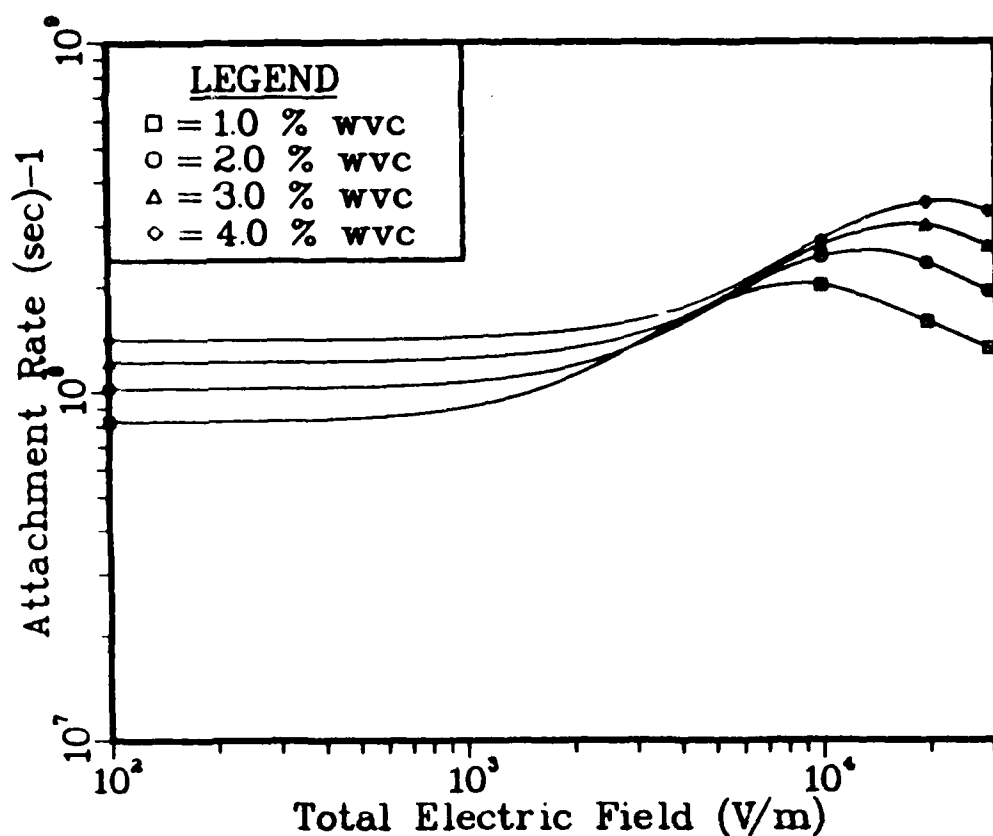


Figure 13. Attachment Rate vs Total Electric Field

on a newer set of experimental data, Pettus and Crevier (Ref 11) developed different equations for the mobility and attachment rate. These fits are slightly more complicated and are not presented here; however, Smith and Radasky (Ref 13) showed an equation which demonstrated the effect of the new data on the electron mobility. The equation (Ref 13:30) limits the maximum allowable mobility such that

$$\mu_{e_{\max}} = \frac{1.5}{(1.0 + 96.77 (w)^{0.789})} \text{ (m}^2\text{/V}\cdot\text{sec)} \quad (5.1)$$

where w is the fraction of water vapor present. This modification is shown in Figure 14 for the one percent case.

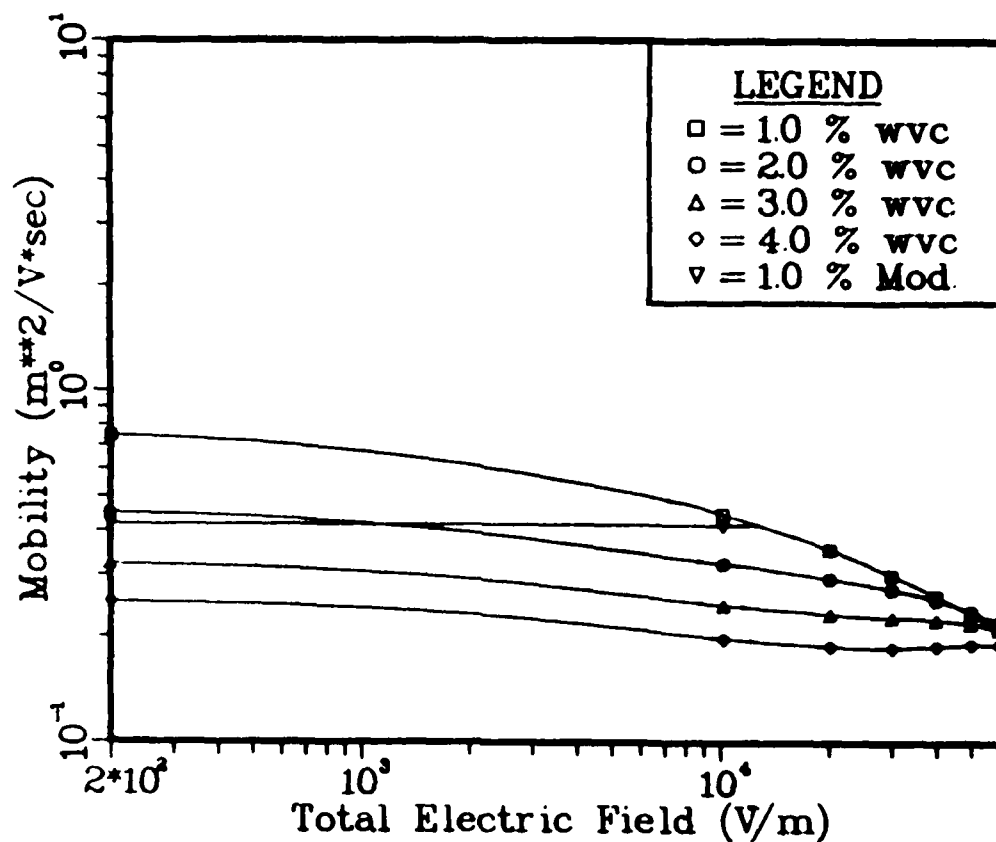


Figure 14. Mobility vs Total Electric Field

It is obvious that these two parameters are not accurately known. The debate has gone on for a number of years and most likely will continue. Overall, the expressions discussed above are felt to be reasonable (Ref 3). Moreover, using them allows variations in the field and the water vapor content to be considered. The exact form of Longley and Longmire's equations is given in Appendix C.

VI. An Improved Numerical Method

As seen in the previous chapter, the ionization rate and Compton current sources are angularly dependent due to the presence of the ground. Furthermore, it was shown that the electron mobility and attachment rate vary with the electric field and the water vapor content of the air. These variations could not be included in the analytic expressions of Longmire, Hill, and Wyatt or in Grover's model. A logical extension to the work of the above-mentioned authors would be to develop a solution to Maxwell's equations which could incorporate the variations in sources and air chemistry parameters.

In this chapter a numerical solution will be presented which allows the angular, the field, and the water vapor dependencies to be included.

Solution Development

As shown earlier (Chapter II), the electric field in the quasi-static phase is derivable from a scalar potential ϕ . Applying this definition to Maxwell's equations resulted in the following differential equation:

$$\begin{aligned} -\frac{1}{r^2} \frac{\partial}{\partial r} (r^2 E_r) - \frac{1}{r \sin \theta} \frac{\partial}{\partial \theta} (\sin \theta E_\theta) - \frac{1}{\sigma} \frac{\partial \sigma}{\partial r} E_r \\ - \frac{1}{\sigma r} \frac{\partial \sigma}{\partial \theta} E_\theta = \frac{1}{\sigma r^2} \frac{\partial}{\partial r} (r^2 J_r) + \frac{1}{r \sin \theta} \frac{\partial}{\partial \theta} (\sin \theta J_\theta) \end{aligned} \quad (6.1)$$

In the previous solutions to this equation, J_r and σ were assumed to be independent of theta and J_θ was set equal to zero (except by Wyatt). Longmire and Wyatt, also, assumed that E_r was small and ignored it. Grover included E_r but this required an approximate model for the conductivity. These restrictions will now be relaxed.

Recalling Eq (3.1) for $\phi(r, \theta)$

$$\phi(r, \theta) = \sum_{\ell=\text{odd}}^{\infty} A_\ell(r) P_\ell(x) \quad (6.2)$$

Let Σ mean $\sum_{\ell=\text{odd}}^{\infty}$. Substituting Eq (6.2) into Eq (6.1) gives

$$\begin{aligned} & \frac{1}{r^2} \frac{\partial}{\partial r} \left(r^2 \frac{\partial}{\partial r} (\Sigma A_\ell(r) P_\ell(x)) \right) + \frac{1}{r^2 \sin \theta} \frac{\partial}{\partial \theta} \left(\sin \theta \frac{\partial}{\partial \theta} (\Sigma A_\ell(r) P_\ell(x)) \right) \\ & + \frac{1}{\sigma} \frac{\partial \sigma}{\partial r} \frac{\partial}{\partial r} (\Sigma A_\ell(r) P_\ell(x)) + \frac{1}{\sigma r^2} \frac{\partial \sigma}{\partial \theta} \frac{\partial}{\partial \theta} (\Sigma A_\ell(r) P_\ell(x)) \\ & = \frac{1}{\sigma r^2} \frac{\partial}{\partial r} (r^2 J_r) + \frac{1}{\sigma r \sin \theta} \frac{\partial}{\partial \theta} (\sin \theta J_\theta) \end{aligned} \quad (6.3)$$

or after expansion and the use of Eq (3.3)

$$\begin{aligned} & \Sigma P_\ell(x) \left[\frac{2}{r} \frac{\partial}{\partial r} A_\ell(r) + \frac{\partial^2 A_\ell(r)}{\partial r^2} - \ell(\ell+1) \frac{A_\ell(r)}{r^2} \right] \\ & + \Sigma \frac{1}{\sigma} \frac{\partial \sigma}{\partial r} \frac{\partial A_\ell(r)}{\partial r} P_\ell(x) - \Sigma \frac{1}{\sigma r^2} \frac{\partial \sigma}{\partial \theta} A_\ell(r) P_\ell^1(x) \\ & = \frac{1}{\sigma} \left[\frac{2J_r}{r} + \frac{\partial J_r}{\partial r} + \frac{1}{r \sin \theta} \frac{\partial}{\partial \theta} (\sin \theta J_\theta) \right] \end{aligned} \quad (6.4)$$

where $P_\ell^1(x)$ is the ℓ 'st Associated Legendre polynomial as before.

Multiplying both sides of Eq (6.4) by $P_m(x)$ and integrating from 0 to 1 gives

$$\begin{aligned} & \Sigma \left[\frac{2}{r} \frac{\partial A_\ell(r)}{\partial r} + \frac{\partial^2 A_\ell(r)}{\partial r^2} - \ell(\ell+1) \frac{A_\ell(r)}{r^2} \right] \int_0^1 P_\ell(x) P_m(x) dx \\ & + \Sigma \int_0^1 \frac{1}{\sigma} \frac{\partial \sigma}{\partial r} \frac{\partial A_\ell(r)}{\partial r} P_\ell(x) P_m(x) dx - \Sigma \int_0^1 \frac{1}{\sigma r^2} \frac{\partial \sigma}{\partial \theta} A_\ell(r) P_\ell^1(x) P_m(x) dx \\ & = \int_0^1 \frac{1}{\sigma} \left[\frac{2J_r}{r} + \frac{\partial J_r}{\partial r} + \frac{1}{r \sin \theta} \frac{\partial}{\partial \theta} (\sin \theta J_\theta) \right] P_m(x) dx \quad (6.5) \end{aligned}$$

Let

$$IA_{\ell,m} = \int_0^1 \frac{1}{\sigma} \frac{\partial \sigma}{\partial r} P_\ell(x) P_m(x) dx \quad (6.6)$$

$$IB_{\ell,m} = \int_0^1 \frac{1}{\sigma} \frac{\partial \sigma}{\partial \theta} P_\ell^1(x) P_m(x) dx \quad (6.7)$$

$$IC_m = \int_0^1 \frac{1}{\sigma} \left[\frac{2J_r}{r} + \frac{\partial J_r}{\partial r} + \frac{1}{r \sin \theta} \frac{\partial}{\partial \theta} (\sin \theta J_\theta) \right] P_m(x) dx \quad (6.8)$$

From the relationship given in Eq (3.6), it is seen that the summation in the first term of Eq (6.5) reduces to

$$\left[\frac{2}{r} \frac{\partial}{\partial r} A_m(r) + \frac{\partial^2}{\partial r^2} A_m(r) - m(m+1) \frac{A_m(r)}{r^2} \right] \frac{1}{2m+1} \quad (6.9)$$

Using this and the defining Eqs (6.6), (6.7), and (6.8), Eq (6.5) becomes

$$\left[\frac{2}{r} \frac{\partial}{\partial r} A_m(r) + \frac{\partial^2}{\partial r^2} A_m(r) - m(m+1) \frac{A_m(r)}{r^2} \right] \frac{1}{2m+1} + \sum \frac{\partial A_\ell(r)}{\partial r} IA_{\ell,m} - \sum \frac{A_\ell(r)}{r^2} IB_{\ell,m} = IC_m \quad (6.10)$$

Removing the terms in the summations where $m = \ell$ and moving the rest to the right-hand side of the equation gives

$$\left[\frac{2}{r} \frac{\partial}{\partial r} A_m(r) + \frac{\partial^2}{\partial r^2} A_m(r) - m(m+1) \frac{A_m(r)}{r^2} \right] \frac{1}{2m+1} + \frac{\partial A_m(r)}{\partial r} IA_{m,m} - \frac{A_m(r)}{r^2} IB_{m,m} = IC_m - \sum_{\substack{\ell=\text{odd} \\ \ell \neq m}}^{\infty} \frac{\partial A_\ell(r)}{\partial r} IA_{\ell,m} + \sum_{\substack{\ell=\text{odd} \\ \ell \neq m}}^{\infty} \frac{A_\ell(r)}{r^2} IB_{\ell,m} \quad (6.11)$$

At this point all derivatives are replaced by their finite difference approximations. A given function $f(x)$ is replaced by

$$f(x) = f(x_n) = f_n \quad (6.12)$$

where n is the n 'th point where $f(x)$ is being determined, i.e. $x_n = n \cdot \Delta x$. Likewise

$$\frac{df(x)}{dx} \approx \frac{f_{n+1} - f_{n-1}}{2\Delta x} \quad (6.13)$$

and

$$\frac{d^2 f(x)}{dx^2} \approx \frac{f_{n+1} - 2f_n + f_{n-1}}{\Delta x^2} \quad (6.14)$$

Applying these relationships to Eqs (6.6) and (6.7) leads to

$$IA_{\ell, m}^n = \int_0^1 \frac{1}{\sigma_n^P} \frac{\sigma_{n+1}^P - \sigma_{n-1}^P}{2\Delta r} P_{\ell}(x) P_m(x) dx \quad (6.15)$$

$$IB_{\ell, m}^n = \int_0^1 \frac{1}{\sigma_n^P} \frac{\sigma_n^{P+1} - \sigma_n^{P-1}}{2\Delta \theta} P_{\ell}^1(x) P_m(x) dx \quad (6.16)$$

where σ_n^P is the value of the conductivity at the n'th radial point and the p'th angle theta.

From the fits for J_{θ} (see Appendix C) it was shown that

$$J_{\theta} = C \cdot (1 - \cos \theta) \quad (6.17)$$

where C is a function of radius and time; hence

$$\frac{\partial J_{\theta}}{\partial \theta} = C \cdot \sin \theta \quad (6.18)$$

Using this result, Eq (6.8) becomes

$$IC_m^n = \int_0^1 \frac{1}{\sigma_n^P} \left[\frac{2J_r^n}{r_n} + \frac{J_r^{n+1} - J_r^{n-1}}{2\Delta r} + \frac{C_n}{r_n} \left[\frac{1 - \cos \theta}{\tan \theta} + \sin \theta \right] \right] P_m(x) dx \quad (6.19)$$

where $r_n = n \cdot \Delta r$ and J_r^n is the radial Compton current at a given range point n.

Finally Eq (6.11) becomes

$$\begin{aligned}
& \left[\frac{2}{r_n} \frac{\Lambda_m^{n+1} - \Lambda_m^{n-1}}{2\Delta r} + \frac{\Lambda_m^{n+1} - 2\Lambda_m^n + \Lambda_m^{n-1}}{\Delta r^2} - m(m+1) \frac{\Lambda_m^n}{r_n^2} \right] \frac{1}{2m+1} \\
& + \frac{\Lambda_m^{n+1} - \Lambda_m^{n-1}}{2\Delta r} IA_{m,m}^n - \frac{\Lambda_m^n}{r_n^2} IB_{m,m}^n = IC_m^n \\
& - \sum_{\substack{\ell=\text{odd} \\ \ell \neq m}}^{\infty} \frac{\Lambda_\ell^{n+1} - \Lambda_\ell^{n-1}}{2\Delta r} IA_{\ell,m}^n + \sum_{\substack{\ell=\text{odd} \\ \ell \neq m}}^{\infty} \frac{\Lambda_\ell^n}{r_n^2} IB_{\ell,m}^n \quad (6.20)
\end{aligned}$$

or after rearrangement

$$\begin{aligned}
& \left[\frac{1}{2m+1} \left(\frac{1}{\Delta r^2} + \frac{1}{r_n \Delta r} \right) + \frac{IA_{m,m}^n}{2\Delta r} \right] \Lambda_m^{n+1} \\
& - \left[\frac{1}{2m+1} \left(\frac{2}{\Delta r^2} + m(m+1) \frac{1}{r_n^2} \right) + \frac{IB_{m,m}^n}{r_n^2} \right] \Lambda_m^n \\
& + \left[\frac{1}{2m+1} \left(\frac{1}{\Delta r^2} - \frac{1}{r_n \Delta r} \right) - \frac{IA_{m,m}^n}{2\Delta r} \right] \Lambda_m^{n-1} = IC_m^n \\
& - \sum_{\substack{\ell=\text{odd} \\ \ell \neq m}}^{\infty} \frac{\Lambda_\ell^{n+1} - \Lambda_\ell^{n-1}}{2\Delta r} IA_{\ell,m}^n + \sum_{\substack{\ell=\text{odd} \\ \ell \neq m}}^{\infty} \frac{\Lambda_\ell^n}{r_n^2} IB_{\ell,m}^n \quad (6.21)
\end{aligned}$$

Comparison of this equation with Eq (3.9) reveals that the complex derivation above has resulted in an equation whose form is similar to the earlier result: namely,

$$a_{m,n} \Lambda_m^{n+1} + b_{m,n} \Lambda_m^n + c_{m,n} \Lambda_m^{n-1} = R_{\ell,m}^n \quad (6.22)$$

where now

$$a_{m,n} = \left[\frac{1}{2m+1} \left(\frac{1}{\Delta r^2} + \frac{1}{r_n \Delta r} \right) + \frac{IA_{m,m}^n}{2\Delta r} \right] \quad (6.23)$$

$$b_{m,n} = - \left[\frac{1}{2m+1} \left(\frac{2}{\Delta r^2} + \frac{m(m+1)}{r_n^2} \right) + \frac{IB_{m,m}^n}{r_n^2} \right] \quad (6.24)$$

$$c_{m,n} = \left[\frac{1}{2m+1} \left(\frac{1}{\Delta r^2} - \frac{1}{\Delta r r_n} \right) - \frac{IA_{m,m}^n}{2\Delta r} \right] \quad (6.25)$$

and

$$\begin{aligned} R_{\ell,m}^n = & IC_m^n - \sum_{\substack{\ell=\text{odd} \\ \ell \neq m}}^{\infty} \frac{A_{\ell}^{n+1} - A_{\ell}^{n-1}}{2\Delta r} IA_{\ell,m} \\ & + \sum_{\substack{\ell=\text{odd} \\ \ell \neq m}}^{\infty} \frac{A_{\ell}^n}{r_n^2} IB_{\ell,m}^n \end{aligned} \quad (6.26)$$

Consequently, the same algorithm that was presented earlier can be used to determine the coefficients A_m^n .

The solution, however, is complicated by a number of factors. In the previous calculations, the coefficients $a_{m,n}$, $b_{m,n}$, $c_{m,n}$ and the right-hand term $R_{\ell,m}^n$ could easily be computed. This is no longer the case. Since the conductivity and Compton current are allowed to vary with theta the integrals in Eqs (6.15), (6.16), and (6.19) are much more complicated and must be evaluated numerically. Moreover, the term $R_{\ell,m}^n$ includes summations which involve the

Legendre polynomial coefficients that are being solved for. Finally, the calculation of sigma is complicated by the field dependence of the electron mobility and attachment rate.

Solution Technique

To solve Eq (6.22), an iterative scheme was used. An initial guess for the field was obtained by ignoring the summation terms on the right-hand side of the equation and using average, field independent, values for μ_e and α_e . Using this first guess as the input, the equation was solved again but the summations were included and the electron parameters were allowed to vary. The new value for the total field obtained here was then compared to the old value at all range points and at one angle. This scheme was continued until the difference between consecutive iterations was less than a specified tolerance at all the range points. It was assumed that convergence along one angle guaranteed convergence everywhere.

The numerical integrals were computed using Romberg integration (Ref 1:206-211). This method is discussed in Appendix D.

The results of calculations made using the algorithm described above are presented in the next chapter.

VII. Results

Applying the algorithm developed in the last chapter, the quasi-static electric fields were computed. The analytic fits for the source terms and the equations for the air chemistry parameters presented in Chapter V were used in the calculations. The results are presented in this chapter along with a comparison to the earlier calculations given in Chapter IV. The effects of some of the physical parameters, also, are discussed.

Test Problem

Using the same yield (10 Mt) and time after the burst (10^{-3} sec), the radial and polar components of the electric field were calculated. The radial field, E_r , is plotted as a function of radius in Figure 15 and polar angle in Figure 16. It is seen from Figure 15 that a sizeable radial field was found for points close to the burst. Note that the field becomes negative at approximately 2000 meters. This occurs when the return current becomes larger than the source current. The polar (theta) field is given in Figures 17 and 18. A peak field of about 45 kV/m was obtained at approximately 1200 meters for $\theta = 90^\circ$.

The difference between these results and the earlier calculations was significant. Shown in Figures 15 and 17 are the peak radial, $E_r(0^\circ)$, (dashed line) and theta, E_θ

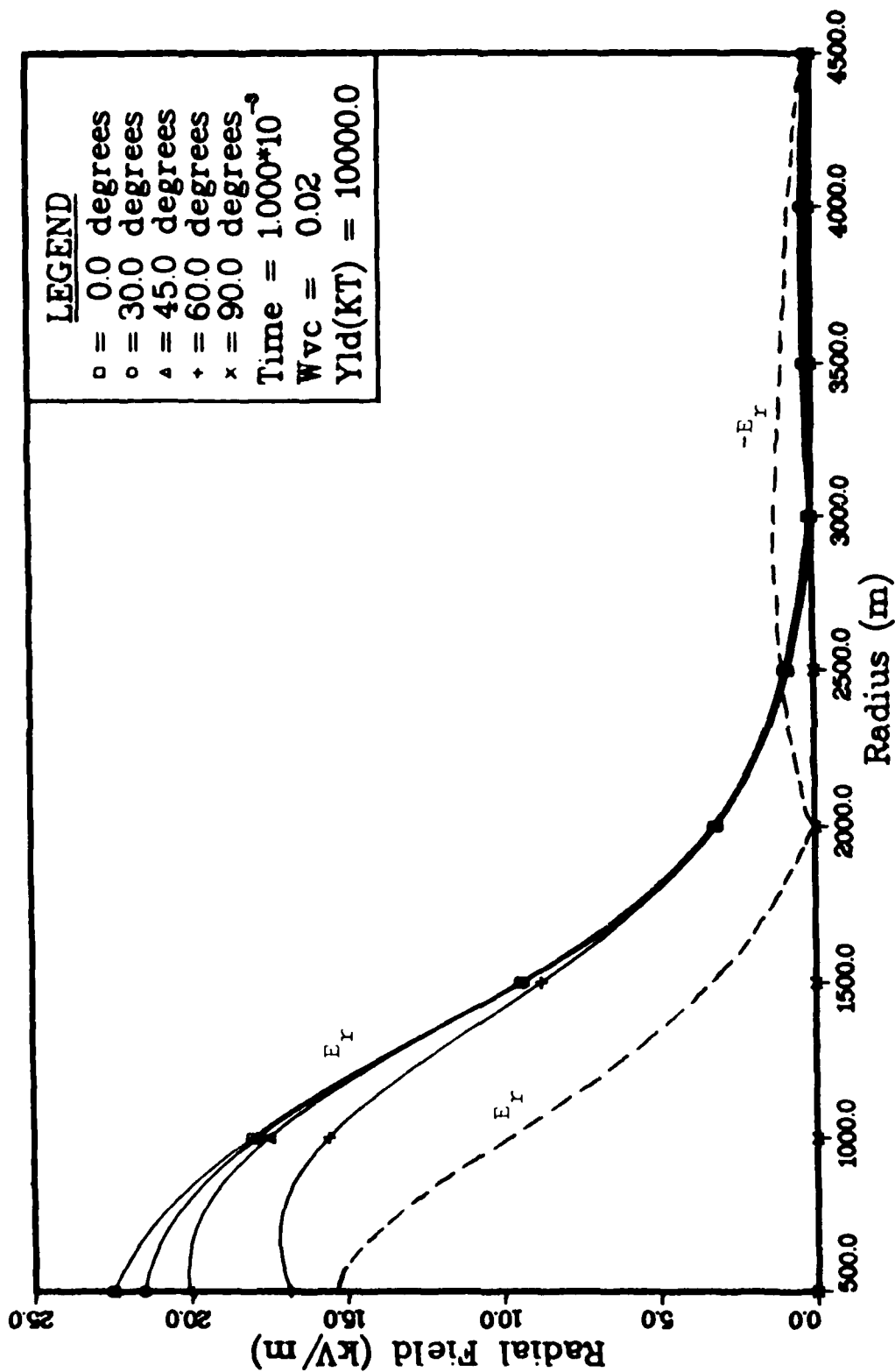


Figure 15. E_r vs Radius, Full Solution
 Initial Solution (Dashed Line, $\theta=0^\circ$) Also Shown

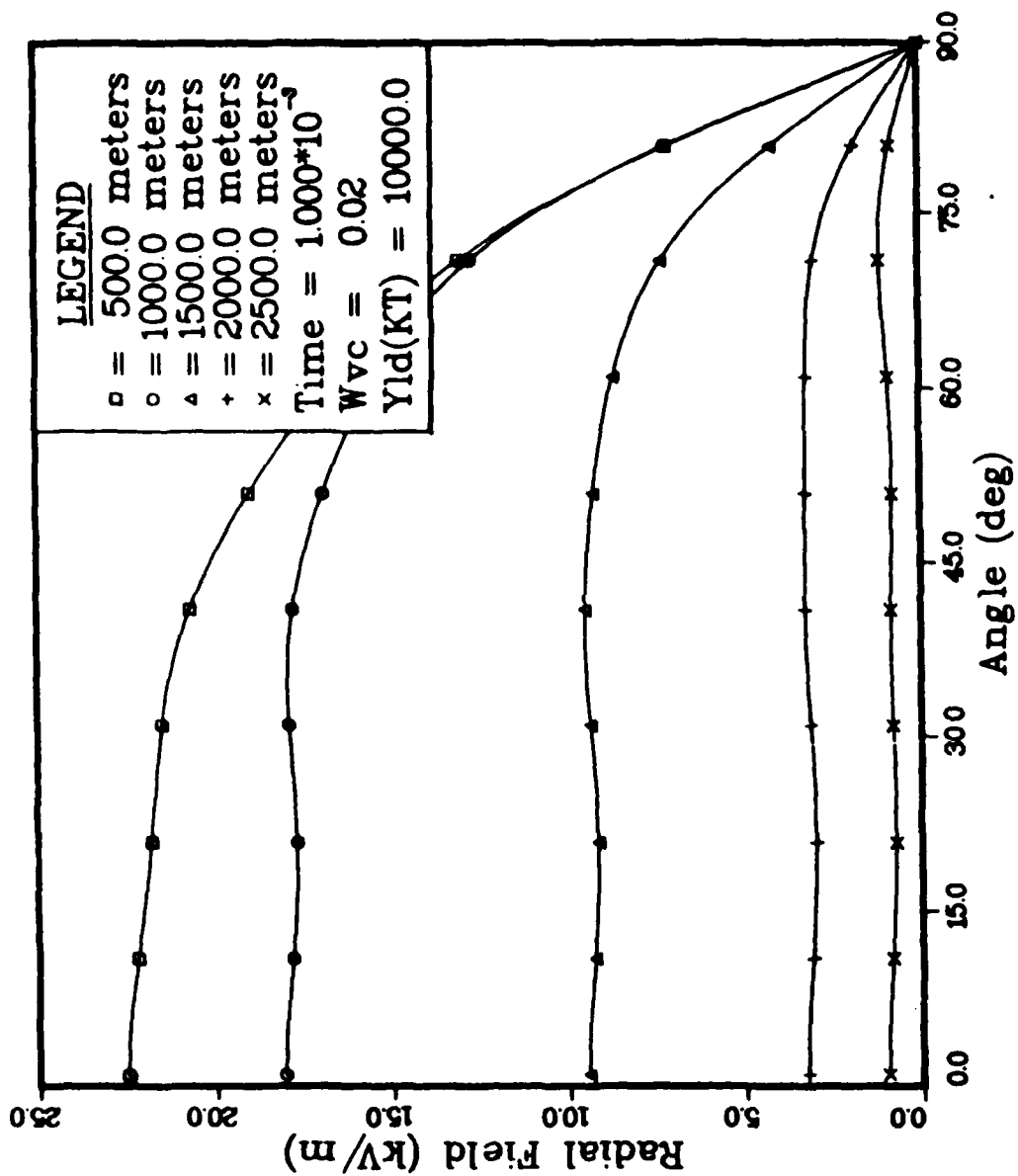


Figure 16. E_r vs Angle, Full Solution

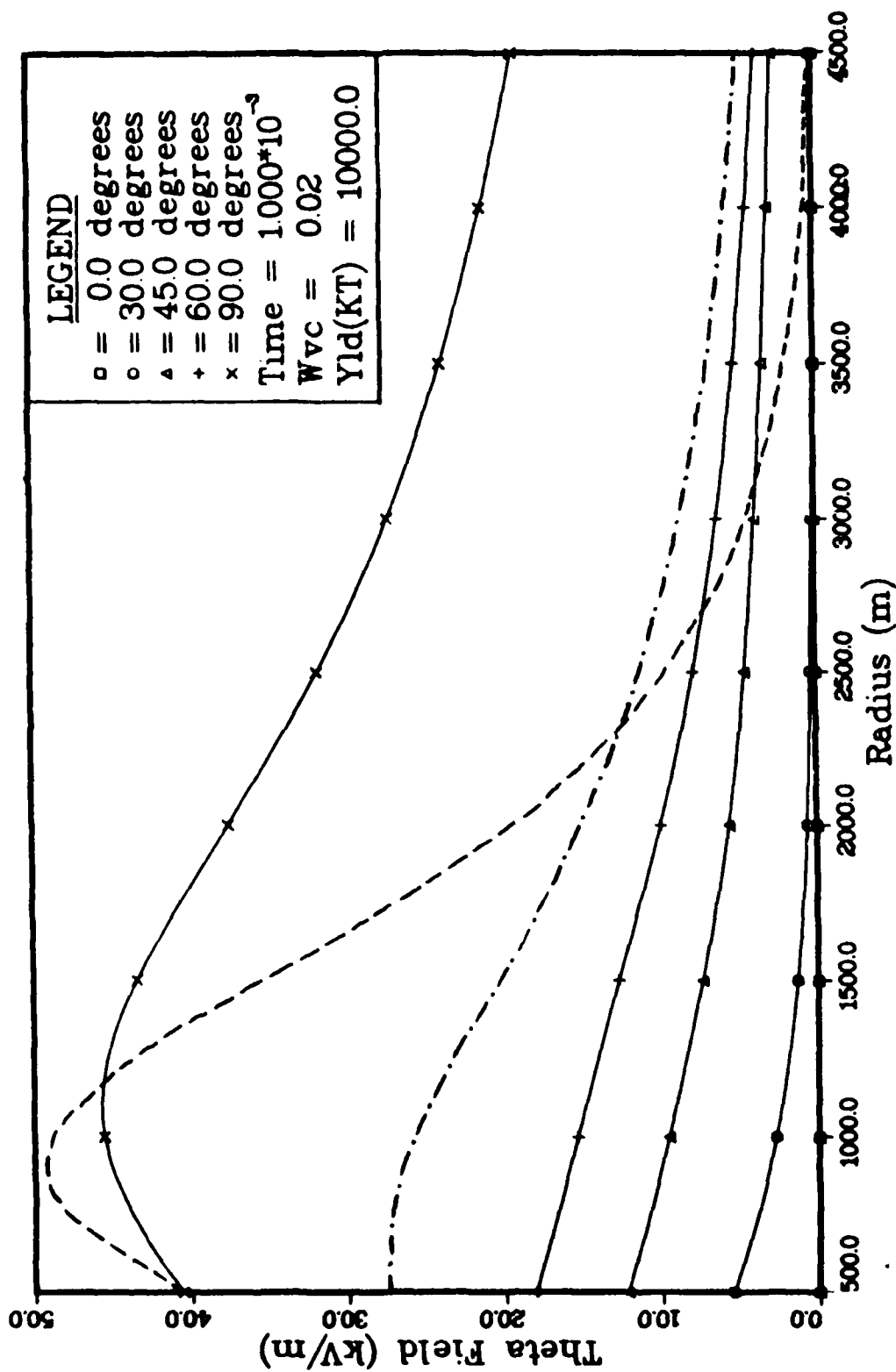


Figure 17. - E_θ vs Radius, Full Solution. Eq. 2.15, (Dashed Line, $\theta = 90^\circ$) and Initial Solution, (Dot-Dashed Line, $\theta = 90^\circ$), Also Shown

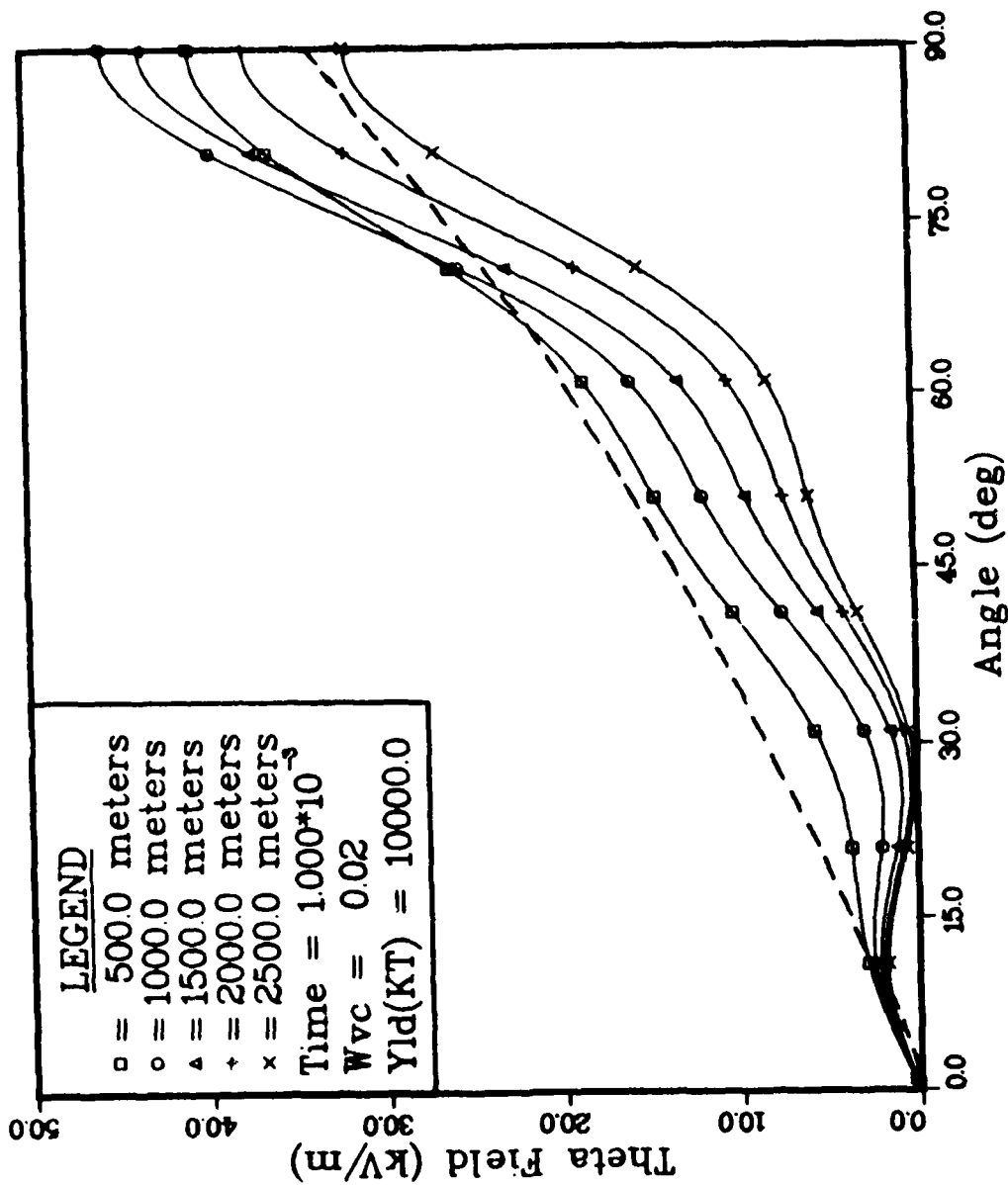


Figure 18. - E_{θ} vs Angle, Full Solution
Eq. 2.15 Shown as a Dashed Line ($r = 1500m$)

(90°), (dot-dash line) fields that were computed earlier using Grover's sources and the air chemistry equations for sigma (see Figures 4-7). The peak fields found using the improved solution were approximately 1.5 times larger than the previous results. In fact, the maximum E_r found with the new solution was almost as large as the peak E_θ from before.

The polar field was found to be at least twice as large as the radial field at their peak angles; the difference being even larger at greater distances.

Longmire's approximate solution at $\theta = 90^\circ$ is shown for comparison in Figure 17 (dashed line). It is seen that the overall shape of the field is quite different than the result obtained in the calculations presented here. In addition, it should be noted that the approximate air chemistry equations were used to compute sigma in Longmire's equation. The inherent limitations of this solution, therefore, should be remembered.

Theta Dependence

It was found in all calculations that the dominant Legendre polynomial coefficient was $A_1(r)$. Recalling Eqs (3.17) and (3.19), one would expect, therefore, that E_r should behave like $\cos\theta$ and E_θ like $\sin\theta$.

From Figure 16 it can be seen that the theta dependence of E_r is generally like $\cos\theta$. Note that at larger ranges E_r becomes nearly theta independent, but the magnitude, also,

is much smaller.

Figure 18 shows, however, that E_θ does not look much like $\sin\theta$. Obviously the theta dependence is complicated by the higher order polynomials. The theta dependence predicted by Longmire's solution was $\tan(\theta/2)$, see Eq 2.15. This equation is plotted in Figure 18 as the dashed line for $r = 1500$ meters.

It was found in the calculations that five polynomials were sufficient to properly describe the theta dependence. More than these were unnecessary because the computed coefficients were much smaller.

Boundary Condition at $r = 0$

To find the values of the integral terms in Eqs (6.15), (6.16), and (6.19), it was necessary to know J_r and σ at $r = 0$. This presented a problem since the fits used to determine these parameters had a $1/r^2$ dependence. Hence, at $r = 0$ J_r and σ would be infinite. This is obviously not possible physically. To avoid the problem, a value of $r = \delta r$ was chosen where δr was allowed to approach zero. Values of $r = 0.001$ meters or smaller resulted in the same final answers.

Field Dependence

To determine the effect of the field dependence of μ_e and α_e the program was run using the average values presented earlier in this work, i.e.

$$\mu_e = 0.25 \text{ m}^2/\text{V}\cdot\text{sec}$$

and

$$\alpha_e = 1.5 \times 10^8 \text{ sec}^{-1}$$

The results are shown in Figures 19 and 20. For comparison the results from the complete solution for E_r at 0° and E_θ at 90° are plotted as dashed lines.

The variation in E_r was found to be quite large, up to 25-30 percent. The difference in E_θ was smaller, but as big as 8-10 percent. It would seem, therefore, that the field dependence of μ_e and α_e is important.

Effect of J_θ

In the earlier calculations that were made (Chapter IV) no theta component of the Compton current was included. It was shown that J_θ was much smaller than J_r except for $r < \lambda$ (Ref 10). To determine its effect, a calculation was made where J_θ was set equal to zero. The results are shown in Figures 21 and 22. There was no difference in the radial field, and as can be seen from Figure 22, the variation in E_θ was very small. The difference was less than 5 percent at 500 meters and the answers were the same for ranges beyond approximately 1500 meters.

Variation in Electron Mobility

As was discussed in Chapter V, recent data has shown that the fit for mobility and attachment rate developed by

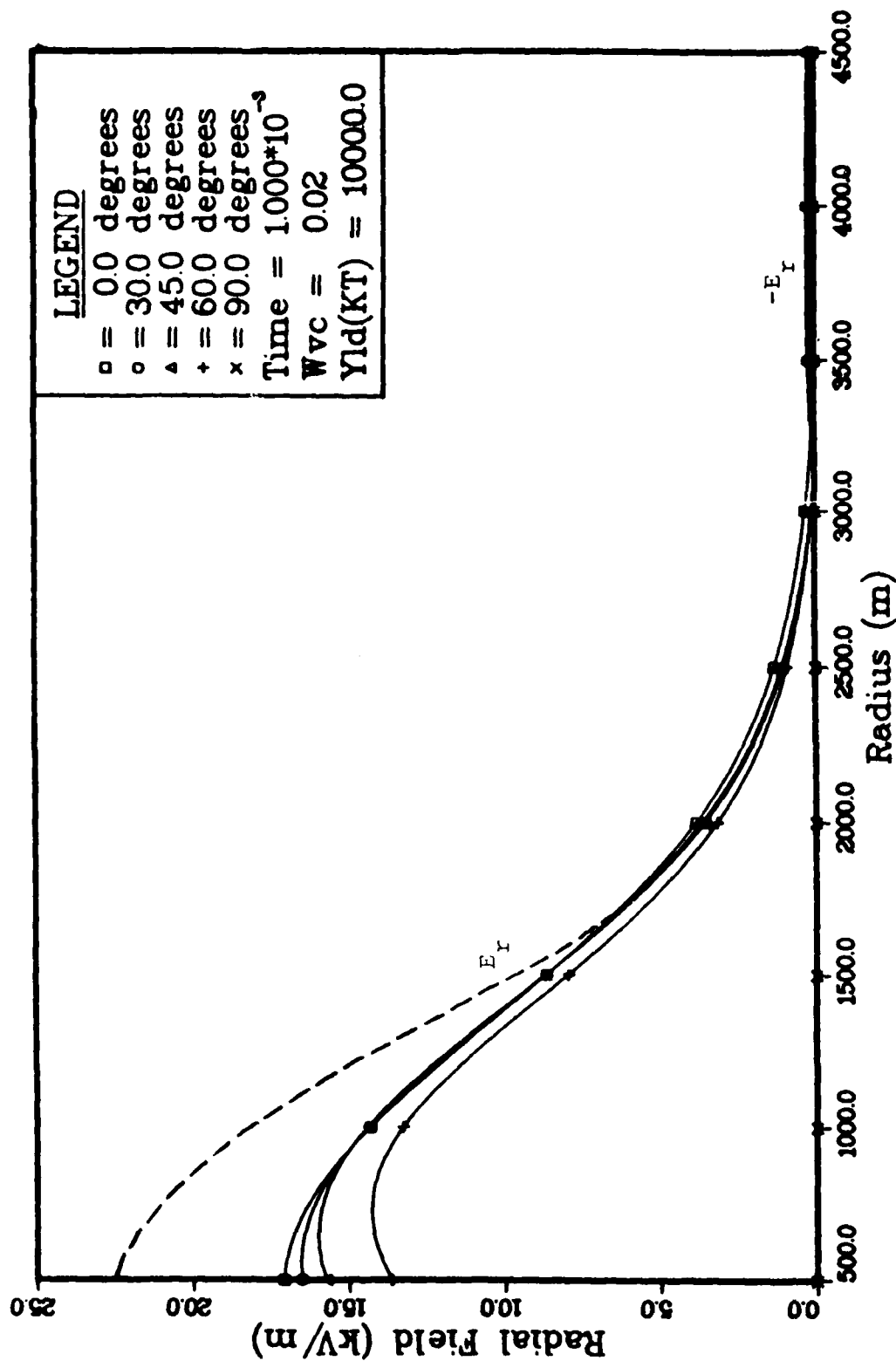


Figure 19. E_r vs Radius, Field Independent
Full Solution Shown as a Dashed Line ($\theta = 0^\circ$)

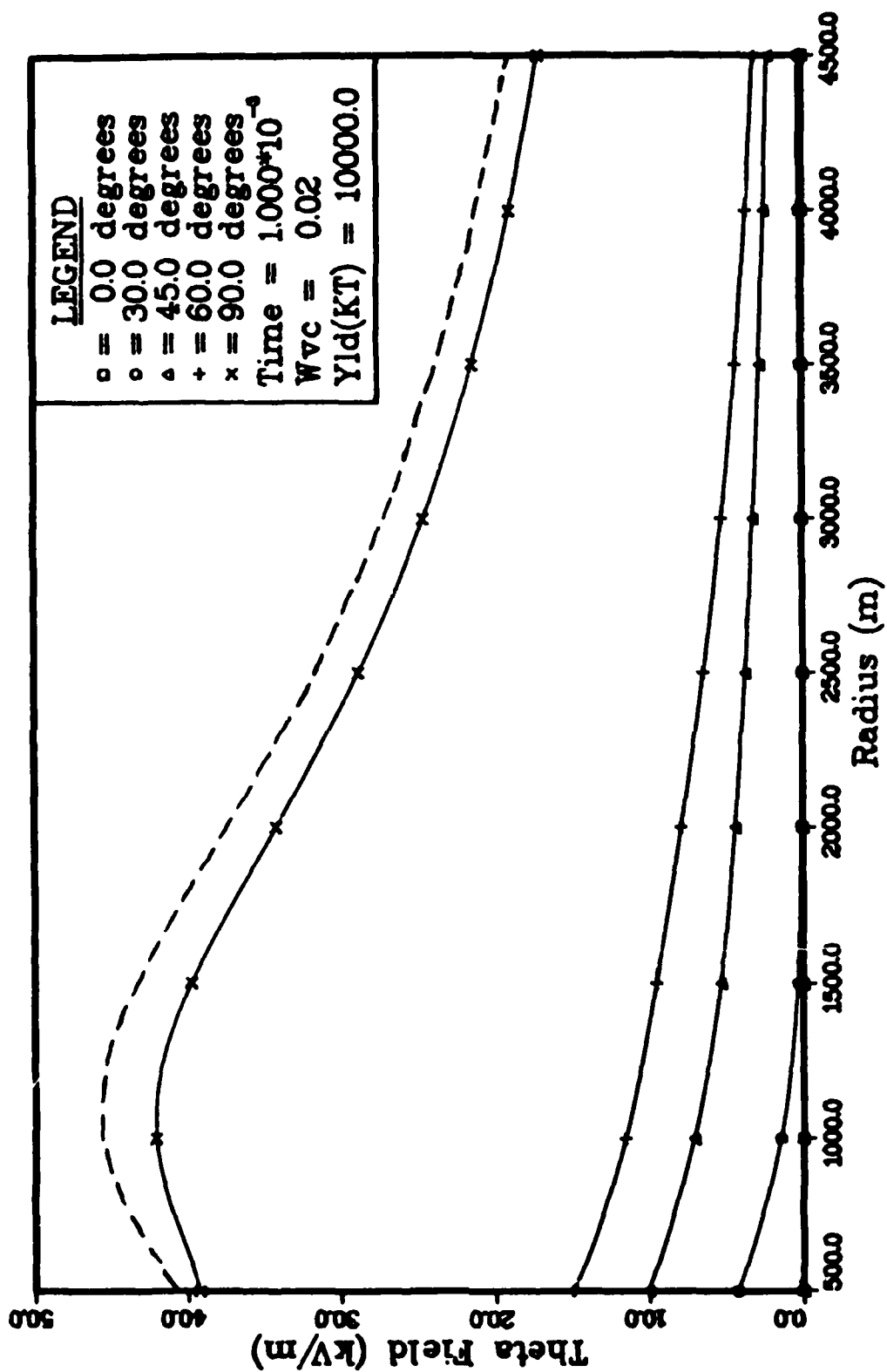


Figure 20. - E_θ vs Radius, Field Independent Full Solution Shown as a Dashed Line ($\theta = 90^\circ$)

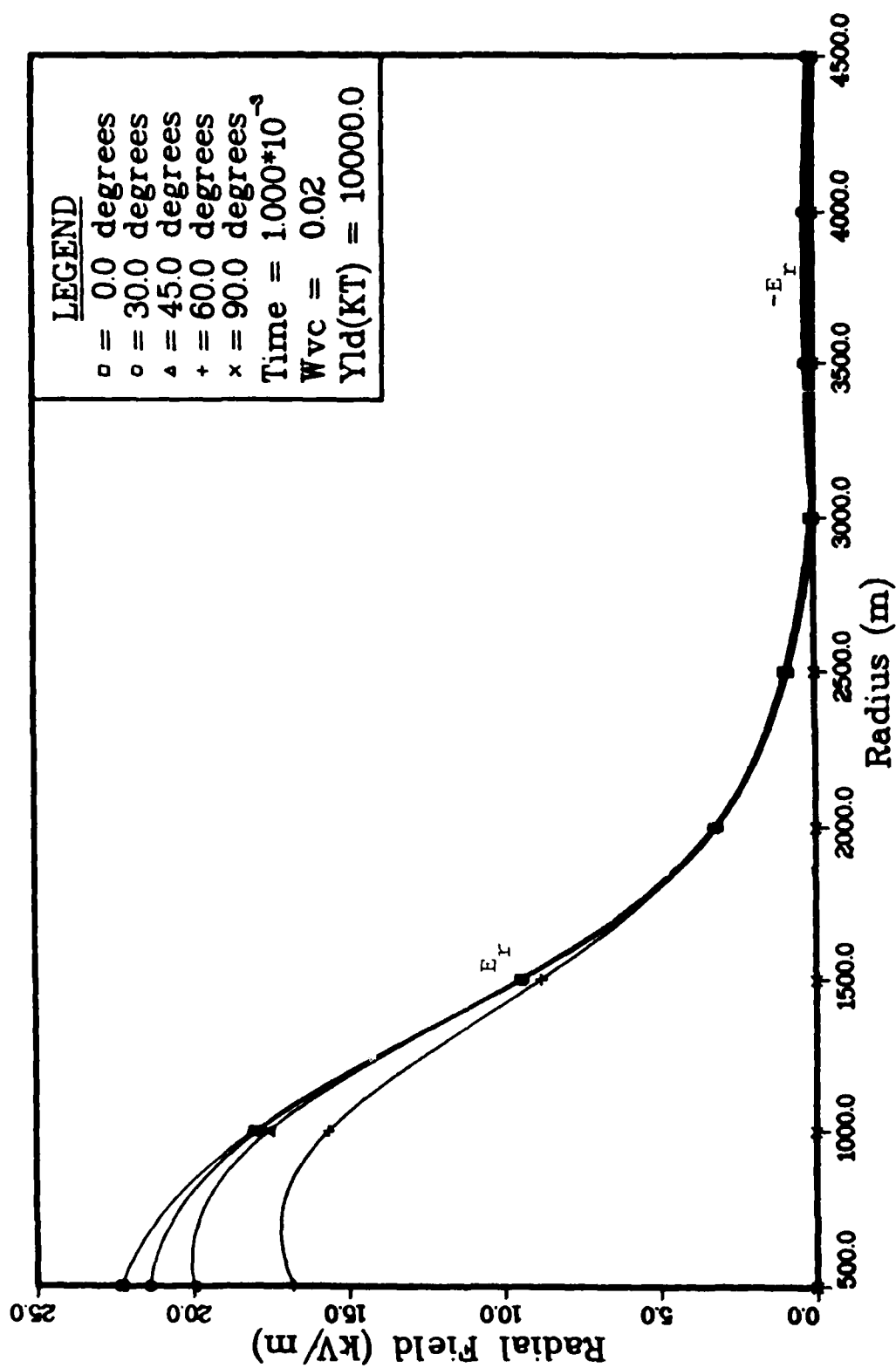


Figure 21. E_r vs Radius, $J_\theta = 0$

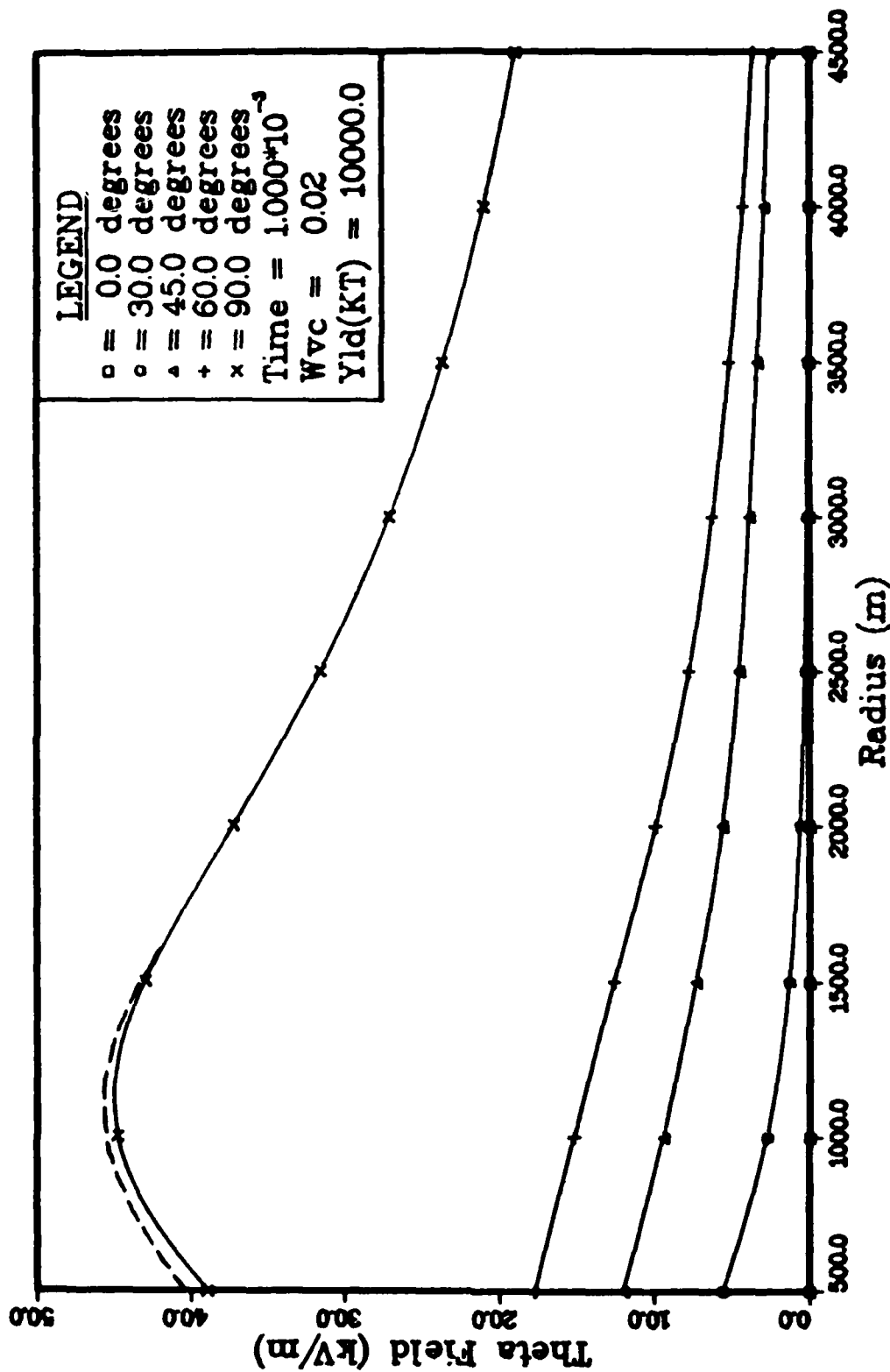


Figure 22. - E_{θ} vs Radius, $J_{\theta} = 0$
 Full Solution Shown as a Dashed Line ($\theta = 90^{\circ}$)

Longley and Longmire might not be correct (Ref 11). In the calculations made in this report, the Longley fits were used along with the modification to the mobility suggested by Smith (Ref 13:30). To see what effect this modification had on the fields, a calculation was made which did not include Smith's equation. The results are given in Figures 23 and 24. Once again the original solutions for E_r at $\theta = 0^\circ$ and E_θ at $\theta = 90^\circ$ are shown for comparison (dashed lines). The variation in E_r and E_θ was less than 2 percent for the peak field values. Obviously the modification makes some difference; however, the air chemistry parameters are not known with enough certainty to suggest any major conclusion (Ref 3:29). It should be pointed out, though, that no change was made in the electron attachment rate equations.

Summary

The results of this section suggest that the polar variation of the ionization rate and Compton current are important for the calculation of the electric fields. In addition, it was seen that variations in the air chemistry parameters and the theta component of the Compton current have some effect on the solutions. In the next chapter a series of parametric studies will be presented which will further show the importance of these parameters.

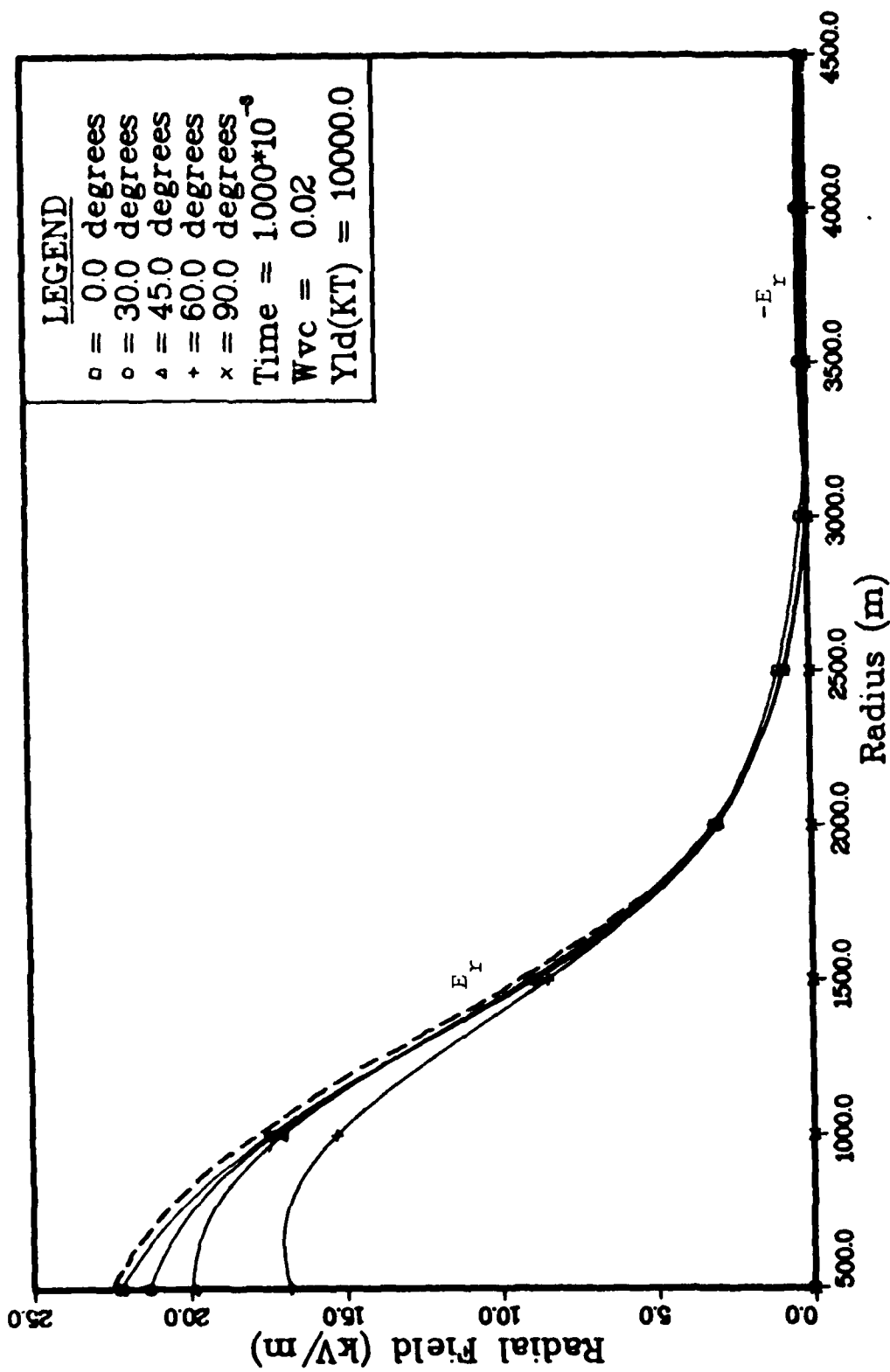


Figure 23. E_r vs Radius, Electron Mobility Not Limited
 Full Solution Shown as a Dashed Line ($\theta = 0^\circ$)

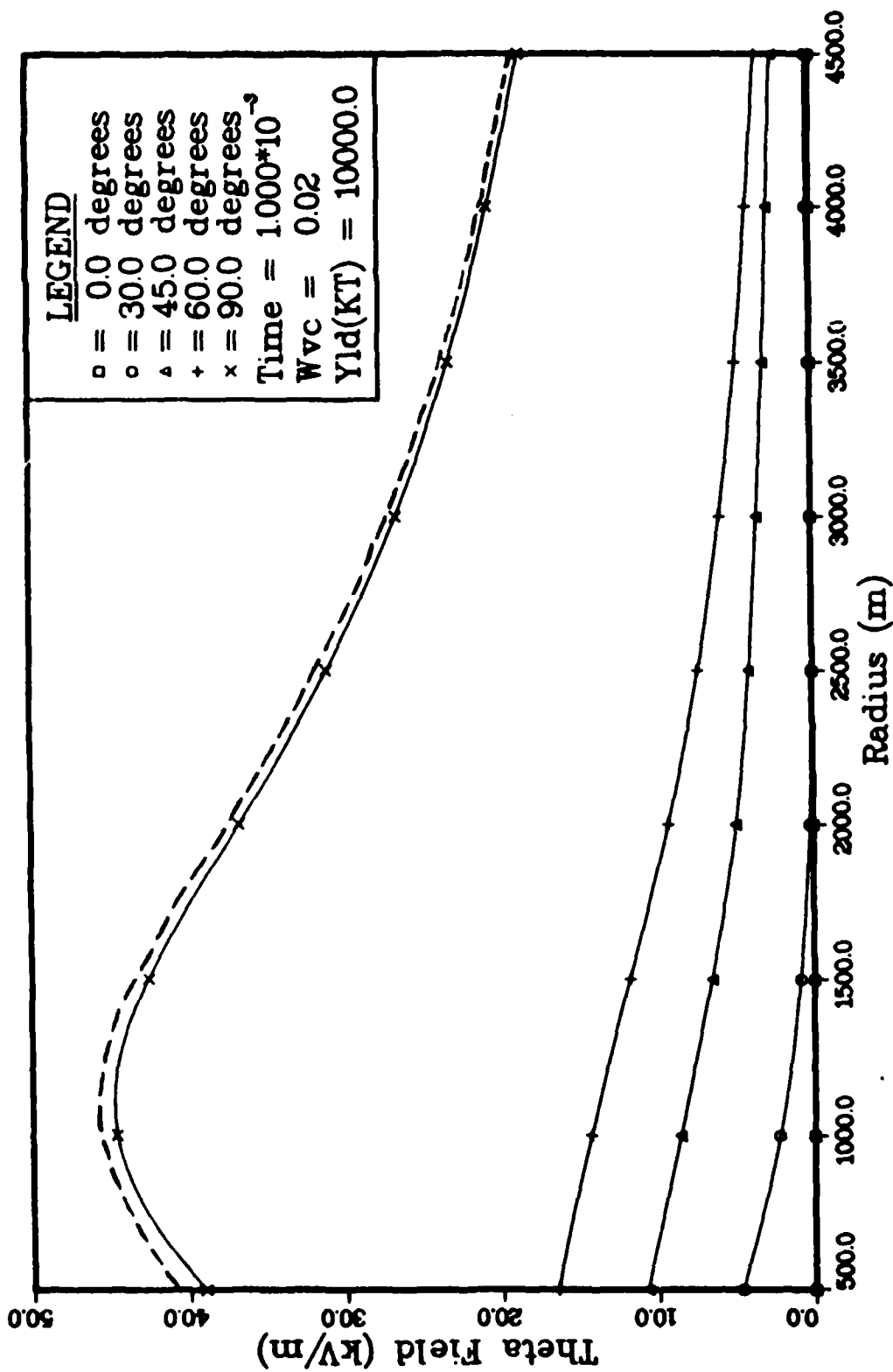


Figure 24. - E_θ vs Radius, Electron Mobility Not Limited
 Full Solution Shown as a Dashed Line ($\theta = 90^\circ$)

VIII. Parametric Studies

Using the code developed from the algorithm in Chapter VI, the impact of changing various parameters was considered. Both the accuracy of the code and the effects of varying physical parameters were studied. The results are presented in this chapter.

Code Accuracy

The computer program used in this report (see Appendix F) was tested by varying the numerical parameters which affected the calculations.

In approximating the derivatives by finite differences, a Δr had to be chosen. It was found that for a total range of 0-5000 meters a Δr of 50 meters was sufficient to guarantee convergence in the solutions; hence only 100 range points were needed. Of course, more could have been used but the added memory requirements and calculation time were unnecessary. A $\Delta \theta$ of one degree was used for the derivative calculations with respect to θ .

As discussed in Appendix D, the Romberg integration technique does not use a predetermined step size when the integrals are calculated. Rather, a so-called "row limit" is selected which allows for any desired accuracy. It was found that a row limit of four was sufficient for calculation of the numerical integrals. Choosing five gave

slightly better accuracy, but the calculation time for a complete solution was doubled.

In the iteration scheme used to find the fields, a tolerance of 100 V/m was selected for the convergence test between two consecutive calculations. In addition, it was determined that the answers were the same regardless of the angle selected for the convergence test.

The final numerical parameter considered was the number of Legendre polynomial coefficients, $A_\ell(r)$, that were necessary to adequately describe the potential function $\phi(r, \theta)$. It was determined that the first five odd terms in the series were sufficient (i.e. $\ell = 1, 3, 5, 7, \& 9$). Using six terms did not improve the answer and required twice as much computer time for a full calculation.

The parameters discussed above are summarized in Table I below.

Table I
Computer Code Parameters Used in Calculations

Number of Range Points	-	100
Δr	-	50 m
$\Delta \theta$	-	1 deg
Romberg Row Limit	-	4
Convergence Tolerance	-	100 V/m
Number of Polynomials	-	1st 5 odd

Time Dependence

Shown in Figure 25 is a plot of the total field along the ground ($\theta = 90^\circ$) vs time for five different ranges.

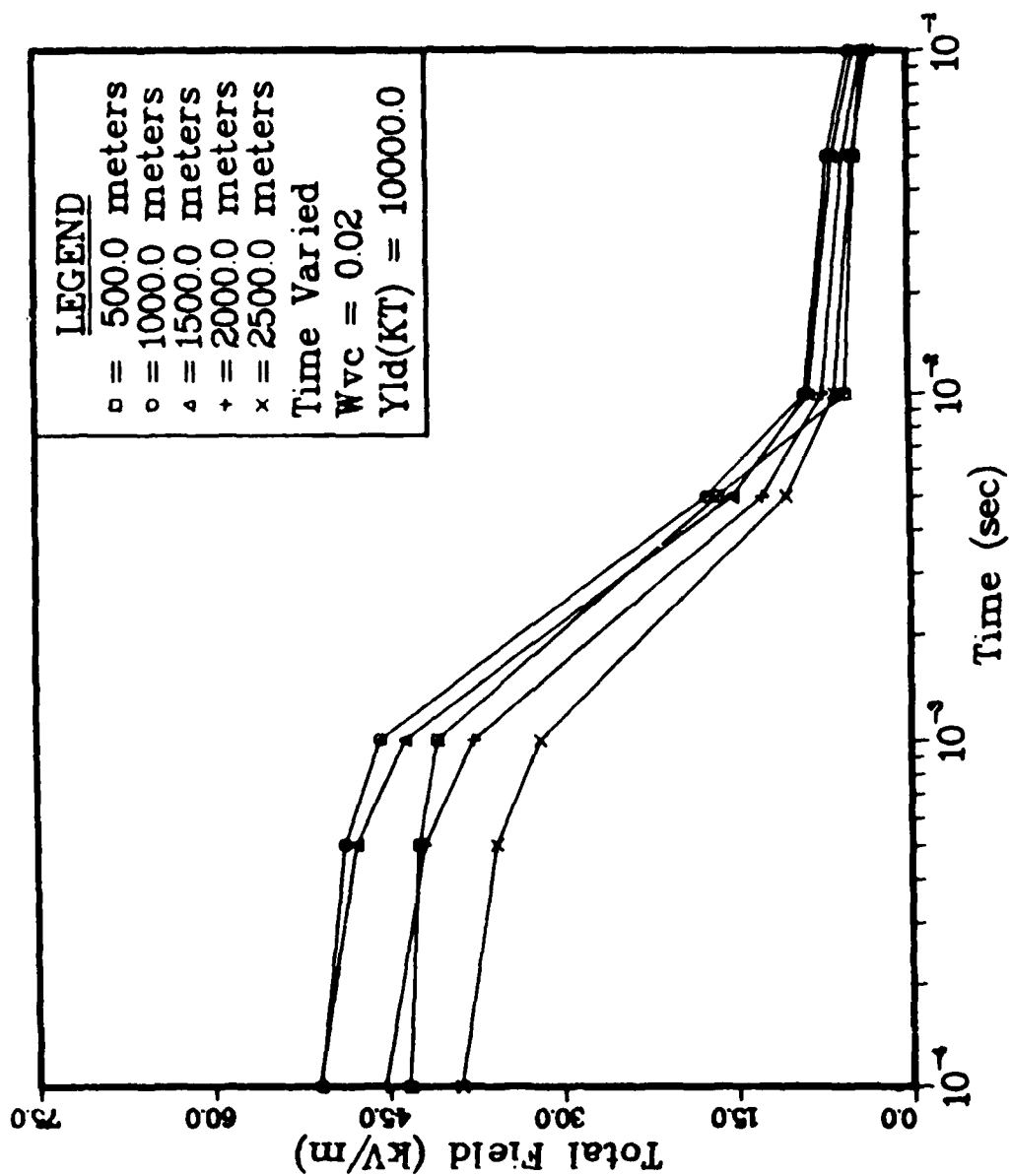


Figure 25. Total Field vs Time, $\theta = 90^\circ$

This field corresponds to the maximum theta component (i.e. $E_r = 0$). The two plateaus appear to agree quite well with the time regimes where either ground or air capture sources dominate. The magnitude of the field is seen to decrease approximately by a factor of ten over the time range shown. This is an interesting result since the current was shown to fall off by two orders of magnitude for the same time range (see Figure 12).

Figure 26 shows the total field at $\theta = 0^\circ$ ($E_\theta = 0$). The time dependence is approximately the same as above, although, the decrease in the total field is less than an order of magnitude. It is seen that for times greater than approximately 10^{-2} seconds the peak radial field at 500 meters is nearly as large as the maximum polar field. This result differs substantially from a curve given in a report by Longmire (Ref 9:45). The calculations presented in this report show a much larger radial field than shown in the above-referenced curve for E_r .

Additional plots for the total field at 10^{-2} and 10^{-1} seconds are given in Appendix E.

Yield Dependence

Figures 27 and 28 show the yield dependence of the total field at $\theta = 90^\circ$ and $\theta = 0^\circ$ respectively. In Figure 27 it is seen that the total field is nearly independent of the yield at 500 meters and falls off slightly for lower yields. For larger distances the total field is

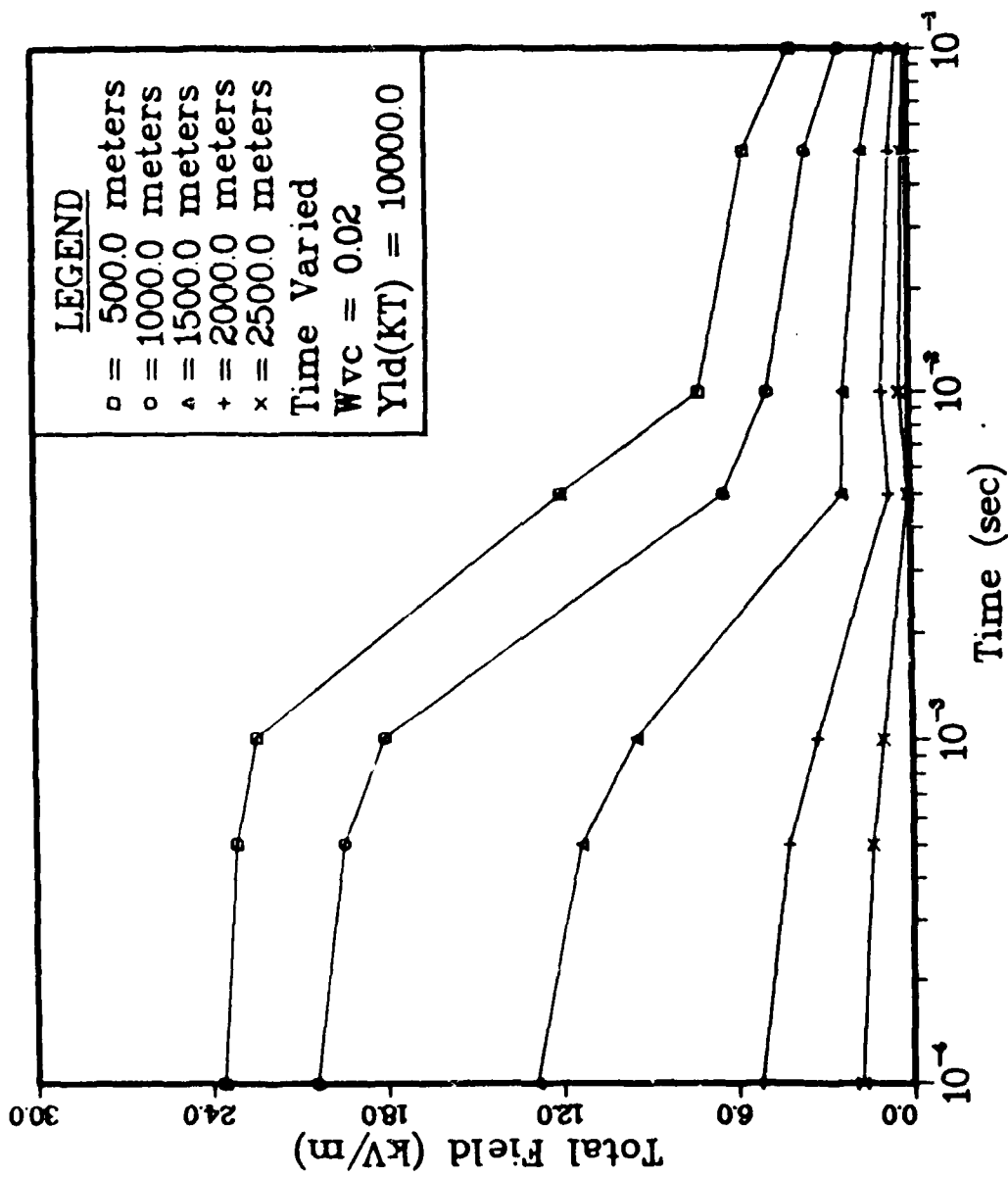


Figure 26. Total Field vs Time, $\theta = 0^\circ$

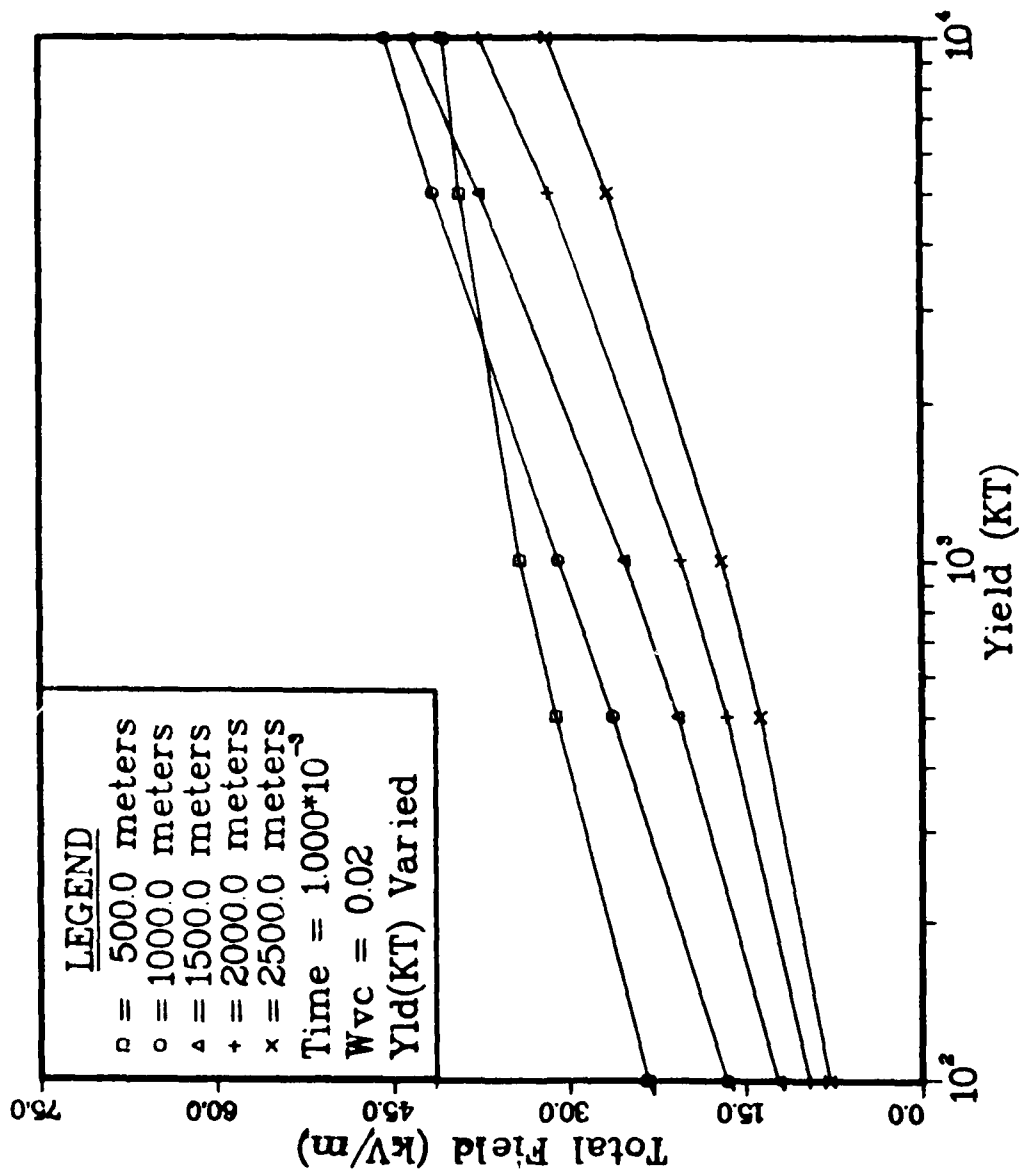


Figure 27. Total Field vs Yield, $\theta = 90^\circ$

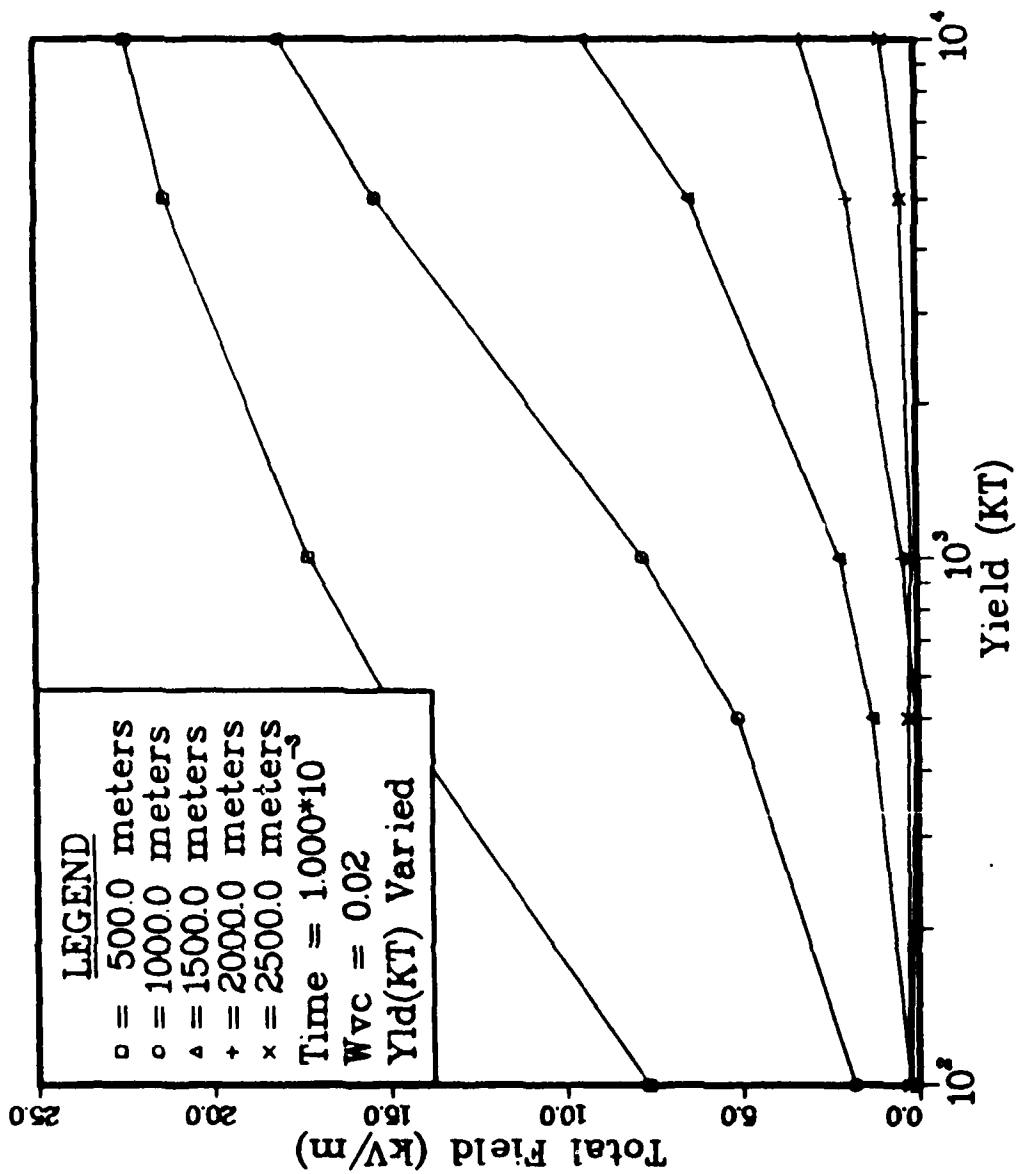


Figure 28. Total Field vs Yield, $\theta = 0^\circ$

more dependent on the yield. This can be explained by considering the ratio of J/σ . For short ranges this ratio is nearly independent of yield because electrons dominate the conductivity. At greater distances the conductivity is dominated by ions and the ratio is no longer yield independent. A similar yield dependence is shown in Figure 28 for the total field at $\theta = 0^\circ$.

Additional curves for 1000 KT and 100 KT are given in Appendix E.

Water Vapor Dependence

The final parameter considered was the effect of various water vapor contents on the total field. In Figures 29 and 30 the total field is plotted as a function of water vapor content in the air. As seen in Figure 29, the field at $\theta = 90^\circ$ varies quite substantially over the range of water vapor fractions shown. Recalling Figures 13 and 14 for the mobility and attachment rate, it was seen that higher water vapor contents decreased the mobility and increased the attachment rate. Thus, as the fraction of water vapor in the air increases the conductivity decreases. Since $E = J/\sigma$, the field should get larger. This result is seen clearly in Figure 29. Note that the dependence is greater for the 500 meter curve due to electron dominated conductivity. For larger ranges where ions dominate, the dependence is slightly less. Figure 30 shows that the field at $\theta = 0^\circ$ does become nearly independent of the water vapor

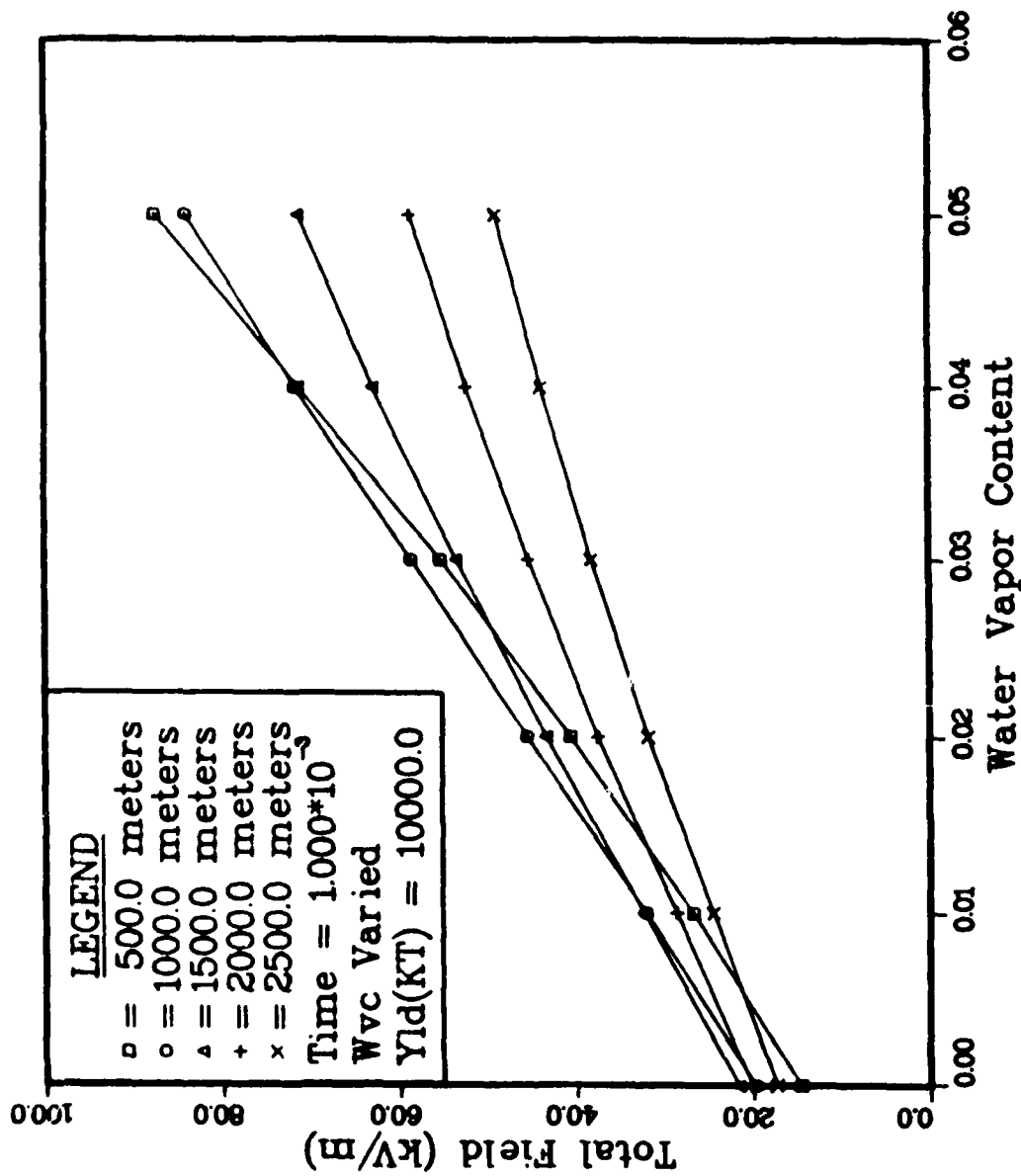


Figure 29. Total Field vs Water Vapor Content, $\theta = 90^\circ$

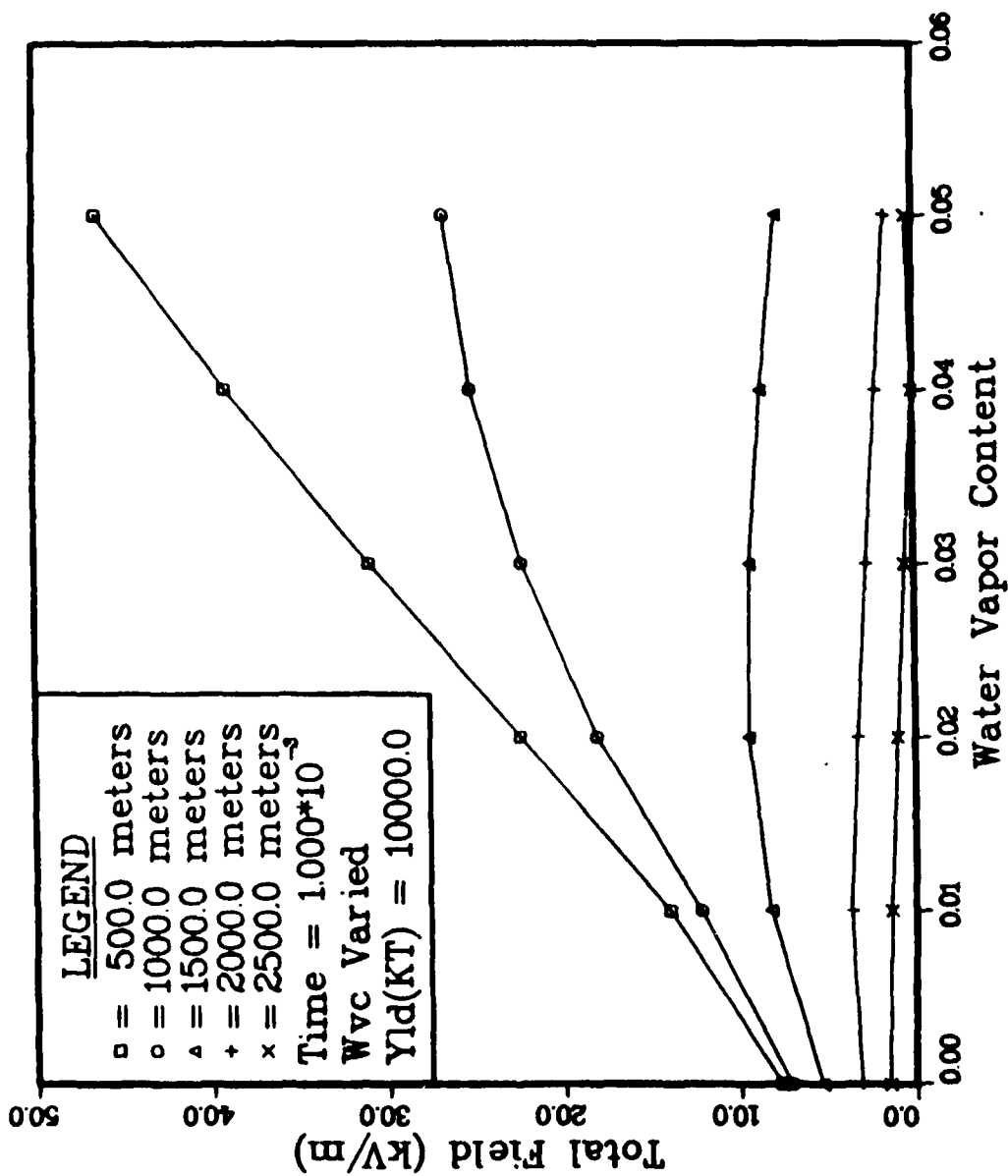


Figure 30. Total Field vs Water Vapor Content, $\theta = 0^\circ$

content for ranges of 1500 meters or larger.

Additional curves for water vapor fractions of 0.00 and 0.04 are given in Appendix E.

IX. Conclusions and Recommendations

Conclusions

In this study the quasi-static EMP fields were calculated using a time-independent numerical method. On the basis of the research and the calculations performed, the following conclusions are made:

1. The angular dependence of the ionization rate and Compton current are important in the calculation of the fields. The peak field values calculated in this work varied by as much as 50 percent from Grover's theta independent calculations (see Figures 15-18). Thus, the results presented in this paper extend Grover's work by using more realistic sources.

2. Even though the radial field is small at late times, its effect is important for a complete solution to Maxwell's equations. In Longmire's analytic development (Ref 9) E_r was ignored and the resulting E_θ field had a limited range of validity. By including E_r , the calculations made in this work provide an improved picture of the late time EMP.

3. The electric fields that result from a surface nuclear burst are dependent on variations in the air chemistry parameters. Using field independent, average values for the electron

mobility and attachment rate resulted in peak field values which were 10 to 30 percent different from the calculations where these parameters were allowed to vary. As shown in Figure 29 the field is also a strong function of the water vapor content of the air.

4. The inclusion of the theta component of the Compton current (J_θ) is not important for EMI calculations as it only changes the fields for points close to the burst. In the test case studied in this work, the variation was less than 5 percent for ranges shorter than 500 meters. The answers were identical for larger ranges.

Recommendations

Based on the results obtained in this study, the following recommendations are suggested:

1. The results of the time-independent calculations presented in this report should be compared to the results obtained with time-dependent codes (such as LEMP) to determine how well the fields are being predicted.
2. The code should be modified to include the new fits (Ref 11) for the electron mobility and attachment rate. A comparison should then be made with the results presented in this work.
3. The validity of the quasi-static approximation should be considered.

Bibliography

1. Burden, Richard L., et al. Numerical Analysis. Boston: Prindle, Weber and Schmidt, 1978.
2. Grover, Morgan K. Some Analytic Models for Quasi-Static Source Region EMP: Application to Nuclear Lightning. RDA-TR-113202-002, R & D Associates, Marina del Rey, California, November 1980. (AD-A109 644).
3. Grover, Morgan K. and F. R. Gilmore. A Review of Data for Electron Mobility, Energy, and Attachment Relevant to EMP Air Chemistry. RDA-TR-110002-C01, R & D Associates, Marina del Rey, California, March 1980. (AD-A098 874).
4. Hill, R. D. "Lightning Induced by Nuclear Bursts," Journal of Geophysical Research, 78: 6355-6358 (September 1973).
5. Jones, C. W. and W. M. Folkner. Gamma-Ray and Neutron EMP Source Comparisons and Uncertainties for Surface Burst EMP Codes. DC-EN-1298-1, Dikewood Industries, Inc., Albuquerque, New Mexico, June 1980. (AD-B051 074L). Unclassified, Limited.
6. Lee, K. S. H. (Editor). EMP Interaction Principles, Techniques and Reference Data, EMP Interaction 2-1. DC-EN-1289, Dikewood Industries, Inc., Albuquerque, New Mexico, December 1980. (AD-A100 508).
7. Longley, H. J. and Conrad L. Longmire. Electron Mobility and Attachment Rate in Moist Air. MRC-N-222, Mission Research Corporation, Santa Barbara, California, December 1975.
8. Longmire, Conrad L. "On the Electromagnetic Pulse Produced by Nuclear Explosions," IEEE Transactions on Antennas and Propagation, AP-26: 3-13 (January 1978).
9. Longmire, Conrad L. and James L. Gilbert. The Theory of EMP Coupling in the Source Region. MRC-R-546, Mission Research Corporation, Santa Barbara, California, February 1980. (AD-A108 751).
10. O'Dell, A. A., C. L. Longmire, and H. J. Longley. The Development of Improved Late-Time Sources for the LEMP Computer Code. MRC-R-104, Mission Research Corporation, Santa Barbara, California, November 1974. (AD-C001 246). Unclassified.

11. Pettus, E. and W. Crevier. Analytic Representation of Electron Mobility and Attachment Data in Dry and Moist Air from Van Lint's HIFX Experiments. MRC-R-576, Mission Research Corporation, Santa Barbara, California, July 1980.
12. Radasky, William A. An Examination of the Adequacy of the Three-Species Air Chemistry Treatment for the Prediction of Surface-Burst EMP. MRC-R-244, Mission Research Corporation, Santa Barbara, California, December 1975. (AD-A025 280).
13. Smith, K. S. and W. A. Radasky. An Examination of the Behavior of the Late-Time Electronic and Ionic Conductivities Appropriate for Surface-Burst EMP Calculations. DC-TN-1505-2, Dikewood Corporation, Albuquerque, New Mexico, March 1982. (AD-B064 200L). Unclassified, Limited.
14. Spiegel, Murray R. Fourier Analysis with Applications to Boundary Value Problems. New York: McGraw Hill Book Company, 1974.
15. Spiegel, Murray R. Mathematical Handbook of Formulas and Tables. New York: McGraw Hill Book Company, 1968.
16. Uman, M. A., et al. "Lightning Induced by Thermonuclear Detonations," Journal of Geophysical Research, 77: 1591-1596 (March 1972).
17. Wyatt, William T. An Improved Model for EMP-Induced Lightning. HDL-TR-1919, Harry Diamond Laboratories, Adelphi, Maryland, April 1980. (AD-A096 811).

Appendix A

Finite Differences in Initial Solution

In this appendix the finite difference approximations which led to Eq (3.9) are presented.

From Maxwell's equations and the Legendre polynomial expansion the following differential equation, Eq (3.8), was obtained:

$$\frac{\partial A_\ell(r)}{\partial r} + \left(\frac{\ell}{r} + \frac{1}{\sigma} \frac{\partial \sigma}{\partial r} \right) \frac{\partial A_\ell(r)}{\partial r} - \ell(\ell+1) \frac{A_\ell(r)}{r^2} = (2\ell+1) \left[\frac{1}{\sigma} \frac{\partial J}{\partial r} + \frac{2}{\sigma^2} J_r \right] \int_0^1 P_\ell(x) dx \quad (A-1)$$

To obtain a numerical solution, all the derivatives in Eq (A-1) are replaced by their central difference approximations. Let $r_n = n \cdot \Delta r$ where n is an integer. Hence, for N range points, Δr is found from $\Delta r = r_{\max}/N$. Then for a given function $f(r)$, the following are obtained:

$$f(r) - f(r_n) = f_n \quad (A-2)$$

Also

$$\frac{df(r)}{dr} \approx \frac{f_{n+1} - f_{n-1}}{2\Delta r} \quad (A-3)$$

and

$$\frac{d^2 f(r)}{dx^2} \approx \frac{f_{n+1} - 2f_n + f_{n-1}}{\Delta r^2} \quad (A-4)$$

Then in Eq (A-1)

$$\frac{\partial^2 A_\ell(r)}{\partial r^2} \Rightarrow \frac{A_{\ell,n+1} - 2A_{\ell,n} + A_{\ell,n-1}}{\Delta r^2}$$

$$\left(\frac{2}{r} + \frac{1}{\sigma} \frac{\partial \sigma}{\partial r} \right) \frac{\partial A_\ell(r)}{\partial r} \Rightarrow \left[\frac{2}{r_n} + \frac{1}{\sigma_n} \frac{\sigma_{n+1} - \sigma_{n-1}}{2\Delta r} \right] \frac{A_{\ell,n+1} - A_{\ell,n-1}}{2\Delta r}$$

$$\frac{A_\ell(r)}{r^2} \Rightarrow \frac{A_{\ell,n}}{r_n^2}$$

$$\left(\frac{1}{\sigma} \frac{\partial J_r}{\partial r} + \frac{2}{\sigma r} J_r \right) \Rightarrow \frac{1}{\sigma_n} \left[\frac{J_r^{n+1} - J_r^{n-1}}{2\Delta r} + \frac{2J_r^n}{r_n} \right]$$

Thus Eq (A-1) becomes

$$\frac{A_{\ell,n+1} - 2A_{\ell,n} + A_{\ell,n-1}}{\Delta r^2} + \left[\frac{2}{r_n} + \frac{1}{\sigma_n} \frac{\sigma_{n+1} - \sigma_{n-1}}{2\Delta r} \right] \frac{A_{\ell,n+1} - A_{\ell,n-1}}{2\Delta r} \quad (A-5)$$

$$- \ell(\ell+1) \frac{A_{\ell,n}}{r_n^2} - (2\ell+1) \frac{1}{\sigma_n} \left[\frac{J_r^{n+1} - J_r^{n-1}}{2\Delta r} + \frac{2J_r^n}{r_n} \right] \int_0^1 P_\ell(x) dx$$

or after rearrangement

$$a_n A_{\ell,n+1} + b_{\ell,n} A_{\ell,n} + c_n A_{\ell,n-1} = R_{\ell,n} \quad (A-6)$$

where

$$a_n = \frac{1}{\Delta r^2} + \frac{1}{2\Delta r} \left[\frac{2}{r_n} + \frac{\sigma_{n+1} - \sigma_{n-1}}{2\Delta r} \right] \quad (A-7)$$

$$b_{\ell,n} = - \left[\frac{2}{\Delta r^2} + \ell(\ell+1) \frac{1}{r_n^2} \right] \quad (A-8)$$

$$\sigma_n = \frac{1}{\Delta r^2} + \frac{1}{2\Delta r} \left[\frac{2}{r_n} + \frac{\sigma_{n+1} - \sigma_{n-1}}{2\Delta r} \right] \quad (\text{A-9})$$

and

$$E_{\psi,n} = (2\ell+1) \frac{1}{\sigma_n} \left[\frac{j_r^{n+1} - j_r^{n-1}}{2\Delta r} + \frac{2j_r^n}{r_n} \right] \int_0^1 P_\ell(x) dx \quad (\text{A-10})$$

AD-A127 303

THE CALCULATION OF LATE-TIME SURFACE BURST EMP
(ELECTROMAGNETIC PULSE) FI..(U) AIR FORCE INST OF TECH
WRIGHT-PATTERSON AFB-OH SCHOOL OF ENGI... J R DOWNEY

2/2

UNCLASSIFIED

MAR 83 AFIT/GNE/PH/83M-5

F/G 18/3

NL

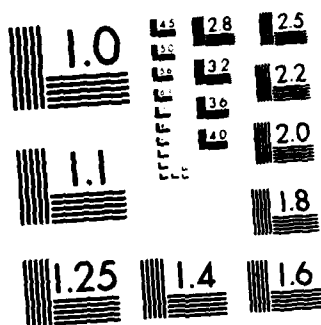
END

DATE

FILMED

5-83

DTIC



MICROCOPY RESOLUTION TEST CHART
NATIONAL BUREAU OF STANDARDS-1963 A

Appendix B

Initial Numerical Results

This appendix contains the results of calculations that were made using Grover's sources and his Model (3) conductivity. These results are discussed in Chapter IV. The figures are grouped as follows:

Figures 31 - 34 ; Fields found using $\sigma_o = 178.0$

Figures 35 - 38 ; Fields found using $\sigma_o = 143.2$

Note that in all figures the absolute value of the field is plotted. Actually E_r is positive and E_θ is negative over most of the range.

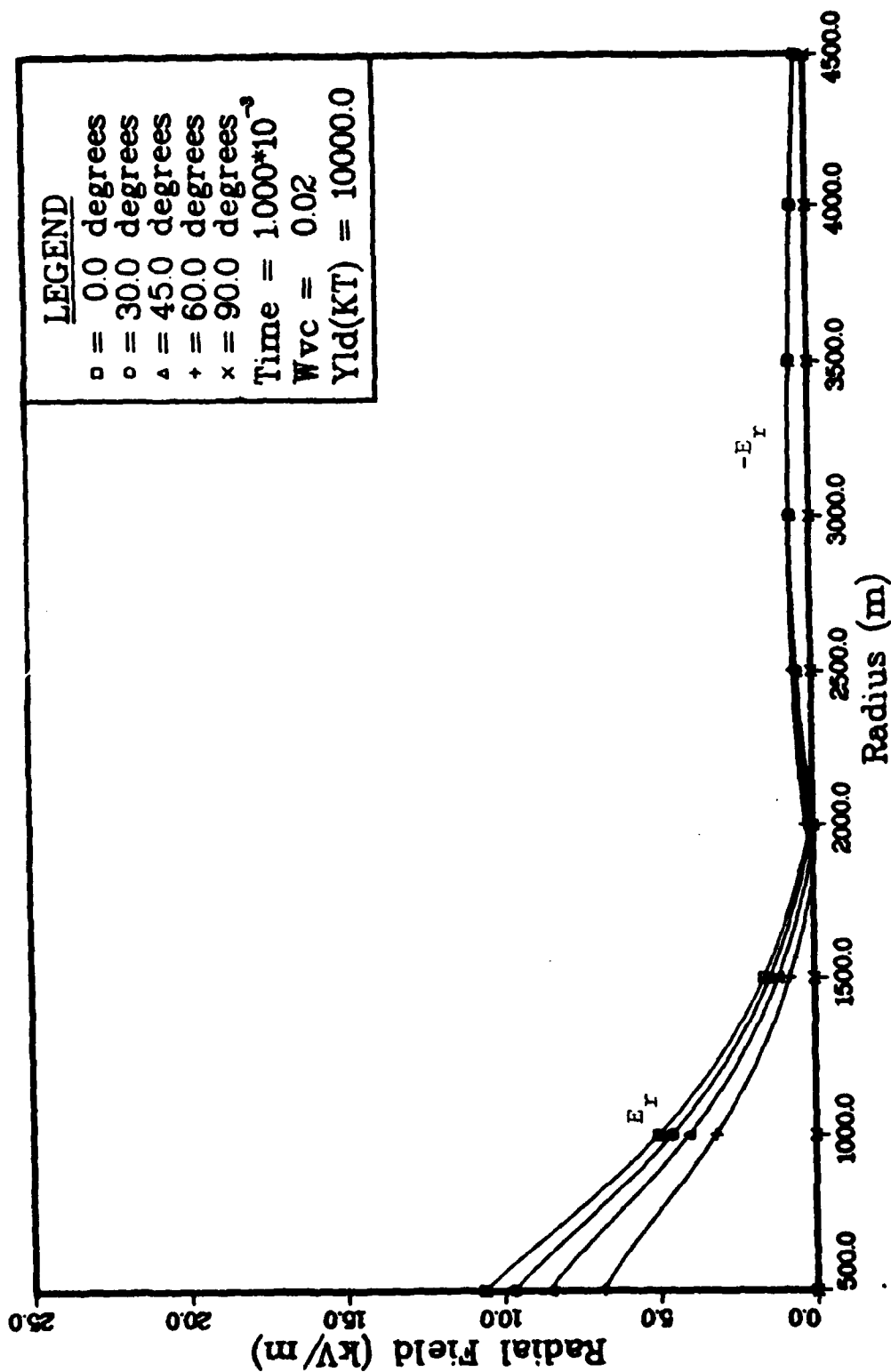


Figure 31. E_r vs Radius, Simplified Sources $\sigma_0 = 178.0$

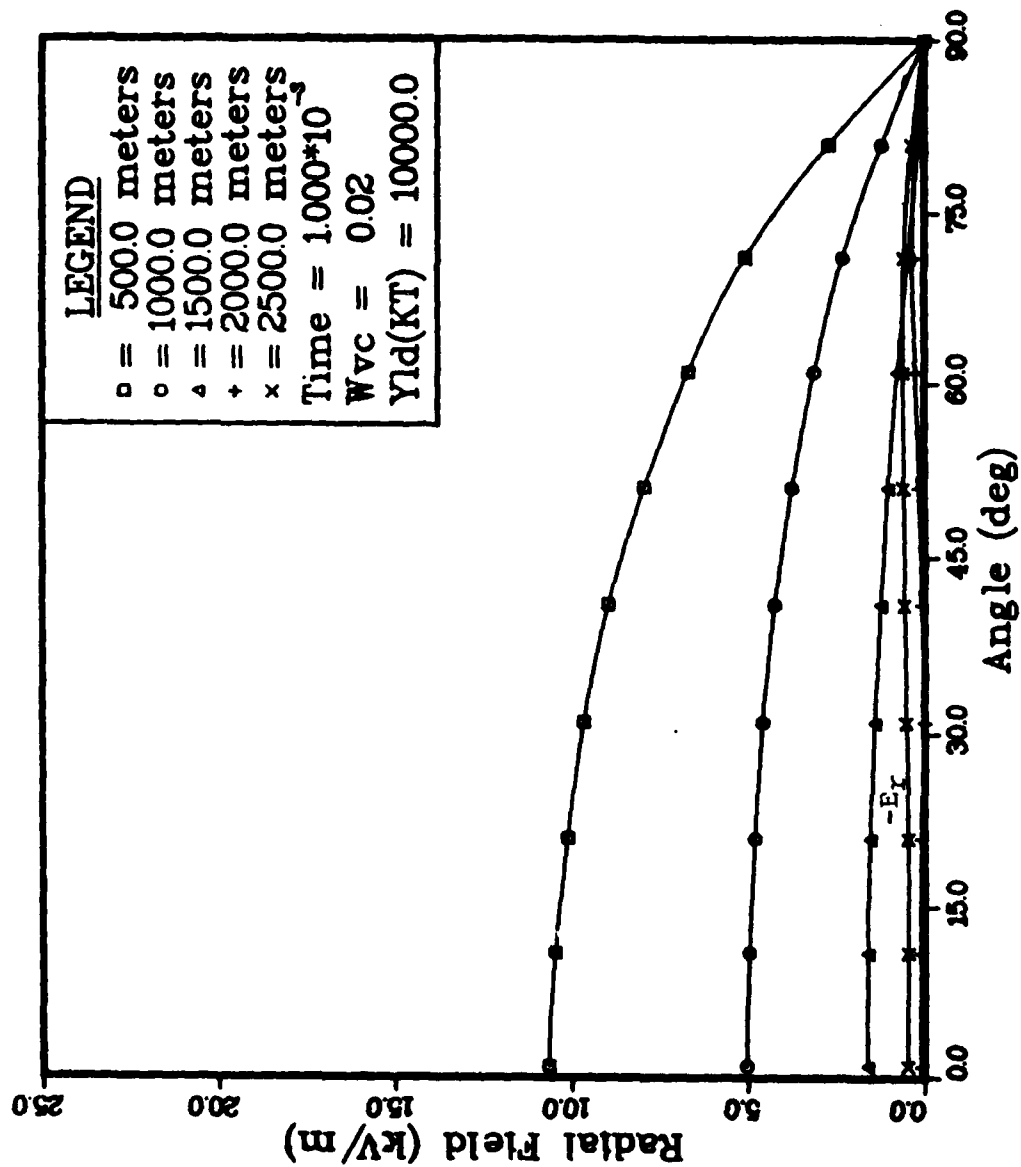


Figure 32. E_r vs Angle, Simplified Sources $\sigma_0 = 178.0$

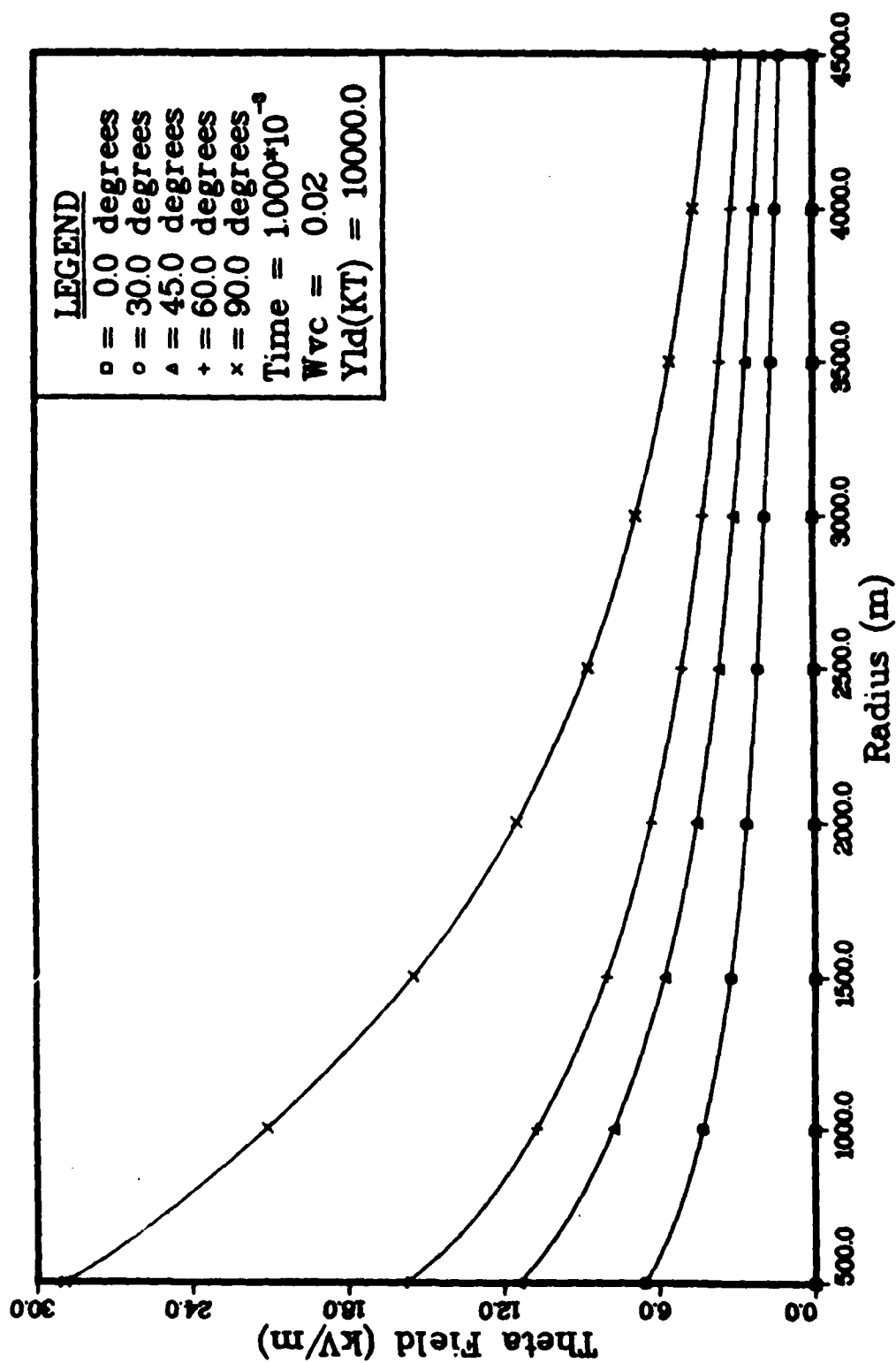


Figure 33. - E_θ vs Radius, Simplified Sources $\sigma_0 = 178.0$

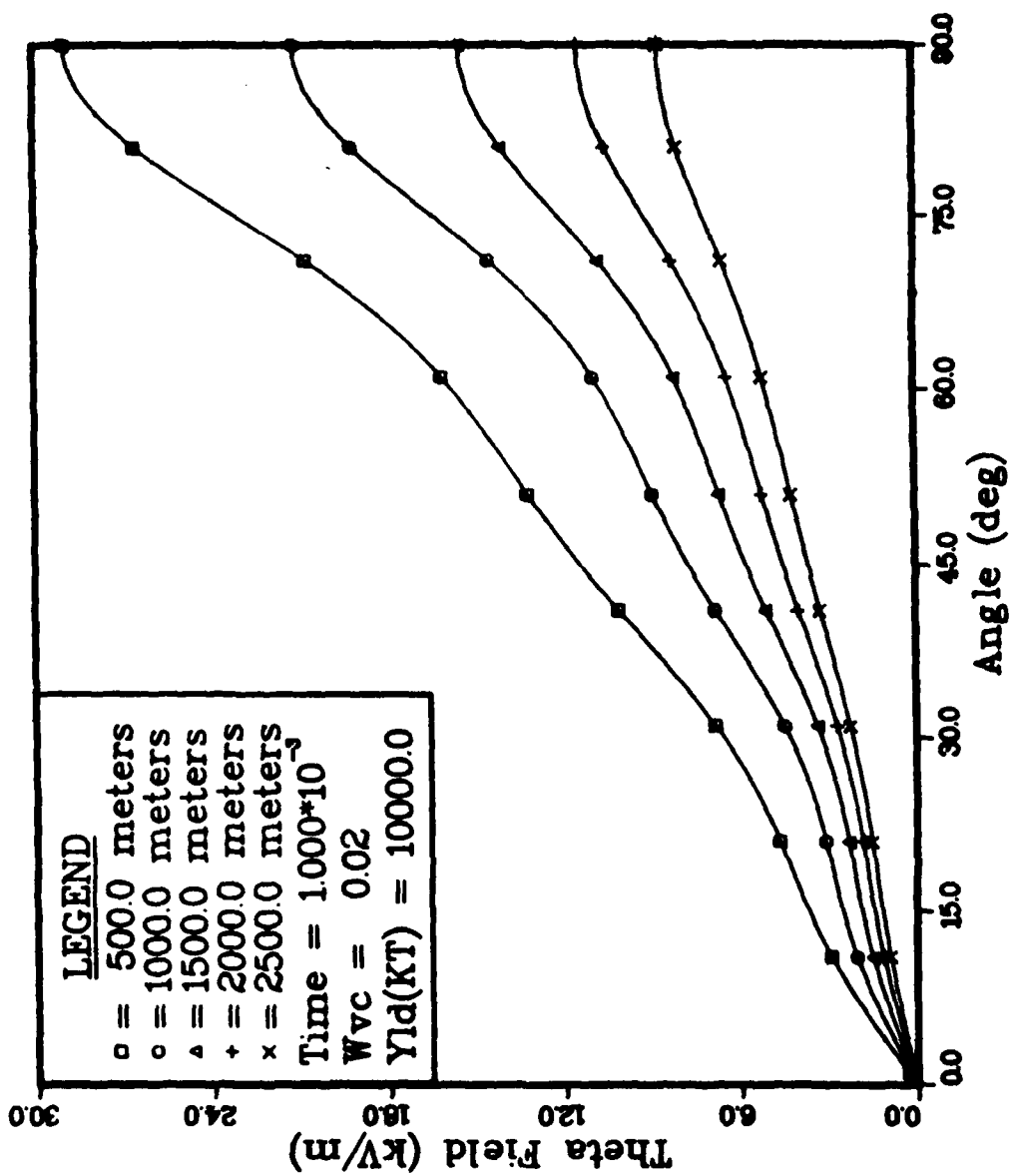


Figure 34. - E_{θ} vs Angle, Simplified Sources $\sigma_0 = 178.0$

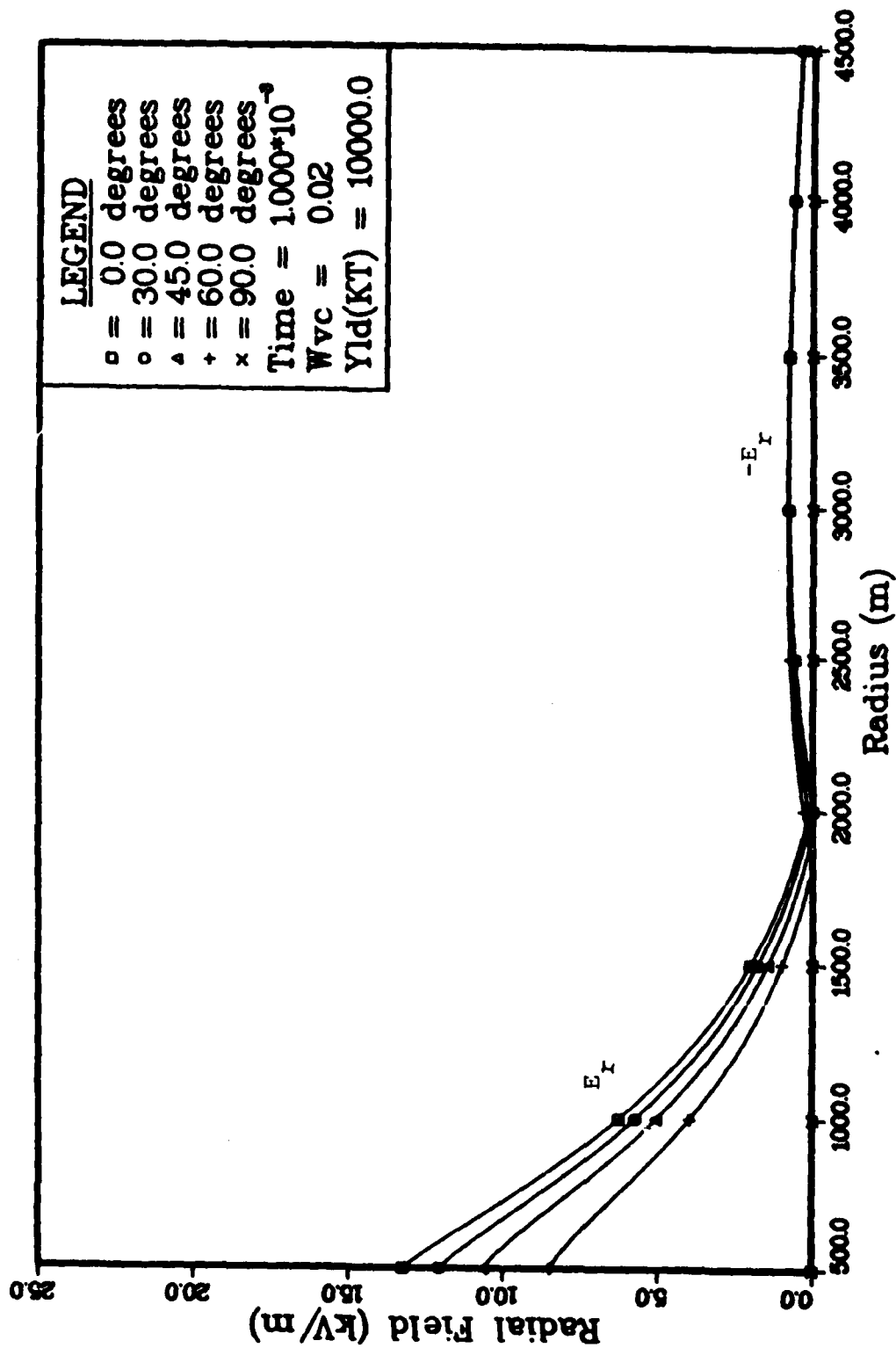


Figure 35. E_r vs Radius, Simplified Sources $\sigma_0 = 143.2$

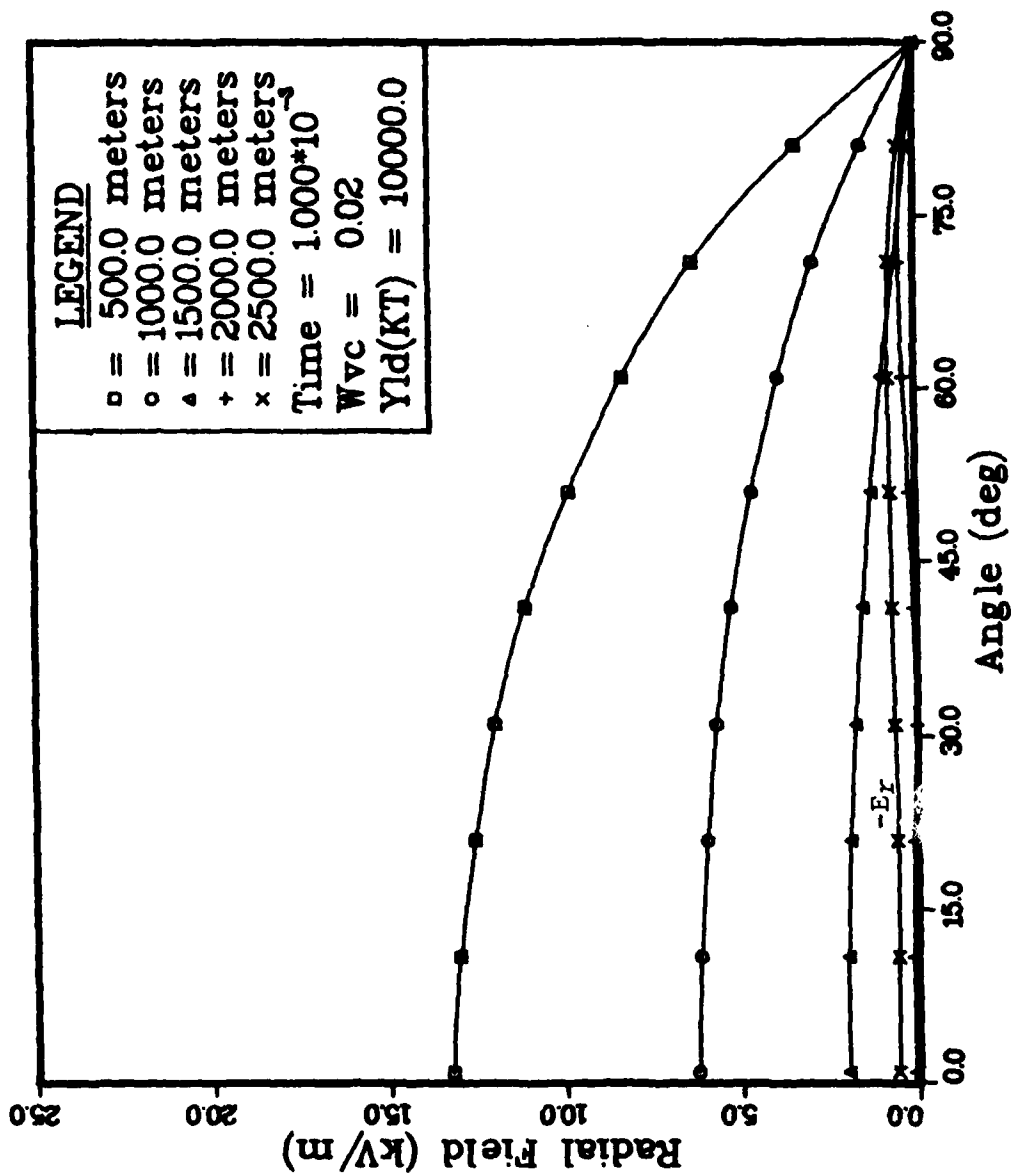


Figure 36. E_r vs Angle, Simplified Sources $\sigma_0 = 143.2$

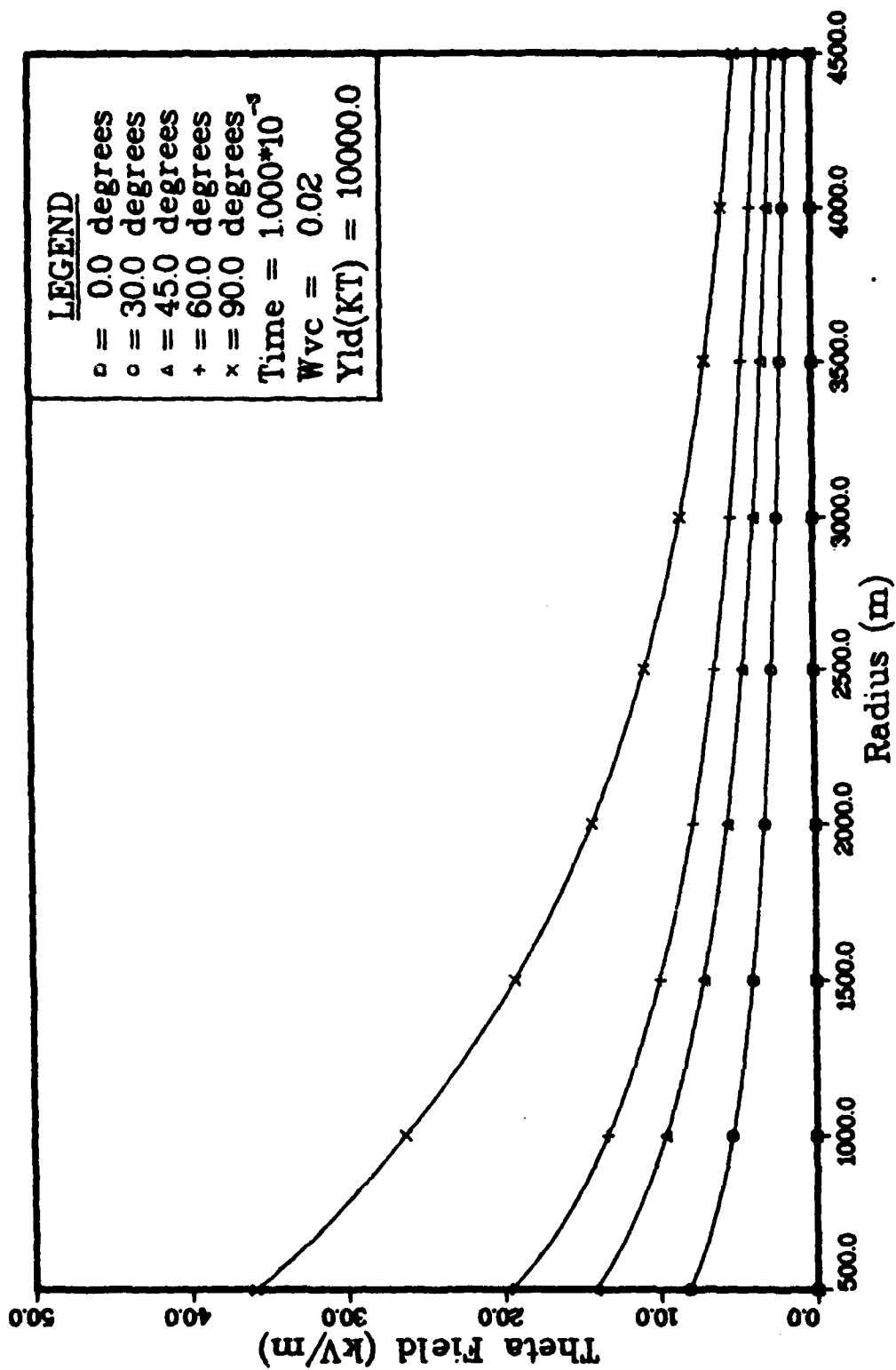


Figure 37. - E_{θ} vs Radius, Simplified Sources $\sigma_0 = 143.2$

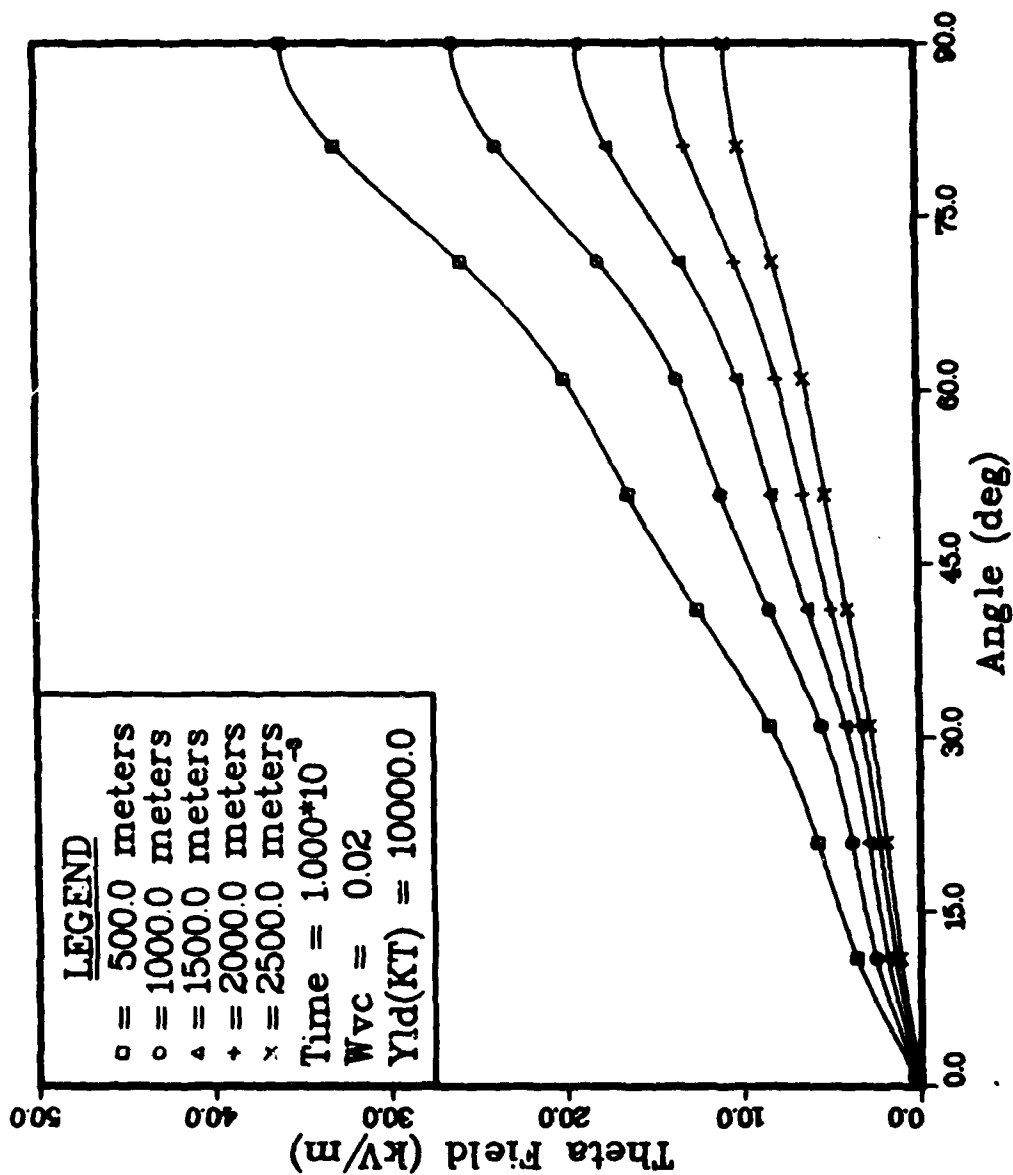


Figure 38. - E_{θ} vs Angle, Simplified Sources $\sigma_0 = 143.2$

Appendix C

Analytic Fits for Sources and
Air Chemistry Parameters

In this appendix the analytic equations for the source terms and air chemistry parameters are presented. These fits were discussed in Chapter V and were used in the calculations presented in Chapters VII and VIII.

Source Terms

The source functions are given in Table II (Ref 10:38). The symbols and units used in these formulas are as follows:

- r = radial distance from the burst (cm)
- μ = $\cos\theta$; θ = polar angle
- Y = total yield (KT)
- $N_t N_a$ = number of neutrons per kiloton
- ρ = air density (mg/cm³)
- t = time (seconds)
- $\dot{\gamma}$ = ionization rate (ion pairs/cm³·sec)
- J_r = radial current density (abamps/cm²)
- J_0 = polar (theta) current density (abamps/cm²)

In all calculations the following values were assumed:

$$N_t N_a = 2.0 \times 10^{23} \text{ neutrons/KT}$$

$$\rho = 1.225 \text{ mg/cm}^3$$

Table II

Analytic Source Functions

Ground Capture Sources

$$\dot{\gamma} = \frac{35 \rho_{YN} N_t a}{r^2} (1 + 1.30\mu) \left(1 - e^{-3.88 \times 10^{-5} \rho r} \right) e^{-3.71 \times 10^{-5} (1 - 0.33\mu) \rho r} - 8.33 \times 10^2 t$$

$$J_r = - \frac{3.9 \times 10^{-22} YN N_t a}{r^2} (1 + 16\mu) \left(1 - e^{-7.75 \times 10^{-5} \rho r} \right) e^{-2.65 \times 10^{-5} \rho r} - 8.33 \times 10^2 t$$

$$J_\theta = + \frac{8.2 \times 10^{-22} YN N_t a}{r^2} (1 - \mu) e^{-4.61 \times 10^{-5} \rho r} - 8.33 \times 10^2 t$$

Air Capture Sources

$$\dot{\gamma} = \frac{2.2 \rho_{YN} N_t a}{r^2} (1 - 0.30\mu) \left(1 - e^{-3.88 \times 10^{-5} \rho r} \right) e^{-3.43 \times 10^{-5} (1 - 0.25\mu) \rho r} - 16.7 t$$

$$J_r = - \frac{2.8 \times 10^{-23} YN N_t a}{r^2} (1 + 1.3\mu) \left(1 - e^{-2.58 \times 10^{-5} \rho r} \right) e^{-2.20 \times 10^{-5} \rho r} - 16.7 t$$

$|J_\theta| \ll |J_r|$ for all r and μ of interest.

Note also that $\dot{\gamma}$, J_r and J_0 were converted to MKS units for use in the program.

Air Chemistry Parameters

To determine the electron mobility and attachment rate, the analytic equations developed by Longley and Longmire (Ref 7) were used except for one modification. The maximum mobility for a given water vapor content was found using Smith's equation, Eq (5.1). In all cases the calculations were made using whatever units the fits were in and at the end the answers were converted to MKS units. The equations are summarized in Table III. The symbols and units used in these formulas are as follows:

- $\epsilon = E/p$ (electrostatic units/atmosphere)
- $\epsilon_0 = \text{esu/atm}$; found from $\epsilon_0 = f(\epsilon, w)$
- $w = \text{fraction of water vapor present}$
- $P = \text{percent water vapor } (P = 100 \cdot w)$
- $\mu_e = \text{electron mobility (cm/sec} \cdot \text{esu)}$
- $\rho_r = \rho_a / \rho_0 = \text{ratio of actual air density to normal}$
- $a_{3a} = \text{three-body attachment rate (sec}^{-1}\text{)}$
- $a_{2a} = \text{two-body attachment rate (sec}^{-1}\text{)}$

In all calculations the following were assumed:

$$\rho_0 = 1.255 \times 10^{-3} \text{ gm/cm}^3$$

$$1 \text{ esu} = 30,020.0 \text{ Volts/m}$$

Table III
Mobility and Attachment Rate Equations

The Mobility

$$\begin{aligned} \epsilon &\equiv E/p \text{ (esu/atmosphere)} & P &\equiv 100 \text{ w} & k &= p^{0.834} \\ \epsilon_0 &= \frac{\epsilon}{1 + Ak}, \text{ for } \epsilon \leq \epsilon_1 & A &= 2.457 \\ & & B &= 0.6884 \\ & & C &= 1.195 \\ & & \epsilon_1 &= 0.07853(1 + Ak) \\ & & \epsilon_2 &= 3.015 + Ck \\ &= \left[\sqrt{\left(\frac{Bk}{2}\right)^2 + \epsilon} - \frac{Bk}{2} \right]^2, \text{ for } \epsilon_1 \leq \epsilon \leq \epsilon_2 \\ &= \epsilon - Ck, \text{ for } \epsilon \geq \epsilon_2 \end{aligned}$$

$$\begin{aligned} \mu_a \left(\frac{\text{cm}}{\text{sec esu}} \right) &= \frac{1.0 \times 10^6}{\rho_r} \left[\frac{16.8 + \epsilon_0}{0.63 + 26.7\epsilon_0} \right]^{0.60} \\ \mu_e(\epsilon) &= \frac{\mu_a(\epsilon_0)}{1 - w + wR(\epsilon_0)} & R(\epsilon_0) &= 1.55 + \frac{210}{1 + 11.8\epsilon_0 + 7.2\epsilon_0^2} \end{aligned}$$

The Attachment Rate

three-body

$$\alpha_{3a}(\text{sec}^{-1}) = 10^8 \rho_r^2 \left[\frac{0.62 + 800\epsilon_0^2}{1 + 10^3 \epsilon_0^2 [\epsilon_0 (1 + 0.03\epsilon_0^2)]^{1/3}} \right]$$

two-body

$$\alpha_{2a}(\text{sec}^{-1}) = 1.22 \times 10^8 \rho_r e^{-21.15/\epsilon_0}$$

$$\alpha_e = (1 - w) [(1 + 34.4w)\alpha_{3a} + \alpha_{2a}]$$

Appendix D

Romberg Integration

To find the numerical integrals in the improved solution, Romberg integration was used. This method is briefly outlined below.

Romberg integration starts by using the trapezoid rule to give a first approximation to the integral. The general formula for trapezoidal integration is

$$\int_a^b f(x) dx = \frac{h}{2} \left[f(a) + f(b) + 2 \sum_{j=1}^{n-1} f(x_j) \right] + O(h^2) \quad (D-1)$$

where $h = (b-a)/n$ and $x_j = a + j \cdot h$ for each $j = 0, 1, \dots, n$. The error term is $O(h^2)$. By applying Richardson extrapolation (Ref 1:208) an improved expression is obtained which converges faster and has an error term of $O(h^4)$. The equation is

$$\int_a^b f(x) dx = \frac{4R_{k,1} - R_{k-1,1}}{3} + O(h^4) \quad (D-2)$$

The $R_{k,1}$ terms are found from

$$R_{1,1} = \frac{h_1}{2} [f(a) + f(b)] \quad (D-3)$$

where $h_1 = b-a$, and in general

$$R_{k,1} = \frac{1}{2} \left[R_{k-1,1} + h_{k-1} \sum_{i=1}^{2^{k-2}} f(a + (i - \frac{1}{2}) h_{k-1}) \right] \quad (D-4)$$

in which $h_k = \frac{1}{2} \cdot h_{k-1}$.

Finally, it can be shown that the technique is generalized to any $R_{n,n}$ such that

$$\int_a^b f(x) \approx R_{n,n} \quad (D-5)$$

where

$$R_{i,j} = \frac{4^{j-1} R_{i,j-1} - R_{i-1,j-1}}{4^{j-1} - 1} \quad (D-6)$$

for each $i = 2, 3, 4, \dots, n$ and $j = 1, 2, \dots, i$. The approximations $R_{i,j}$ can be represented as in Figure 39.

$$\begin{array}{ccccccc}
 R_{1,1} & & & & & & \\
 R_{2,1} & R_{2,2} & & & & & \\
 R_{3,1} & R_{3,2} & R_{3,3} & & & & \\
 R_{4,1} & R_{4,2} & R_{4,3} & R_{4,4} & & & \\
 & & & & \cdot & & \\
 & & & & \cdot & \cdot & \\
 & & & & & & \cdot \\
 R_{n,1} & R_{n,2} & R_{n,3} & R_{n,4} & \cdot & \cdot & \cdot \quad R_{n,n}
 \end{array}$$

Figure 39. Generalized Romberg Terms

Hence the integral is seen to converge diagonally.

Note that no predetermined step size (h) is chosen. Thus,

the integral is computed by selecting a maximum "row limit" n and determining all the terms in Figure 39 until $R_{n,n}$ is found. The method is fast because once $R_{i,1}$ is known, all other terms in the row are found using this and the value of $R_{i-1,j-1}$ from the previous row. The complete algorithm which was built into the computer program is given in Figure 40.

Romberg Algorithm

Select a positive integer n . Let $h_1 = b-a$ and perform the following:

1. Set $i = 1$ and $j = 1$. Set $R_{1,1} = \frac{h_1}{2} [f(a) + f(b)]$
2. Add 1 to i
3. If $i > n$ go to Step 9
4. Set $h_i = \frac{1}{2} \cdot h_{i-1}$. Set

$$R_{i,1} = \frac{1}{2} \left[R_{i-1,1} + h_{i-1} \sum_{k=1}^{2^{i-2}} f(a + (k-\frac{1}{2})h_{i-1}) \right]$$
5. Add 1 to j
6. If $j > i$, set $j = 1$ and go to Step 2
7. Set

$$R_{i,j} = \frac{2^{2(j-1)} R_{i,j-1} - R_{i-1,j-1}}{2^{2(j-1)} - 1}$$
8. Go to Step 5
9. The procedure is complete and $R_{n,n}$ approximates

$$\int_a^b f(x) dx$$

Figure 40. Romberg Algorithm (Ref 1:210)

Appendix E
Parametric Studies

This appendix contains the results of calculations made using the complete solution algorithm. The plots represent a series of parametric studies where the time, the yield, and the water vapor content were varied. The figures are grouped according to the parameter studied.

Time Dependence (t)

Figures 41 - 42 ; Data for $t = 10^{-2}$ sec

Figures 43 - 44 ; Data for $t = 10^{-1}$ sec

Yield Dependence (Yld)

Figures 45 - 46 ; Data for Yld = 1000 KT

Figures 47 - 48 ; Data for Yld = 100 KT

Water Vapor Content (Wvc)

Figures 49 - 50 ; Data for Wvc = 0.00

Figures 51 - 52 ; Data for Wvc = 0.04

The total field was found by taking the square root of $E_r^2 + E_0^2$.

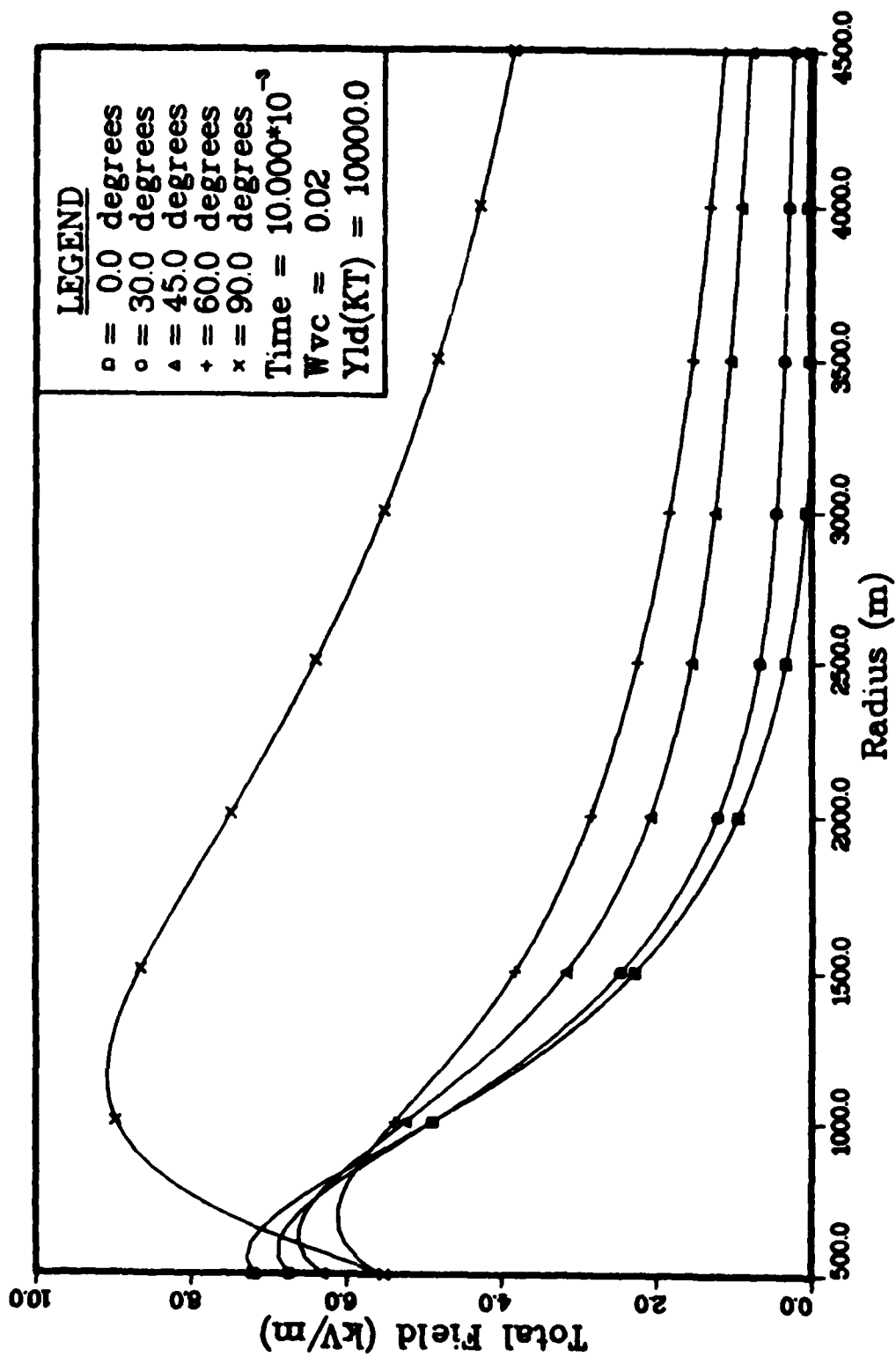


Figure 41. Total Field vs Radius, Full Solution $t = 10^{-2}$ sec

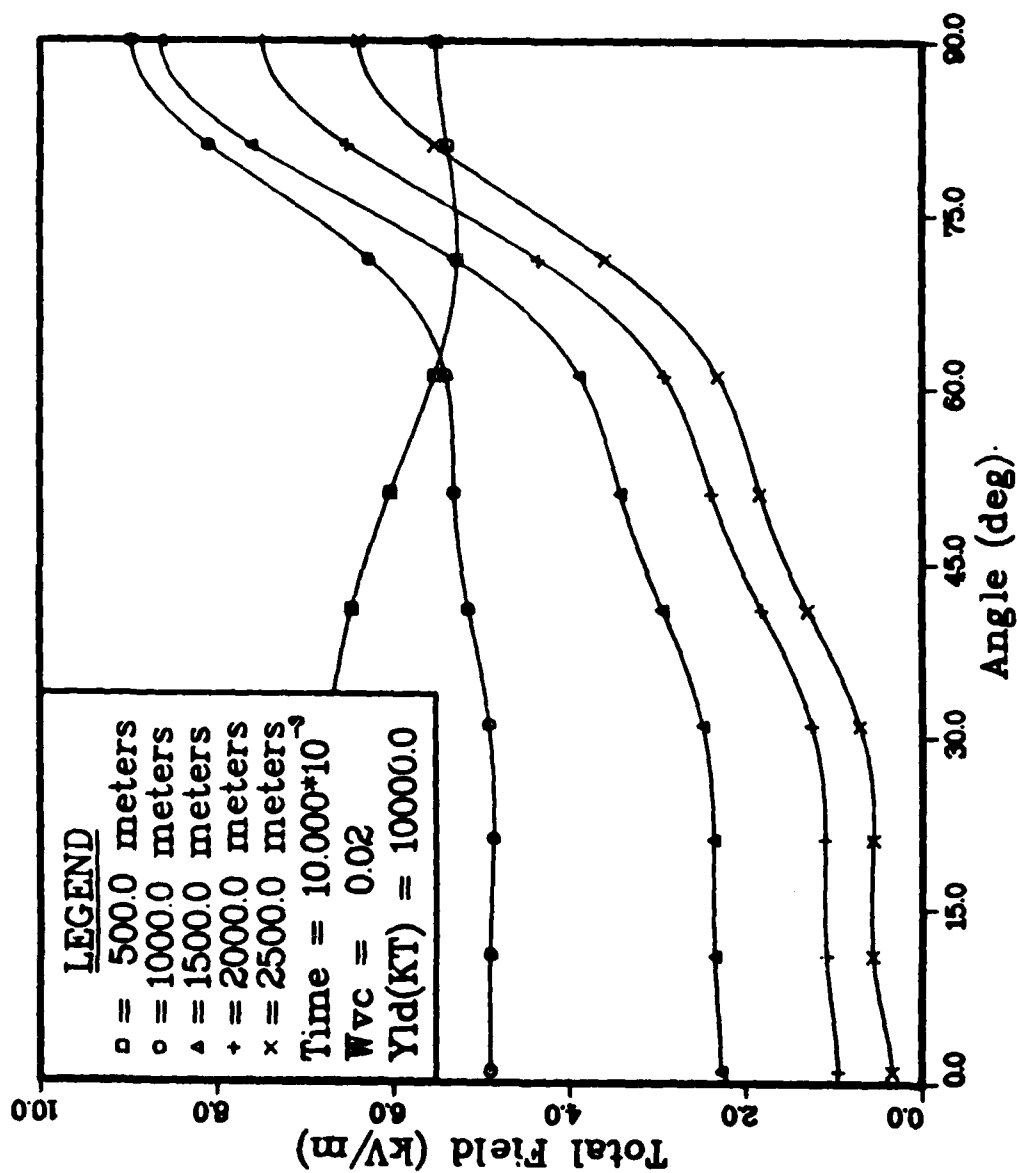


Figure 42. Total Field vs Angle, Full Solution $t = 10^{-2}$ sec

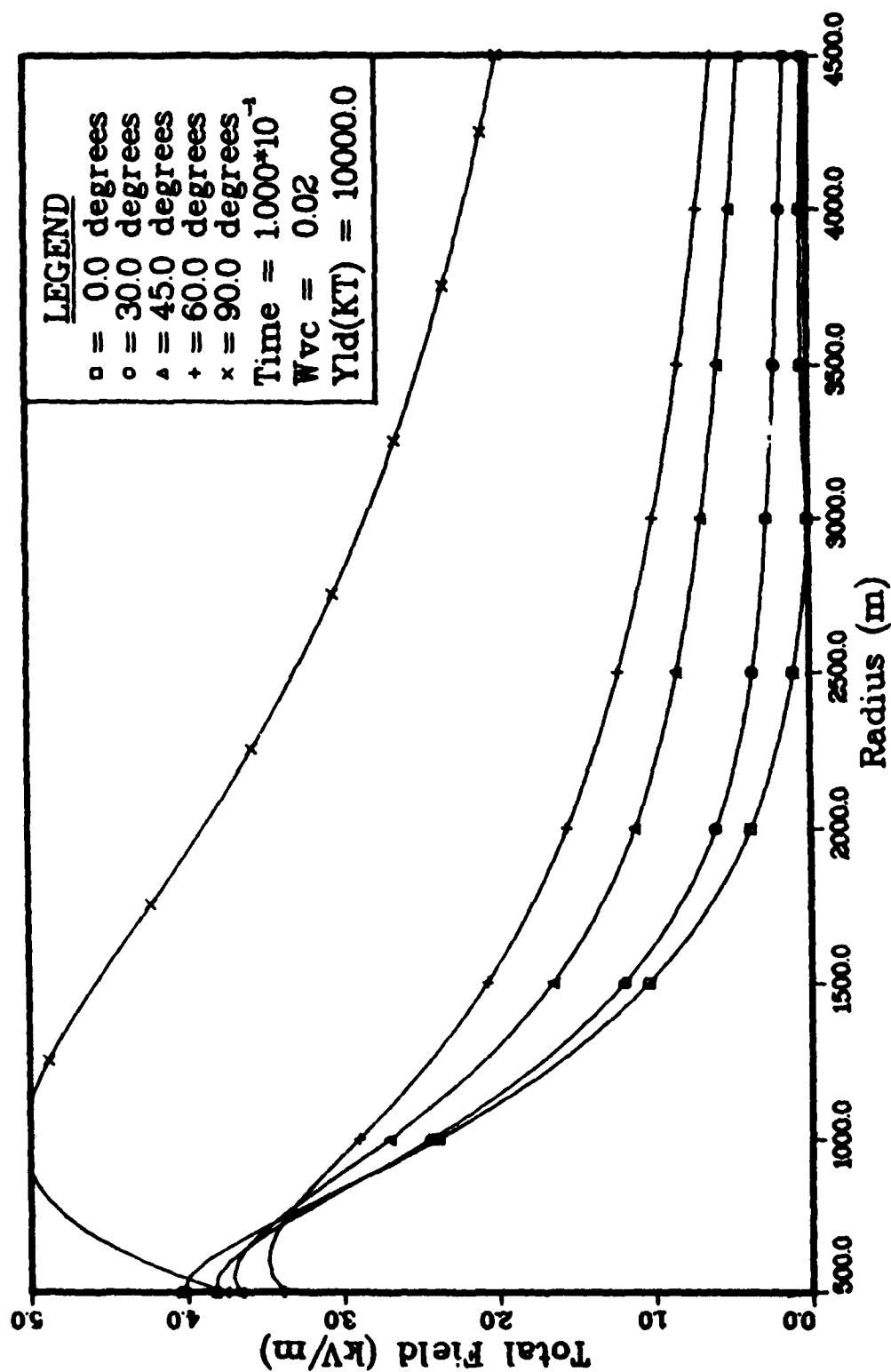


Figure 43. Total Field vs Radius, Full Solution $t = 10^{-1}$ sec

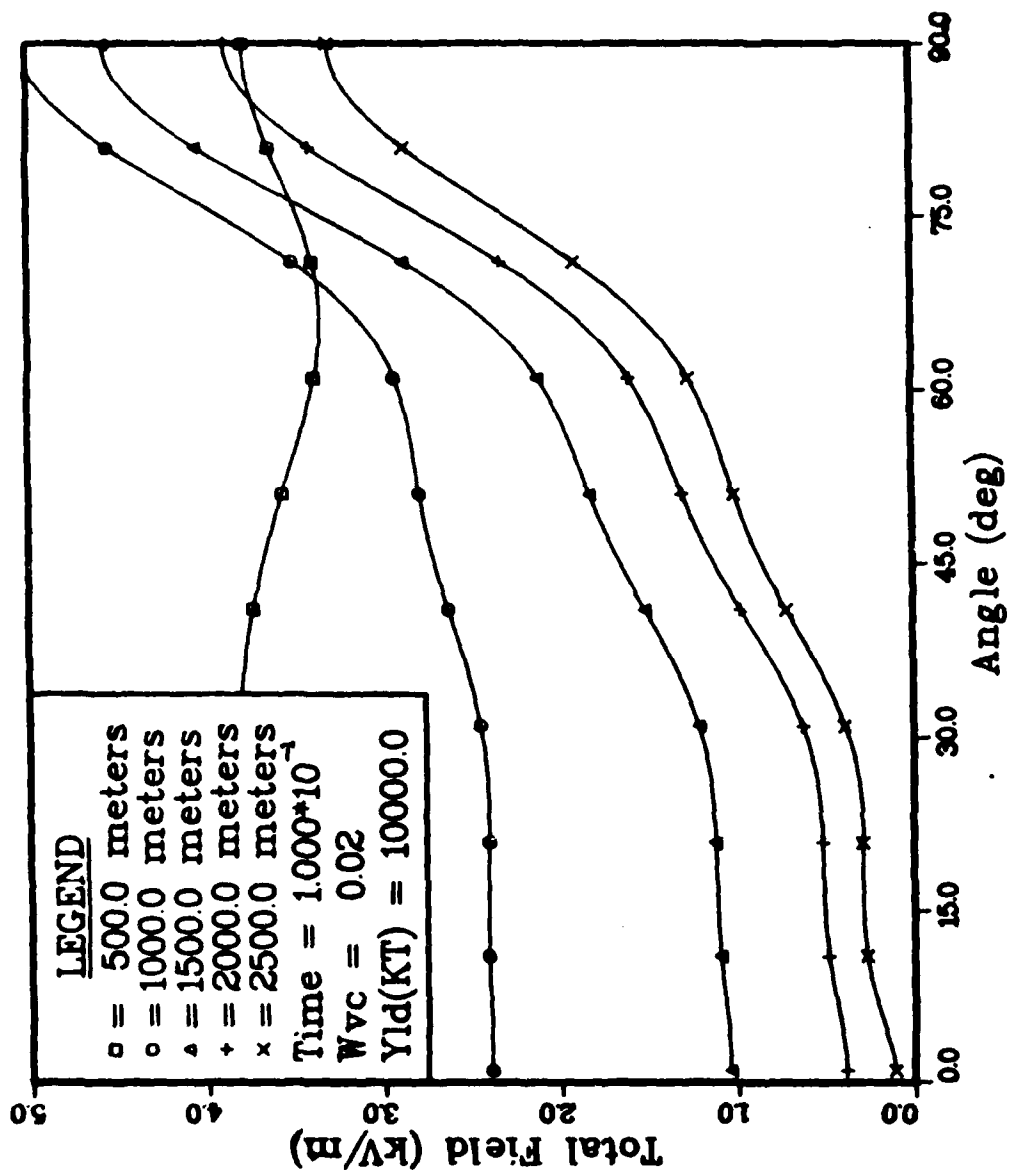


Figure 44. Total Field vs Angle, Full Solution $t = 10^{-1}$ sec

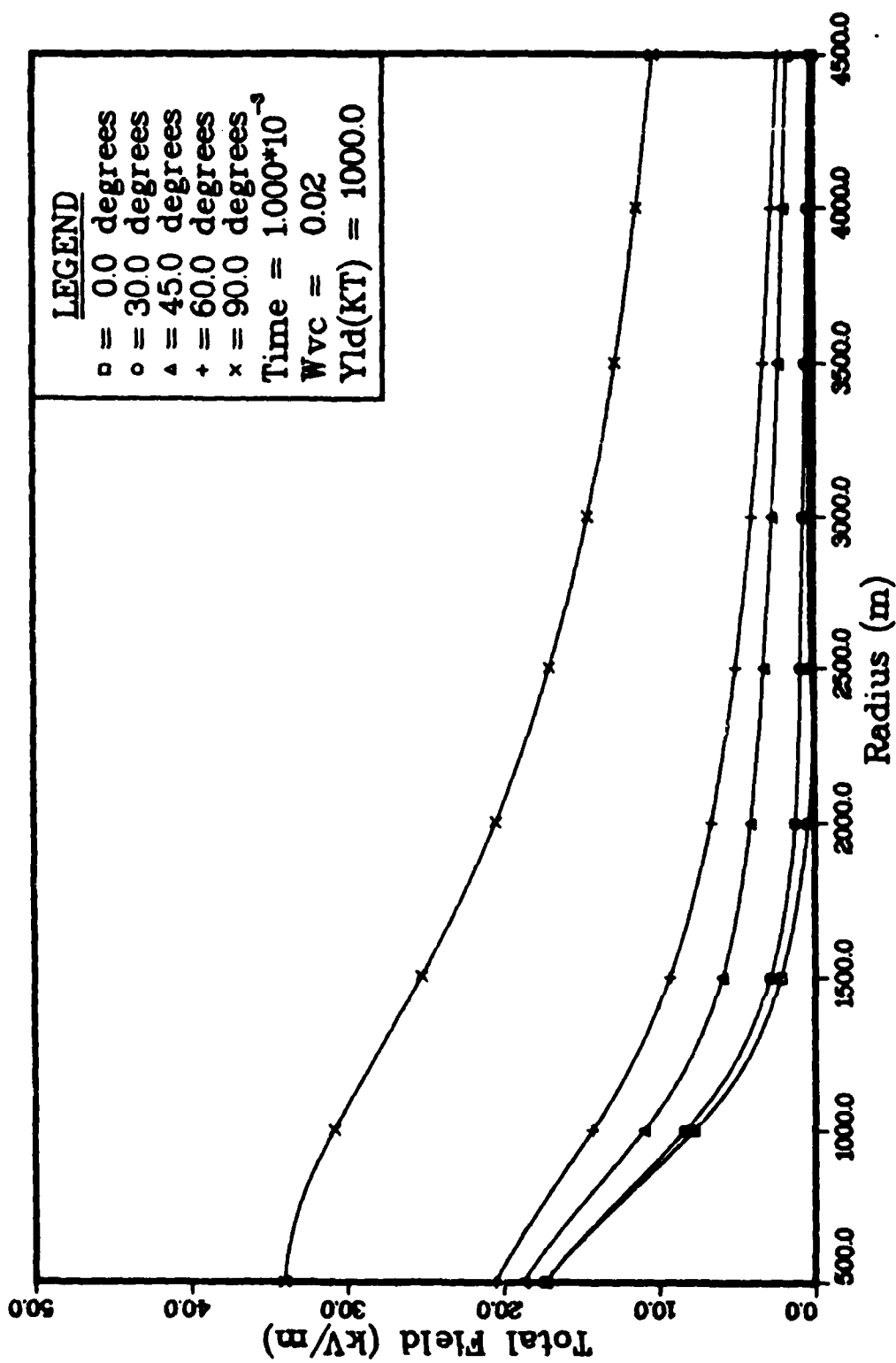


Figure 45. Total Field vs Radius, Full Solution Yld = 1000 KT

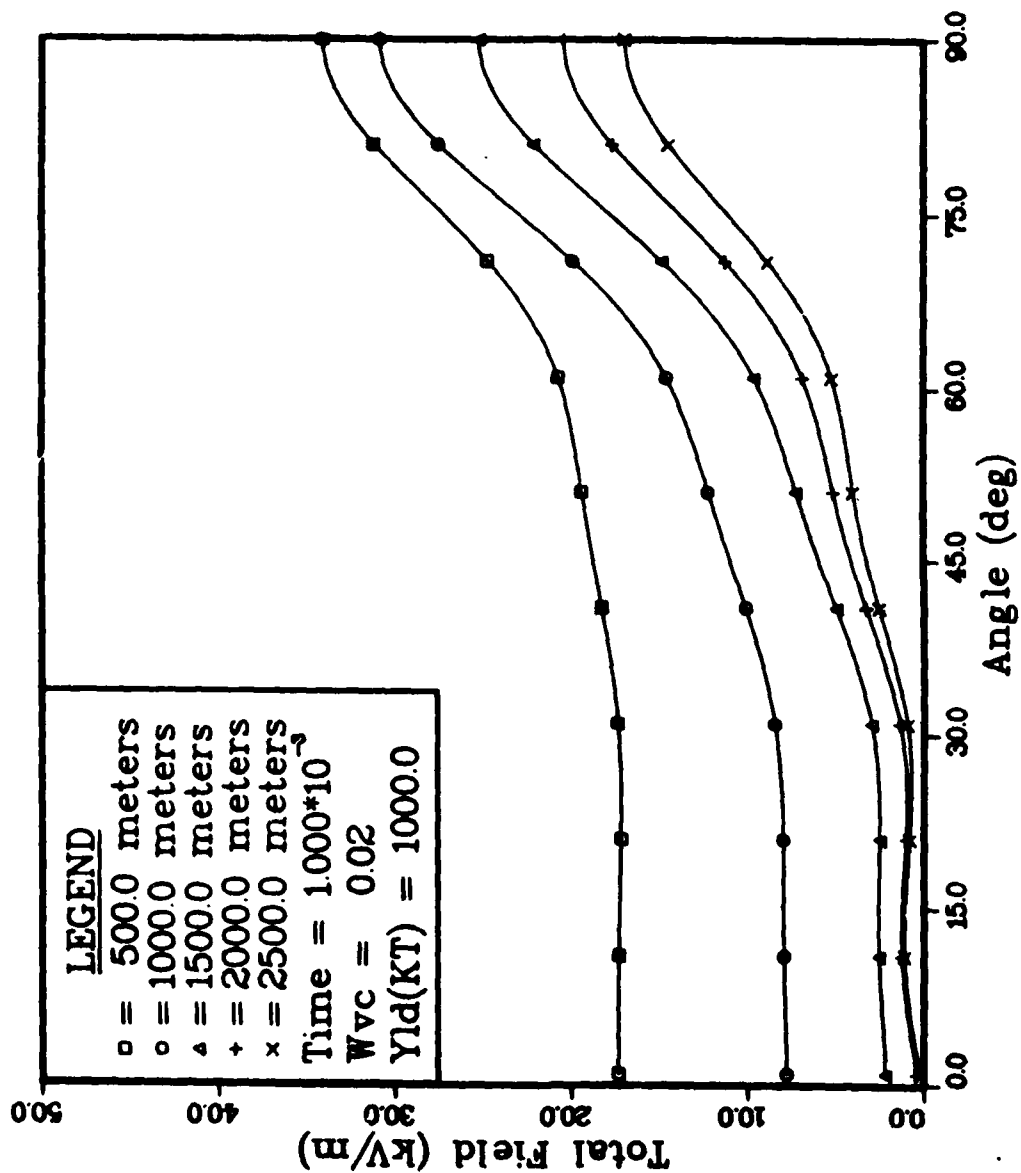


Figure 46. Total Field vs Angle, Full Solution Yld = 1000 KT

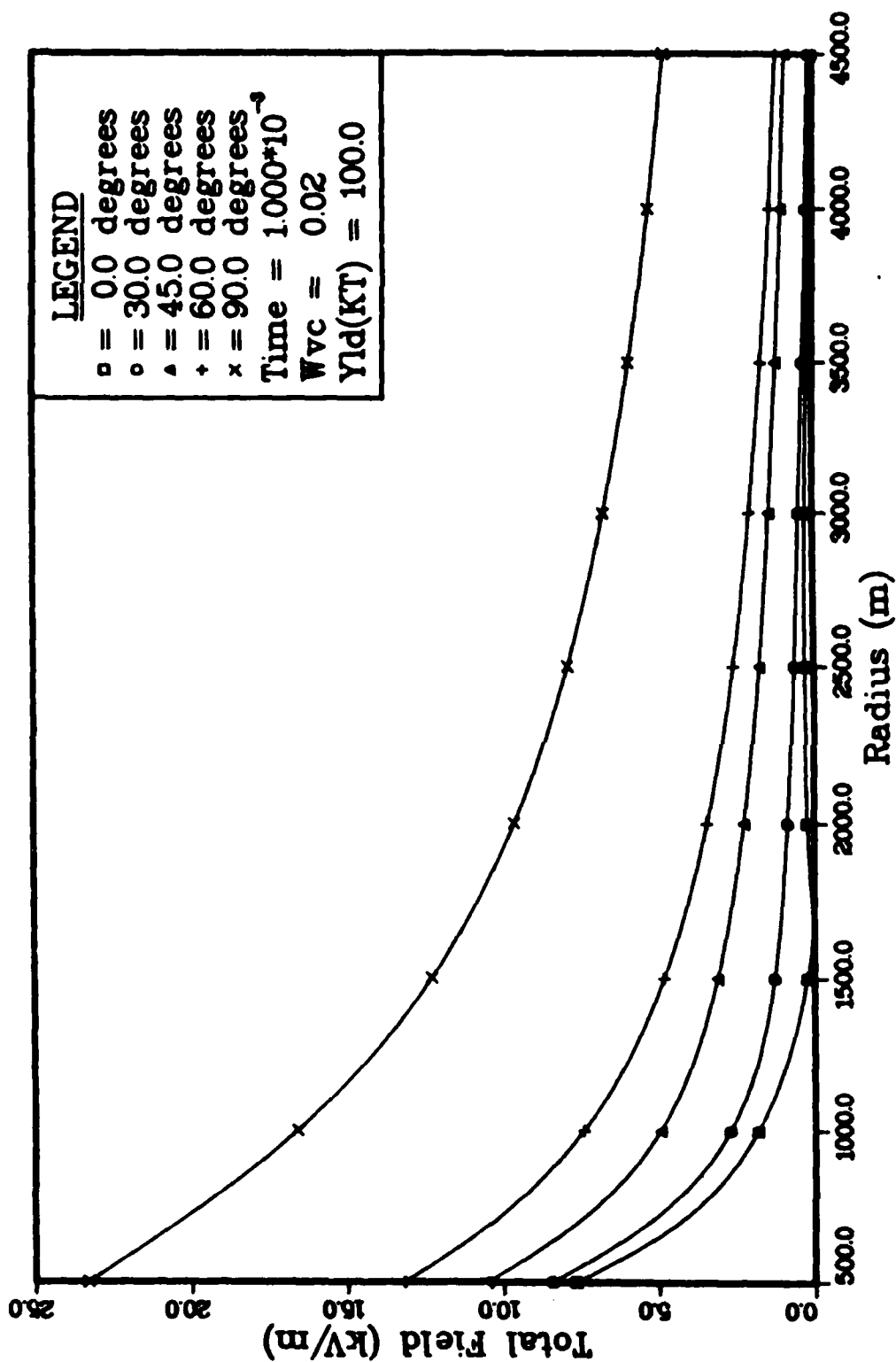


Figure 47. Total Field vs Radius, Full Solution $Yld = 100$ KT

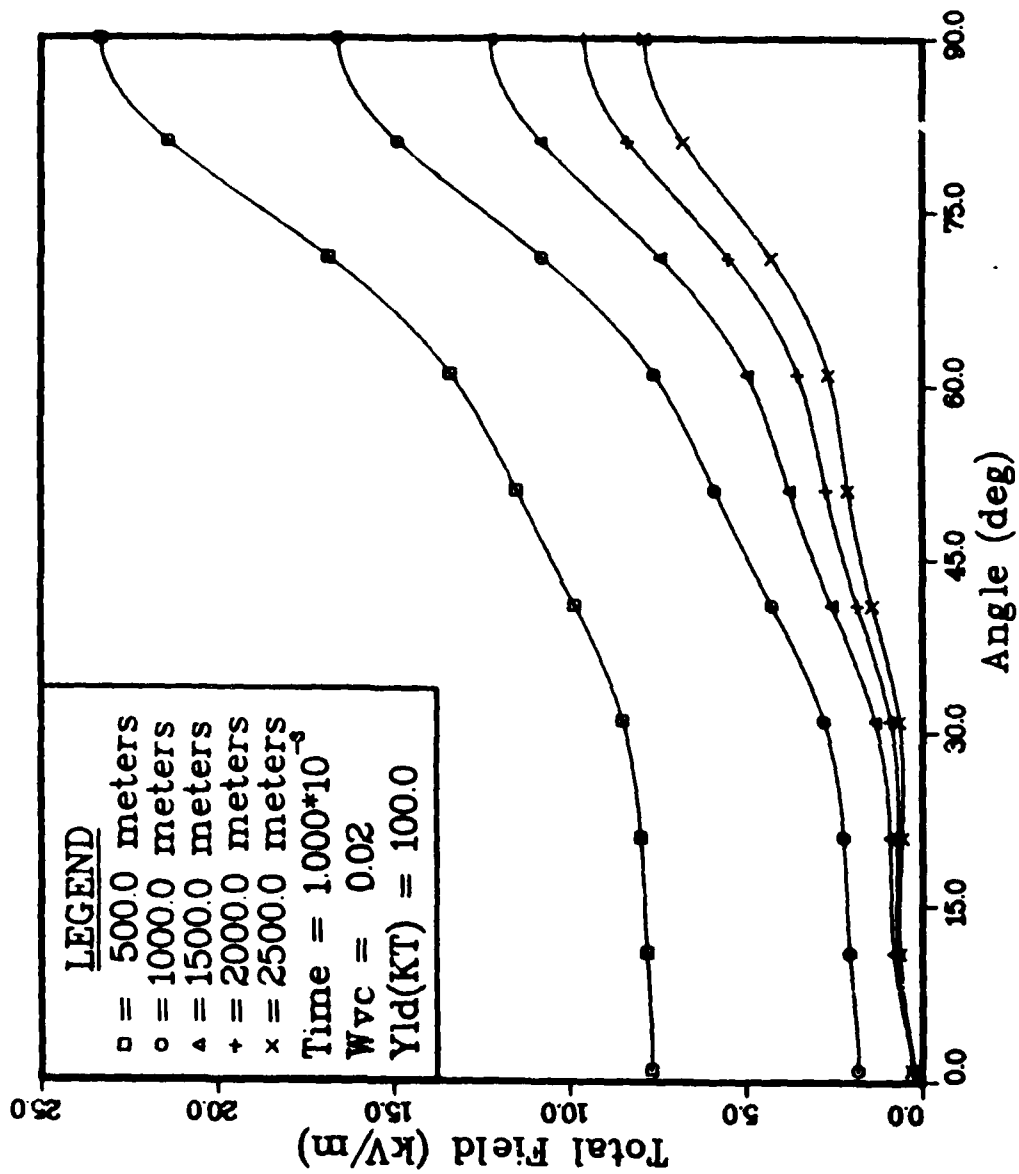


Figure 48. Total Field vs Angle, Full Solution Yld = 100 KT

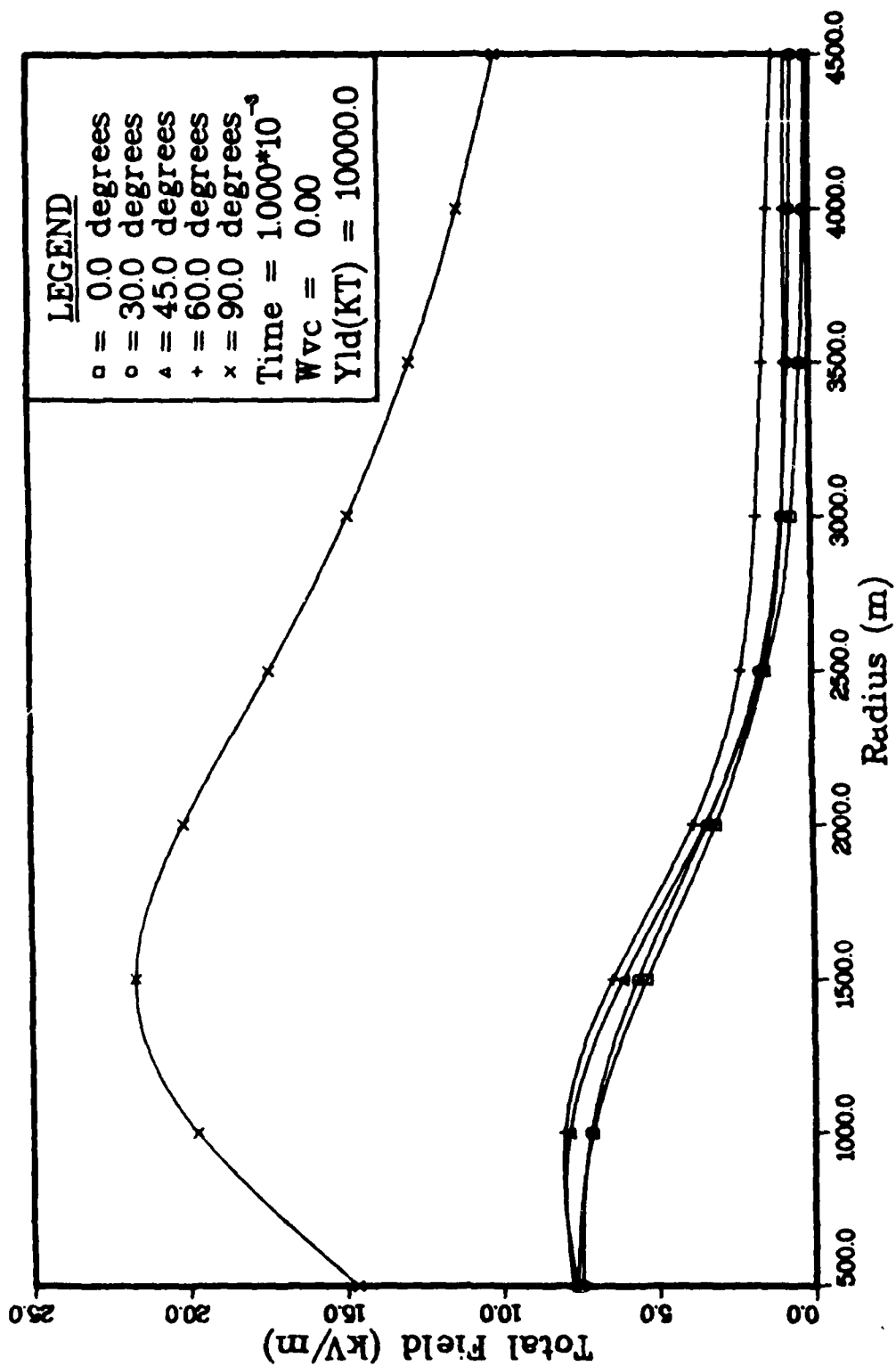


Figure 49. Total Field vs Radius, Full Solution $W_{vc} = 0.00$

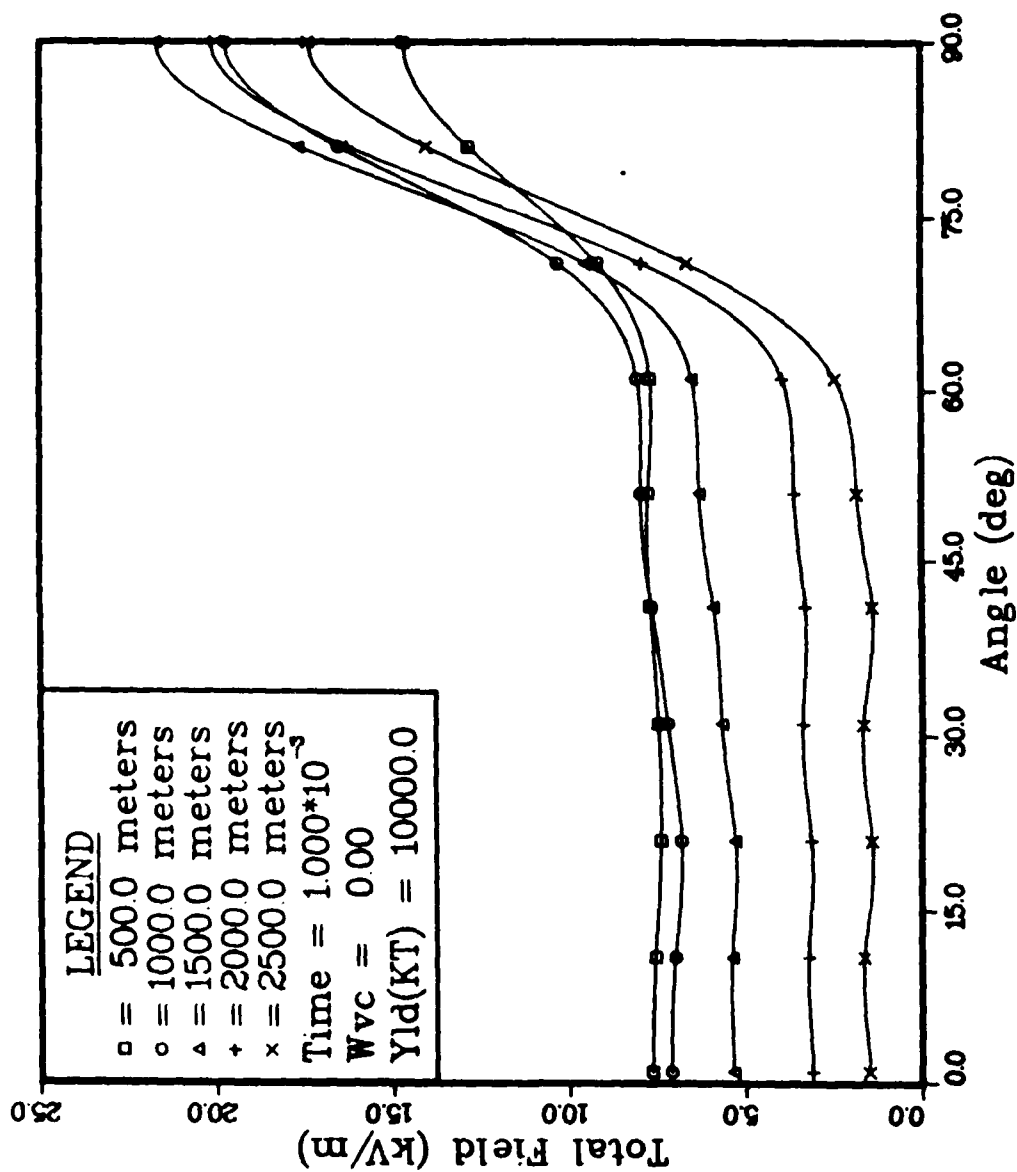


Figure 50. Total Field vs Angle, Full Solution Wvc = 0.00

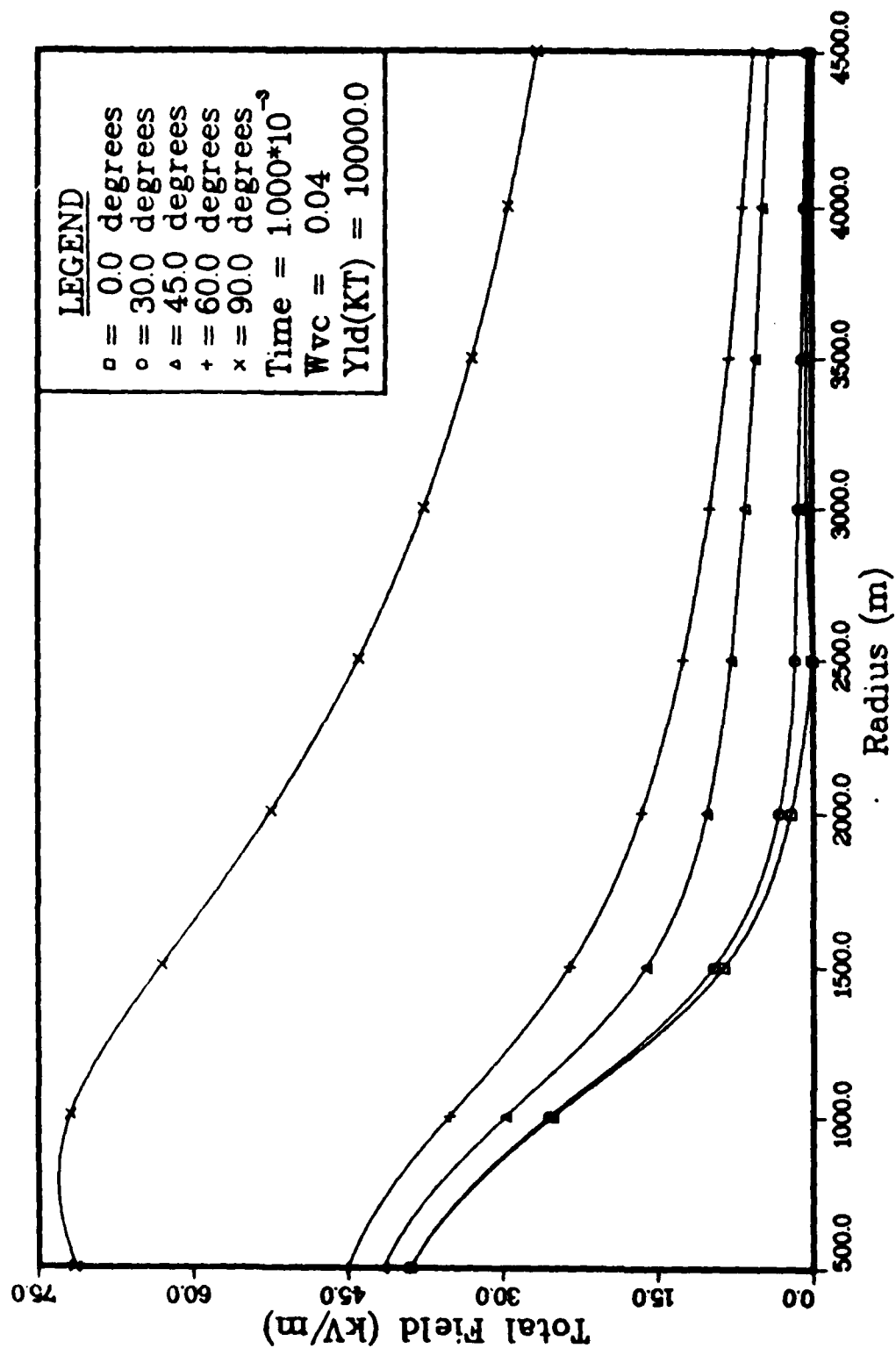
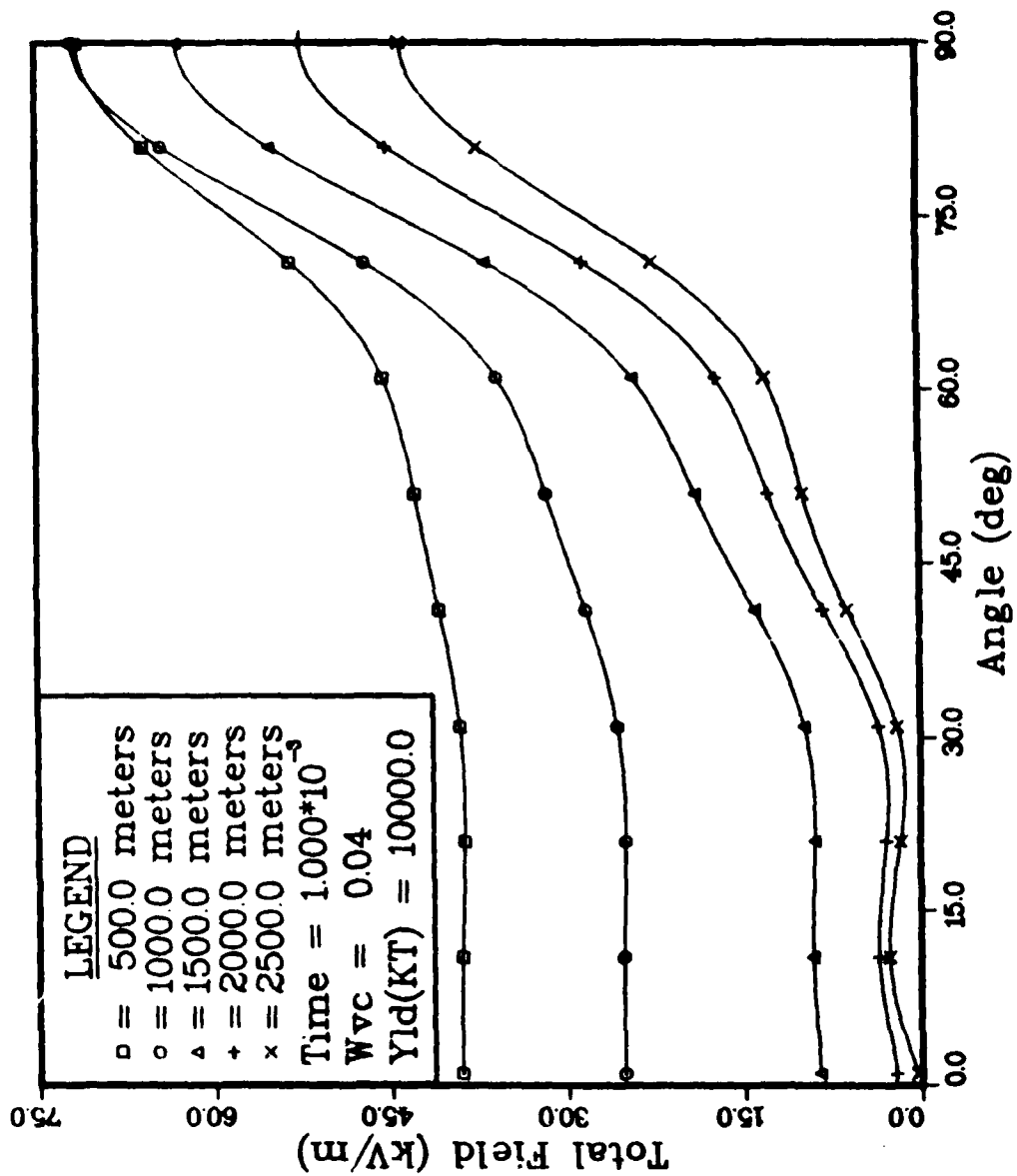


Figure 51. Total Field vs Radius, Full Solution $W_{vc} = 0.04$



Appendix F

Program Description and Listing

The program used to find the late-time EMP was written in FORTRAN V. Every effort was made to include descriptive comments and documentation. Structured programming techniques were applied and many of the calculations are made in various subroutines. The program complies with the 1977 ANSI standard and should, therefore, be transportable.

Other than possible changes in the numerical accuracy of the calculations the only input to the program is the time, the yield, the water vapor content, and the relative air density. The atmospheric pressure was taken to be one atmosphere (sea-level).

A flow diagram for the program is given in Figure 53.

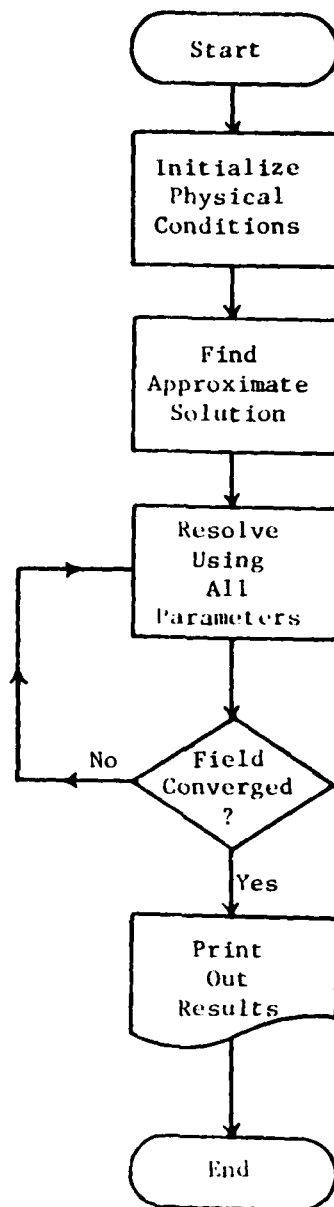


Figure 53. Program Flow Diagram

PROGRAM LTEMP

THIS PROGRAM IS DESIGNED TO FIND THE LATE TIME
ELECTRIC FIELD THAT WOULD RESULT FROM A NUCLEAR BURST.
THE PROGRAM USES FITS FOR THE IONIZATION RATE, AND THE
RADIAL AND THETA COMPTON CURRENT COMPONENTS THAT WERE
DEVELOPED BY O'DELL, LONGMIRE, AND LONGLEY FOR USE WITH
LEMP-2.

THE PROBLEM IS FIRST SOLVED BY ASSUMING NO FIELD
DEPENDENCE ON THE CONDUCTIVITY. THE TOTAL FIELD FOUND
HERE IS THEN USED AS THE INPUT TO THE FIELD DEPENDENT
CALCULATION. NOTE ALSO THAT THE INITIAL ANSWER USES A
SIMPLIFIED APPROXIMATION FOR FINDING THE LEGENDRE POLYNOMIAL
COEFFICIENTS.

VARIABLES

REAL INT1(100,7),INT2(100,7),RAD(100),SIGMA1,SIGMAC
REAL AL(7,0:102),A,B,C,E(0:100),F(0:100),THTA,JTHTAC
REAL DR,DIV,CSANG(5),TIME,WVC,TOL,OH,DT,VAL1,VAL2,VAL3
REAL ETHTA(100,5),ERAD(100,5),ETOT(100,5),ROM1(5,5,7)
REAL RHS(100,7),ROM2(5,5,7),SUM2(7),LGDRLP,ALGDRP
REAL YLD,NPKT,RDEN,LL,UL,H,ANG1,ANG2,ROM3(5,5,7)
REAL DETOT(100),NETOT(100),CTANG,SUM3(7),LVAL1,LVAL2,LVAL3
REAL JRADC,HVAL1,HVAL2,HVAL3,ANG,SUM1(7)
REAL ROM4(5,5,7,7),ROM5(5,5,7,7),SUM4(7,7),SUM5(7,7)
REAL LGPL(5,8,7),LGPL1(7),LGPL0(7),ALPL0(7),ALPL1(7)
REAL ALPL(5,8,7),LGPLS0(7),LGPLS1(7),ALPLS0(7)
REAL ALPLS1(7),ALPLS(5,8,7),LGPLS(5,8,7)
INTEGER I,J,K,NL,M,N,OL,L,COUNT,NR,MAXI,CODE
INTEGER SL,OSL

BEGIN LTEMP

INITIALIZE THE NUMBER OF RANGE POINTS, LEGENDRE
POLYNOMIALS, TIME, YIELD, AND NEUTRONS/KT.
N=100

```
C NL=5
C TIME=1.0E-3
C YLD=10000.0
C NPKT=2.0E+23
C
C ATMOSPHERIC CONDITIONS.
C RDEN=1.0
C WVC=0.02
C
C INITIALIZE 5 ANGLE VALUES (COSINE OF ANGLE).
C DATA(CSANG(I),I=1,5)/1.0,0.8660254,0.70712,0.5,0.0/
C
C SOLVE THE PROBLEM FIRST BY ASSUMING NO FIELD
C DEPENDENCE AND BY APPROXIMATING THE LEGENDRE
C COEFFICIENTS.
C
C FIND THE THETA DEPENDENT INTEGRAL TERMS IN THE
C DIFFERENTIAL EQUATION USING ROMBERG INTEGRATION.
C DR=5000.0/N
C DIV=1/DR**2
C NR=5
C LL=0.0
C UL=1.0
C DT=1.0*3.1415926/180.0
C ASSUME FIELD INDEPENDENT CONDUCTIVITY.
C CODE=1
C RAD(1)=DR
C DO 5 M=1,N
C   RAD(M)=DR*M
C   I=1
C   J=1
C   H=UL-LL
C   THTA=ACOS(0.0)
C   ANG1=ABS(COS(THTA+DT))
C   ANG2=ABS(COS(THTA-DT))
C   SIGMA1=SIGMAC(AL,0.0,DR,NL,M,WVC,TIME,YLD,NPKT,RDEN,CODE)
```

```

+      LVAL1=1/(SIGMA1*DR**2)*(SIGMAC(AL,0.0,DR,NL,M+1,WVC,TIME,  

+      YLD,NPKT,RDEN,CODE)-SIGMAC(AL,0.0,DR,NL,M-1,WVC,TIME,YLD,  

+      NPKT,RDEN,CODE))  

+      LVAL2=1/(2*DT*SIGMA1)*(SIGMAC(AL,ANG1,DR,NL,M,WVC,TIME,  

+      YLD,NPKT,RDEN,CODE)-SIGMAC(AL,ANG2,DR,NL,M,WVC,TIME,YLD,  

+      NPKT,RDEN,CODE))  

+      LVAL3=1/SIGMA1*(2/(DR*M)*JFADC(DR*M,0.0,TIME,YLD,NPKT,RDEN)+  

+      1/(2*DR)*(JRADC(DR*(M+1),0.0,TIME,YLD,NPKT,RDEN)-  

+      JRADC(DR*(M-1),0.0,TIME,YLD,NPKT,RDEN))+  

+      JTHTAC(DR*M,TIME,YLD,NPKT,RDEN/RADCM)*(1-COS(THTA))//  

+      TAN(THTA)+SIN(THTA)))  

+      THTA=ACOS(1.0)  

+      ANG1=ABS(COS(THTA+DT))  

+      ANG2=ABS(COS(THTA-DT))  

+      SIGMA1=SIGMAC(AL,1.0,DR,NL,M,WVC,TIME,YLD,NPKT,RDEN,CODE)  

+      HUAL1=1/(SIGMA1*DR**2)*(SIGMAC(AL,1.0,DR,NL,M+1,WVC,TIME,  

+      YLD,NPKT,RDEN,CODE)-SIGMAC(AL,1.0,DR,NL,M-1,WVC,TIME,YLD,  

+      NPKT,RDEN,CODE))  

+      HUAL2=1/(2*DT*SIGMA1)*(SIGMAC(AL,ANG1,DR,NL,M,WVC,TIME,  

+      YLD,NPKT,RDEN,CODE)-SIGMAC(AL,ANG2,DR,NL,M,WVC,TIME,YLD,  

+      NPKT,RDEN,CODE))  

+      HUAL3=1/SIGMA1*(2/(DR*M)*JRADC(DR*M,1.0,TIME,YLD,NPKT,RDEN)+  

+      1/(2*DR)*(JRADC(DR*(M+1),1.0,TIME,YLD,NPKT,RDEN)-  

+      JRADC(DR*(M-1),1.0,TIME,YLD,NPKT,RDEN)))  

+      DO 10 L=1,NL  

+      IF(M.EQ.1)THEN  

+        OL=2*L-1  

+        LGPL0(L)=LGDRPL(LL,OL)  

+        LGPL1(L)=LGDRPL(UL,OL)  

+        ALPL0(L)=ALGDRP(LL,OL)  

+        ALPL1(L)=ALGDRP(UL,OL)  

+      END IF  

+      ROM1(1,1,L)=H/2*(LVAL1*(LGPL0(L))*X2+  

+      HUAL1*(LGPL1(L))*X2)  

+      ROM2(1,1,L)=H/2*(LVAL2*LGPL0(L)*XALPL0(L)+  

+      HUAL2*LGPL1(L)*XALPL1(L))

```

```

10      ROM3(1,1,L)=H/2*(LVAL3*LGPL0(L)+HVAL3*LGPL1(L))
      CONTINUE
C
C
20      ITERATIVE LOOP FOR INTEGRATION.
      CONTINUE
      I=I+1
      IF(I.GT.NR) THEN
        DO 21 L=1,NL
          INT1(M,L)=ROM1(NR,NR,L)
          INT2(M,L)=ROM2(NR,NR,L)
          RHS(M,L)=ROM3(NR,NR,L)*(2*(2*L-1)+1)
21      CONTINUE
        ELSE
          OH=H
          H=OH*0.5
          DO 22 L=1,NL
            SUM1(L)=0.0
            SUM2(L)=0.0
            SUM3(L)=0.0
22      CONTINUE
          DO 23 K=1,2*(I-2)
            ANG=LL+(K-0.5)*OH
            THTA=ACOS(ANG)
            ANG1=ABS(COS(THTA+DT))
            ANG2=ABS(COS(THTA-DT))
            SIGMA1=SIGMAC(AL,ANG,DR,NL,M,WVC,TIME,YLD,NPKT,RDEN,CODE)
            VAL1=1/(SIGMA1*DR*2)*(SIGMAC(AL,ANG,DR,NL,M+1,WVC,TIME,
              YLD,NPKT,RDEN,CODE)-SIGMAC(AL,ANG,DR,NL,M-1,WVC,TIME,YLD
              ,NPKT,RDEN,CODE))*OH
            VAL2=1/(2*DT*SIGMA1)*(SIGMAC(AL,ANG1,DR,NL,M,WVC,TIME,
              YLD,NPKT,RDEN,CODE)-SIGMAC(AL,ANG2,DR,NL,M,WVC,TIME,YLD,
              NPKT,RDEN,CODE))*OH
            VAL3=1/SIGMA1*(2/(DR*M)*JRADCD(DR*M,ANG,TIME,YLD,NPKT,RDEN)
              +1/(2*DR)*JRADCD(DR*(M+1),ANG,TIME,YLD,NPKT,RDEN)-
              JRADC(DR*M)

```

```

+
      TAN(THTA)+SIN(THTA)))XOH
DO 24 L=1,NL
  IF (M.EQ.1) THEN
    LGPL(I,K,L)=LGDRPL(ANG,2XL-1)
    ALPL(I,K,L)=ALGDRP(ANG,2XL-1)
  END IF
  SUM1(L)=SUM1(L)+VAL1*LGPL(I,K,L)**2
  SUM2(L)=SUM2(L)+VAL2*LGPL(I,K,L)*ALPL(I,K,L)
  SUM3(L)=SUM3(L)+VAL3*LGPL(I,K,L)
CONTINUE
CONTINUE
DO 25 L=1,NL
  ROM1(I,1,L)=0.5*(ROM1(I-1,1,L)+SUM1(L))
  ROM2(I,1,L)=0.5*(ROM2(I-1,1,L)+SUM2(L))
  ROM3(I,1,L)=0.5*(ROM3(I-1,1,L)+SUM3(L))
CONTINUE
DO 26 J=2,I
  DO 27 L=1,NL
    ROM1(I,J,L)=((2)**(2*(J-1))*ROM1(I,J-1,L)-
      ROM1(I-1,J-1,L))/((2)**(2*(J-1))-1)
    ROM2(I,J,L)=((2)**(2*(J-1))*ROM2(I,J-1,L)-
      ROM2(I-1,J-1,L))/((2)**(2*(J-1))-1)
    ROM3(I,J,L)=((2)**(2*(J-1))*ROM3(I,J-1,L)-
      ROM3(I-1,J-1,L))/((2)**(2*(J-1))-1)
  CONTINUE
CONTINUE
GO TO 20
END IF
CONTINUE
5
C
C
  FIND COEFFICIENTS FOR A GIVEN L.
DO 30 L=1,NL
  OL=2XL-1
  F(N)=0.0
  E(N)=1.0
  DO 40 M=N,1,-1

```

```

A=DIV+1/(DR* $\text{RAD}(M)$ )+(2* $\text{OL}+1$ )/(2* $\text{DR}$ )* $\text{INT}1(M,L)$ 
B=-(2* $\text{DIV}+\text{OL}*(\text{OL}+1)/\text{RAD}(M)**2+(2*\text{OL}+1)/\text{RAD}(M)**2*\text{INT}2(M,L)$ )
C=2* $\text{DIV}-A$ 
E(M-1)=-C/(A*E(M)+B)
F(M-1)=(RHS(M,L)-A*F(M))/(A*E(M)+B)
CONTINUE
AL(L,0)=0.0
AL(L,1)=F(0)
DO 50 I=2,N
  AL(L,I)=AL(L,I-1)*E(I-1)+F(I-1)
CONTINUE
AL(L,N+1)=AL(L,N)
AL(L,N+2)=AL(L,N)
CONTINUE
30
C
C
C
  FIND THE ELECTRIC FIELD COMPONENTS AND THE MAGNITUDE
  OF THE TOTAL ELECTRIC FIELD (AT 5 DIFFERENT ANGLES).
DO 60 I=1,N
DO 70 J=1,5
  ERAD(I,J)=0.0
  ETHTA(I,J)=0.0
  DO 80 K=1,NL
    ERAD(I,J)=ERAD(I,J)-(AL(K,I+1)-AL(K,I-1))/
      (2* $\text{DR}$ )* $\text{LGDRPL}(\text{CSANG}(J),2*K-1)$ 
    ETHTA(I,J)=ETHTA(I,J)+1/ $\text{RAD}(I)$ *AL(K,I)*
       $\text{ALGDRP}(\text{CSANG}(J),2*K-1)$ 
    CONTINUE
  ETOT(I,J)= $\text{SQRT}(\text{ETHTA}(I,J)**2+\text{ERAD}(I,J)**2)$ 
  CONTINUE
CONTINUE
60
C
C
C
  NOW SOLVE THE PROBLEM BY INCLUDING THE FIELD DEPENDENCE
  OF THE CONDUCTIVITY. THE LEGENDRE COEFFICIENTS ABOVE
  SERVE AS THE FIRST GUESS (INPUT) FOR THIS PART OF THE
  PROBLEM.
CODE=0

```

```

C
C
C      CHOOSE CONVERGENCE TEST ANGLE, MAXIMUM NUMBER OF ITERATIONS,
      TOLERANCE, AND ROW LIMIT FOR ROMBERG INTEGRATION.
      CTANG=CSANG(5)
      MAXI=15
      TOL=100.0
      NR=4

C
C      FIND THE TOTAL FIELD AT ALL RANGE POINTS AND THE TEST
      ANGLE USING THE COEFFICIENTS FROM THE THETA INDEPENDENT
      CALCULATION.
      DO 90 I=1,N
        DETOT(1)=ETOT(1,5)
        CONTINUE
      90

C
C      ITERATIVE LOOP FOR FIELD DEPENDENT CALCULATION.

      COUNT=0
      CONTINUE
      COUNT=COUNT+1
      100

C
C      FIND THE THETA DEPENDENT INTEGRAL TERMS IN THE
      DIFFERENTIAL EQUATION USING ROMBERG INTEGRATION.
      DO 110 M=1,N
        I=1
        J=1
        H=UL-LL
        THTA=ACOS(0.0)
        ANG1=ABS(COS(THTA+DT))
        ANG2=ABS(COS(THTA-DT))
        SIGMA1=SIGMAC(AL,0.0,DR,NL,M,WVC,TIME,YLD,NPKT,RDEN,CODE)
        LVAL1=1/(SIGMA1*DR*2)*X(SIGMAC(AL,0.0,DR,NL,M+1,WVC,TIME,
          YLD,NPKT,RDEN,CODE)-SIGMAC(AL,0.0,DR,NL,M-1,WVC,TIME,YLD,
          NPKT,RDEN,CODE))
        LVAL2=1/(2*DT*SIGMA1)*X(SIGMAC(AL,ANG1,DR,NL,M,WVC,TIME,
          YLD,NPKT,RDEN,CODE)-SIGMAC(AL,ANG2,DR,NL,M,WVC,TIME,YLD,
          +
          +
          +

```

```

+      NPKT,RDEN, CODE))
+      LVAL3=1/SIGMAI*(2/(DR*M)*JRADC(DR*M,0.0,TIME,YLD,NPKT,RDEN)+
+      1/(2*DR)*(JRADC(DR*(M+1),0.0,TIME,YLD,NPKT,RDEN)-
+      JRADC(DR*(M-1),0.0,TIME,YLD,NPKT,RDEN)) +
+      JTHTA(C(DR*M,TIME,YLD,NPKT,RDEN)/RAD(M)*(1-COS(THTA))
+      TAN(THTA)+SIN(THTA)))
+      THTA=ACOS(1.0)
+      ANG1=ABS(COS(THTA+DT))
+      ANG2=ABS(COS(THTA-DT))
+      SIGMAI=SIGMAC(AL,1.0,DR,NL,M,WVC,TIME,YLD,NPKT,RDEN,CODE)
+      HVAL1=1/(SIGMAI*DR*Z)*(SIGMAC(AL,1.0,DR,NL,M+1,WVC,TIME,
+      YLD,NPKT,RDEN,CODE)-SIGMAC(AL,1.0,DR,NL,M-1,WVC,TIME,YLD,
+      NPKT,RDEN,CODE))
+      HVAL2=1/(2*DT*SIGMAI)*(SIGMAC(AL,ANG1,DR,NL,M,WVC,TIME,
+      YLD,NPKT,RDEN,CODE)-SIGMAC(AL,ANG2,DR,NL,M,WVC,TIME,YLD,
+      NPKT,RDEN,CODE))
+      HVAL=1/SIGMAI*(2/(DR*M)*JRADC(DR*M,1.0,TIME,YLD,NPKT,RDEN)+
+      1/(2*DR)*(JRADC(DR*(M+1),1.0,TIME,YLD,NPKT,RDEN)-
+      JRADC(DR*(M-1),1.0,TIME,YLD,NPKT,RDEN)))
+      DO 120 L=1,NL
+      ROM1(1,1,L)=H/2*(LVAL1*(LGPL0(L))*2+
+      HVAL1*(LGPL1(L))*2)
+      ROM2(1,1,L)=H/2*(LVAL2*LGPL0(L)*ALPL0(L)+
+      HVAL2*LGPL1(L)*ALPL1(L))
+      ROM3(1,1,L)=H/2*(LVAL3*LGPL0(L)+HVAL3*LGPL1(L))
+      DO 121 SL=1,NL
+      IF(M.EQ.1.AND.COUNT.EQ.1) THEN
+      OSL=2*SL-1
+      LGPLS0(SL)=LGDRPL(LL,OSL)
+      LGPLS1(SL)=LGDRPL(UL,OSL)
+      ALPLS0(SL)=ALGDRP(LL,OSL)
+      ALPLS1(SL)=ALGDRP(UL,OSL)
+      END IF
+      IF(SL.EQ.L) THEN
+      ROM4(1,1,L,SL)=0.0
+      ROM5(1,1,L,SL)=0.0

```

```

ELSE
  ROM4(1,1,L,SL)=H/2*(L*VAL1*LGPL0(L)*LGPLS0(SL)+
    + HVAL1*LGPL1(L)*LGPLS1(SL))
  ROM5(1,1,L,SL)=H/2*(L*VAL2*ALPLS0(SL)*LGPL0(L)+
    + HVAL2*ALPLS1(SL)*LGPL1(L))
  END IF
  CONTINUE
CONTINUE
C
C ITERATIVE LOOP FOR INTEGRATION.
CONTINUE
I=I+1
IF(1.6T.NR) THEN
  DO 140 L=1,NL
    INT1(M,L)=ROM1(NR,NR,L)
    INT2(M,L)=ROM2(NR,NR,L)
    RHS(M,L)=ROM3(NR,NR,L)
    DO 141 SL=1,NL
      RHS(M,L)=RHS(M,L)-1/(2*DR)*AL(SL,M+1)-AL(SL,M-1))*
        + ROM4(NR,NR,L,SL)+1/RAD(M)**2*AL(SL,M)*ROM5(NR,NR,L,SL)
    CONTINUE
  CONTINUE
ELSE
  OH=H
  H=OH*0.5
  DO 150 L=1,NL
    SUM1(L)=0.0
    SUM2(L)=0.0
    SUM3(L)=0.0
    DO 151 SL=1,NL
      SUM4(L,SL)=0.0
      SUM5(L,SL)=0.0
    CONTINUE
  CONTINUE
  DO 160 K=1,2*(I-2)
    ANG=LL+(K-0.5)*OH

```

```

      THTA=ACOS(ANG)
      ANG1=ABS(COS(THTA+DT))
      ANG2=ABS(COS(THTA-DT))
      SIGNH1=SIGNH(VAL,ANG,DR,NL,M,WVC,TIME,YLD,NPFT,RCEN,CODE)
      VAL1=1+(SIGNH1*DR*2)*SIGNH(VAL,HVS,1,1,NL,M+1,WVC,TIME,
      YLD,NPFT,RCEN,CODE)-SIGNH(VAL,HVS,DR,NL,M+1,WVC,TIME,
      NPFT,RCEN,CODE)*OH
      VAL2=1+(2*DT)*SIGNH1*(SIGNH(VAL,HVS,1,1,NL,M,WVC,TIME,
      YLD,NPFT,RCEN,CODE)-SIGNH(VAL,HVS,DR,NL,M,WVC,TIME,
      NPFT,RCEN,CODE))*OH
      VAL3=1+(SIGNH1*(2*(DR*M)*JFAC(DR*M)+JFAC(DR*M)+JFAC(
      +1/(2*DR)*JFAC(DR*(M+1)+ANG,TIME,YLD,NPFT,RCEN,
      JFAC(DR*(M+1)+ANG,TIME,YLD,NPFT,RCEN))*
      JFAC(DR*M,TIME,YLD,NPFT,RCEN)+RAD(1-COS(THTA))
      TAN(THTA)+SIN(THTA))*OH
      DO 170 L=1,NL
        SUM1(L)=SUM1(L)+VAL1*LGPL(I,K,L)**2
        SUM2(L)=SUM2(L)+VAL2*LGPL(I,K,L)*HLPL(I,K,L)
        SUM3(L)=SUM3(L)+VAL3*LGPL(I,K,L)
      DO 171 SL=1,NL
        IF(M.EQ.1.AND.COUNT.EQ.1)THEN
          LGPLS(I,K,SL)=LGDRPL(ANG,2*SL-1)
          ALPLS(I,K,SL)=ALGDRP(ANG,2*SL-1)
        END IF
        SUM4(L,SL)=SUM4(L,SL)+VAL1*LGPL(I,K,L)*
          LGPLS(I,K,SL)
        SUM5(L,SL)=SUM5(L,SL)+VAL2*LGPL(I,K,L)*
          ALPLS(I,K,SL)
      CONTINUE
      CONTINUE
      CONTINUE
      DO 180 L=1,NL
        ROM1(I,1,L)=0.5*(ROM1(I-1,1,L)+SUM1(L))
        ROM2(I,1,L)=0.5*(ROM2(I-1,1,L)+SUM2(L))
        ROM3(I,1,L)=0.5*(ROM3(I-1,1,L)+SUM3(L))
      DO 181 SL=1,NL

```

171
170
160

```

181 IF(SL.EQ.L) THEN
180   ROM4(I,1,L,SL)=0.0
      ROM5(I,1,L,SL)=0.0
      ELSE
        ROM4(I,1,L,SL)=0.5*(ROM4(I-1,1,L,SL)+SUM4(L,SL))
        ROM5(I,1,L,SL)=0.5*(ROM5(I-1,1,L,SL)+SUM5(L,SL))
      END IF
      CONTINUE
      DO 190 J=2,I
        DO 200 L=1,NL
          ROM1(I,J,L)=((2)**(2*(J-1))*ROM1(I,J-1,L)-
            ROM1(I-1,J-1,L))/((2)**(2*(J-1))-1)
          ROM2(I,J,L)=((2)**(2*(J-1))*ROM2(I,J-1,L)-
            ROM2(I-1,J-1,L))/((2)**(2*(J-1))-1)
          ROM3(I,J,L)=((2)**(2*(J-1))*ROM3(I,J-1,L)-
            ROM3(I-1,J-1,L))/((2)**(2*(J-1))-1)
          DO 201 SL=1,NL
            ROM4(I,J,L,SL)=((2)**(2*(J-1))*ROM4(I,J-1,L,SL)-
              ROM4(I-1,J-1,L,SL))/((2)**(2*(J-1))-1)
            ROM5(I,J,L,SL)=((2)**(2*(J-1))*ROM5(I,J-1,L,SL)-
              ROM5(I-1,J-1,L,SL))/((2)**(2*(J-1))-1)
          END IF
        CONTINUE
      CONTINUE
      GO TO 130
    END IF
  CONTINUE
110
C
C
      FIND COEFFICIENTS FOR A GIVEN L.
      DO 210 L=1,NL
        OL=2*L-1
        F(N)=0.0
        E(N)=1.0
        DO 220 M=N,1,-1
          A=DIV+1/(DR*RAD(M))+(2*OL+1)/(2*DR)*INT1(M,L)

```

```

      B=- (2*DIV+OL*(OL+1)/RAD(M)**2+(2*OL+1)/RAD(M)**2*INT2(M,L))
      C=2*DIV-A
      E(M-1)=-C/(A+E(M)+B)
      F(M-1)=-((2*OL+1)*RHS(M,L)-A*F(M))/(A+E(M)+B)
220    CONTINUE
      AL(L,0)=0.0
      AL(L,1)=F(0)
      DO 230 I=2,N
        AL(L,I)=AL(L,I-1)*E(I-1)+F(I-1)
230    CONTINUE
      AL(L,N+1)=AL(L,N)
      AL(L,N+2)=AL(L,N)
210    CONTINUE

C
C
C      FIND THE VALUE OF THE TOTAL FIELD AT ALL RANGE POINTS AND
      THE SPECIFIED ANGLE AND CHECK FOR GOODNESS OF FIT.
      DO 240 I=1,N
        NETOT(I)=ETOTC(AL,CTANG,DR,NL,I)
240    CONTINUE
      DC 250 I=5,N
        IF (ABS(NETOT(I)-OETOT(I)).LE.TOL) THEN
          ELSE
            DO 260 J=1,N
              OETOT(J)=NETOT(J)
              CONTINUE
            IF (COUNT.LT.MAXI) THEN
              GO TO 100
            END IF
          END IF
        CONTINUE
250    CONTINUE

C
C
C      FIND THE ELECTRIC FIELD COMPONENTS AND THE MAGNITUDE
      OF THE TOTAL ELECTRIC FIELD (AT 5 DIFFERENT ANGLES).
      DO 270 I=1,N
        DO 280 J=1,5
          ERAD(I,J)=0.0

```

```

      ETHTA(I,J)=0.0
      DO 290 K=1,NL
        ERAD(I,J)=ERAD(I,J)-(AL(K,I+1)-AL(K,I-1))/
          (2*DR)*LGORPL(CSANG(J),2*K-1)
        ETHTA(I,J)=ETHTA(I,J)+1/RAD(I)*AL(K,I)*
          ALGORPL(CSANG(J),2*K-1)
      CONTINUE
      ETOT(I,J)=SORT(ETHTA(I,J)**2+ERAD(I,J)**2,
      CONTINUE
      CONTINUE
      CONTINUE
      PRINT OUT RESULTS.
      PRINT 300,TIME
      FORMAT(///,28X,'TIME =',1X,1P1E13.4,/)
      PRINT 310,WVC
      FORMAT(28X,'WVC =',1X,F5.2,/)
      PRINT 320,YLD
      FORMAT(28X,'YIELD(KT) =',1X,F9.2,/)
      PRINT 330,COUNT
      FORMAT(28X,'NO. ITERATIONS =',1X,I3,/)
      IF(NL.EQ.5)THEN
        PRINT 340
        FORMAT(26X,'POLYNOMIAL COEFFICIENTS',/)
        PRINT 350
        FORMAT(4X,'RP',7X,'A1',11X,'A3',11X,'A5',11X,'A7',11X,'A9',/)
        DO 360 I=0,N,5
          PRINT 370,I,(AL(J,I),J=1,NL)
          FORMAT(3X,I3,2X,1P5E13.4)
        CONTINUE
      END IF
      PRINT 380
      FORMAT(/,32X,'RADIAL FIELD',/)
      PRINT 390
      FORMAT(4X,'RP',7X,'0',11X,'20',11X,'45',11X,'60',11X,'90',/)
      DO 400 I=5,N,5

```

```

410 PRINT 410,I,(ERAD(I,J),J=1,5)
400 FORMAT(3X,13,2X,1P5E13.4)
CONTINUE
420 PRINT 420
FORMAT(/,32X,'THETA FIELD',/)
430 PRINT 430
FORMAT(4X,'RP',7X,' 0',11X,'20',11X,'45',11X,'60',11X,'90',/)
DO 440 I=5,N,5
450 PRINT 450,I,(ETHA(I,J),J=1,5)
440 FORMAT(3X,13,2X,1P5E13.4)
CONTINUE
460 PRINT 460
FORMAT(/,32X,'TOTAL FIELD',/)
470 PRINT 470
FORMAT(4X,'RP',7X,' 0',11X,'20',11X,'45',11X,'60',11X,'90',/)
DO 480 I=5,N,5
490 PRINT 490,I,(ETOT(I,J),J=1,5)
480 FORMAT(3X,13,2X,1P5E13.4)
CONTINUE
501 PRINT 501
FORMAT(///)
END

C REAL FUNCTION INZRTC(RAD,CSANG,TIME,YLD,NPKT,RDEN)
C
C THIS FUNCTION GIVES THE IONIZATION RATE FOR
C ANY RADIUS, ANGLE, TIME, YIELD, NO. OF NEUTRONS/KT,
C AND RELATIVE AIR DENSITY.
C
C VARIABLES
C REAL RAD,RADC,CSANG,TIME,YLD,NPKT
C REAL RDEN,RHO,GCS,ACS
C BEGIN INZRTC
C IF(ABS(RAD-0.001).LE.0.001)THEN

```

```

RAD=0.001
END IF
RHO=RDEN*1.225
RADC=RAD*100
GCS=35.0*PHO*(LD*NPKT/(RADC)**2*(1+1.3*CSANG))*
  (1-EXP(-3.88E-5*RHO*RADC))*EXP(-3.71E-5*(1-0.33*
  CSANG)*RHO*RADC-8.33E+2*TIME)
ACS=2.2*RHO*(LD*NPKT/(RADC)**2*(1-0.3*CSANG))*
  (1-EXP(-3.88E-5*RHO*RADC))*EXP(-3.43E-5*(1-0.25*
  CSANG)*RHO*RADC-16.7*TIME)
INZRTC=(GCS+ACS)*1.0E+6
END

```

```

REAL FUNCTION JRADC(RAD,CSANG,TIME,YLD,NPKT,RDEN)

```

THIS FUNCTION GIVES THE RADIAL CURRENT FOR
ANY RADIUS, ANGLE, TIME, YIELD, NO. OF NEUTRONS/KT,
AND RELATIVE AIR DENSITY.

```

VARIABLES

```

```

REAL RAD,RADC,CSANG,TIME,YLD,NPKT
REAL RDEN,RHO,GCS,ACS

```

```

BEGIN JRADC

```

```

IF (ABS(RAD-0.001).LE.0.001) THEN

```

```

RAD=0.001

```

```

END IF

```

```

RHO=RDEN*1.225

```

```

RADC=RAD*100.0

```

```

GCS=3.9E-22*YLD*NPKT/(RADC)**2*(1+16*CSANG)*

```

```

  (1-EXP(-7.75E-5*RHO*RADC))*EXP(-2.65E-5*RHO*RADC-
  8.33E+2*TIME)

```

```

ACS=2.8E-23*YLD*NPKT/(RADC)**2*(1+1.3*CSANG)*

```

```

  (1-EXP(-2.58E-5*RHO*RADC))*EXP(-2.2E-5*RHO*RADC-
  16.7*TIME)

```



```

C
C
C
      BEGIN ETOTC
      ETOTC=SQRT((ERADC(AL,CSANG,DR,NL,I))**2+
+      (ETHTAC(AL,CSANG,DR,NL,I))**2)
      END
C
      REAL FUNCTION SIGMAC(AL,CSANG,DR,NL,I,WVC,TIME,YLD,NPKT,
+      RDEN,CODE)
C
C      THIS FUNCTION GIVES THE CONDUCTIVITY AT ANY RADIUS AND
C      ANGLE VALUE. THE WATER VAPOR CONTENT AND TOTAL FIELD EFFECTS
C      ARE INCLUDED.
C
C      VARIABLES
      REAL AL(7,0:102),CSANG,DR,WVC,TIME,YLD,NPKT
      REAL RDEN,MUI,MUE,MUA,KA,KN,ARGE,AC,BC,CC,KC
      REAL PWVC,EPS0,ESU,EP51,EP52,KA3,KA2,R
      REAL MUEMAX,INZRT,INZRTC,ETOTC
      INTEGER I,NL,CODE
C
      BEGIN SIGMAC
C
      IF(CODE.EQ.1)THEN
        FIELD INDEPENDENT CONDUCTIVITY.
        MUE=0.25
        MUI=2.5E-4
        KA=1.5E+8
        KN=2.0E-12
        INZRT=INZRTC(IXDR,CSANG,TIME,YLD,NPKT,RDEN)
        SIGMAC=1.6E-19*(INZRT/KA*MUE+2*MUI*SQRT(INZRT/KN))
      ELSE
        FIELD DEPENDENT CONDUCTIVITY.
        DATA FOR LONGMIRE FITS (MUE & KA).
        DATA AC,BC,CC/2.457,0.6884,1.195/
        KN=2.0E-12

```

```

MUI=2.5E-4
PWVC=100.0*WVC
KC=PWVC**X(0.834)
EPS1=0.07853*(1+AC*KC)
EPS2=3.015+CC*KC
MUEMAX=1.5/(1.0+96.97*(WVC)**X(0.787))
ESU=ETOTC(AL,CSANG,DR,NL,1)/30020.0
IF(ESU.LE.EPS1) THEN
    EPS0=ESU/(1+AC*KC)
ELSE IF(ESU.GT.EPS1.AND.ESU.LE.EPS2) THEN
    EPS0=(SQRT((BC*KC/2)**2+ESU)-BC*KC/2)**2
ELSE
    EPS0=ESU-CC*KC
END IF
MUA=1.0E+6/RDENX((16.8+EPS0)/(0.63+26.7*EPS0))**X(0.60)
R=1.55+210/(1+11.8*EPS0+7.2*EPS0**2)
MUE=MUA/(1-WVC+WVC*R)/3.002E+6
IF(MUE.GE.MUEMAX) THEN
    MUE=MUEMAX
END IF
KA3=1.0E+8*RDENX**2*((0.62+800*EPS0**2)/(1+1.0E+3*EPS0**2)*
    (EPS0*(1+0.03*EPS0**2))**X(0.33333333))
IF(EPS0.LT.1.1) THEN
    ARG=25.0
ELSE
    ARG=-21.15/EPS0
END IF
IF(ABS(ARG).GT.20.0) THEN
    KA2=0.0
ELSE
    KA2=1.22E+8*RDENX*EXP(-21.15/EPS0)
END IF
KA=((1-WVC)*((1+34.4*WVC)*KA3+KA2)
INZRT=INZRTC(1*DR,CSANG,TIME,YLD,NPKT,RDEN)
SIGMAC=1.6E-19*(INZRT/KA*MUE+2*MUI*SQRT(INZRT/KN))
END IF

```



```

C
C
      BEGIN ALGDRP
      IF(L.EQ.0) THEN
        ALGDRP=0.0
      ELSE IF(L.EQ.1) THEN
        ALGDRP=SQRT(ABS(1-CSHNG**2))
      ELSE
        AP(0)=0.0
        AP(1)=SQRT(ABS(1-CSHNG**2))
        DO 10 I=2,L
          AP(I)=(2.0*I-1.0)/(I-1.0)*CSHNG*H(I-1)+I/(1.0-I)*AP(I-2)
        CONTINUE
        ALGDRP=AP(L)
      END IF
      END
10

```

Vita

James R. Downey was born 27 January 1959 in Corry, Pennsylvania. He graduated from Corry Area High School in 1977 and attended Grove City College, Grove City, Pennsylvania where he earned a Bachelor of Science degree in physics. Upon graduation, he was commissioned in the United States Air Force through the ROTC program. In August of 1981 he entered active duty as a graduate student at the Air Force Institute of Technology, Wright-Patterson A.F.B., Ohio.

Permanent Address: 160 Johnson Street
Corry, Pennsylvania 16407

UNCLASSIFIED

SECURITY CLASSIFICATION OF THIS PAGE (When Data Entered)

REPORT DOCUMENTATION PAGE		READ INSTRUCTIONS BEFORE COMPLETING FORM
1. REPORT NUMBER AFIT/CNR/PH/83M-5	2. GOVT ACCESSION NO. 17-4121-5	3. RECIPIENT'S CATALOG NUMBER
4. TITLE (and Subtitle) THE CALCULATION OF LATE-TIME SURFACE BURST EMP FIELDS USING A TIME-INDEPENDENT NUMERICAL METHOD		5. TYPE OF REPORT & PERIOD COVERED MS Thesis
7. AUTHOR(s) James R. Downey 2Lt USAF		6. PERFORMING ORG. REPORT NUMBER
9. PERFORMING ORGANIZATION NAME AND ADDRESS Air Force Institute of Technology (AFIT-EN) Wright-Patterson AFB OH 45433		8. CONTRACT OR GRANT NUMBER(s)
11. CONTROLLING OFFICE NAME AND ADDRESS		10. PROGRAM ELEMENT, PROJECT, TASK AREA & WORK UNIT NUMBERS
14. MONITORING AGENCY NAME & ADDRESS (if different from Controlling Office)		12. REPORT DATE March 1983
		13. NUMBER OF PAGES 148
		15. SECURITY CLASS. (of this report) UNCLASSIFIED
		15a. DECLASSIFICATION DOWNGRADING SCHEDULE
16. DISTRIBUTION STATEMENT (of this Report) Approved for Public Release; Distribution Unlimited		
17. DISTRIBUTION STATEMENT (of the abstract entered in Block 20, if different from Report)		
18. SUPPLEMENTARY NOTES Approved for public release; IAW AFR 190-17. LYNN E. WOLAVER Deputy for Research and Professional Development Air Force Institute of Technology (ATC) Wright-Patterson AFB OH 45433 7 APR 1983		
19. KEY WORDS (Continue on reverse side if necessary and identify by block number) EMP Late-Time Air Conductivity Surface Burst Quasi-Static		
20. ABSTRACT (Continue on reverse side if necessary and identify by block number) A numerical solution was developed to find the quasi-static EMP fields resulting from a surface nuclear burst. By ignoring the time derivatives in Maxwell's equations and expanding the electrostatic potential in Legendre polynomials, a set of differential equations was obtained that was dependent on r only (r = radius from burst). By employing finite differences, a tri-diagonal matrix equation was obtained that was parallel to the z axis of the field. This equation was solved using an iterative scheme. <i>sent</i> (Continued on Reverse)		

DD FORM 1 JAN 73 1473

EDITION OF 1 NOV 65 IS OBSOLETE

UNCLASSIFIED

SECURITY CLASSIFICATION OF THIS PAGE (When Data Entered)

UNCLASSIFIED

SECURITY CLASSIFICATION OF THIS PAGE (When Data Entered)

BLOCK 20: ABSTRACT (Continued)

Analytic curve fits based on Monte Carlo data were used to determine the air ionization rate and Compton current. This permitted the angular variation of these sources to be included in the calculations. In addition, the electron air chemistry parameters were allowed to vary with the local electric field and water vapor content of the air. This was accomplished by the use of previously developed equations for these terms.

Field calculations were made and compared to previous analytic results. The differences were found to be as great as 50 percent for peak field values. A limited parametric study was performed to consider the effects of varying the time, the yield, and the water vapor content.

UNCLASSIFIED

SECURITY CLASSIFICATION OF THIS PAGE (When Data Entered)